Dyke reactivation across the frictional-viscous transition: Precambrian deformation of Scourie dyke margins in NW Scotland

LAURA JANE SCOTT

Dyke reactivation across the frictional-viscous transition: Precambrian deformation of Scourie dyke margins in NW Scotland

Loch Assynt in the sunshine, fieldwork September 2017

Laura Jane Scott

This thesis is submitted as fulfilment for an MScR in Geology, Department of Earth Sciences, Durham University, 2018

Basement-hosted regional dyke swarms are recognised worldwide and represent lithosphere-scale anisotropies that may significantly influence later deformation. Several Precambrian deformation events have affected the Lewisian Complex of NW Scotland, with the Badcallian (ca. 2.75Ga) and Inverian (ca. 2.5Ga) predating and the Laxfordian (ca. 1.75Ga) and 'Late Laxfordian' (ca. 1.55Ga) postdating the regional Scourie dyke swarm (ca. 2.4Ga). Brittle-ductile reactivation and reworking of these dykes is widely reported but has lacked detailed description. The present study focuses on dykes in the Assynt Terrane that show a range of contact relationships and reactivation styles. The dyke at *Lochinver* (NC087219) preserves undeformed intrusive contacts, with obvious ~1.5cm chilled margins. Two dykes at *Achmelvich* (NC056250 and NC055248) show different reactivation styles. One preserves local developments (<1.2m) of schistose viscous mylonites with dextral shear sense indicators in mica schists at both contacts. The style of deformation, veining and associated metamorphism is consistent with Laxfordian deformation in the nearby Canisp Shear Zone. The second dyke has ductile dextral deformation on its southern margin, but the northern margin preserves a complex history of localised ductile and later brittle reactivation associated with pseudotachylytes, parallel to the dyke margin and as injections into the surrounding gneisses. Shear sense indicators suggest this deformation, along with later cross-cutting zeolite veins, are associated with sinistral shearing. *Loch Assynt* (NC2125) shows evidence for localised (1-5cm) sinistral ultramylonites and pseudotachylytes at the dyke margins, overprinted by brittle sinistral reactivation; both associated with widespread epidote and localised copper mineralisation – there is little evidence for schistose mylonites. Re-Os geochronology of the copper mineralisation yields an age of 1.55Ga. Thus, field and microstructural observations show at least three phases of brittle-ductile reactivation along dyke margins broadly correlated with Laxfordian and 'Late Laxfordian' events, both are kinematically coherent and distinct. Favourable regional tectonic stresses can therefore lead to tectonic inheritance within the geological record.

Table of Contents

List of Figures

List of Tables

List of abbreviations

Bio*	Biotite
BLG	Bulging (recrystallisation)
BVT*	Brittle-viscous transition (also known as the brittle-ductile, or brittle-plastic)
Cat*	Cataclasite
CPO	Crystal Preferred Orientation
CSZ	Canisp Shear Zone
Epi*	Epidote
Fsp*	Feldspar
GBAR	Grain boundary area reduction
GBM	Grain boundary migration (recrystallisation)
GBS	Grain boundary sliding
Gt-sill-plag-qz	Garnet-sillimanite-plagioclase-quartz
Hb*	Hornblende
LAF*	Loch Assynt Fault
Psd*	Pseudotachylyte
SGR	Subgrain rotation (recrystallisation)
SPO	Shape Preferred Orientation
Qtz*	Quartz

** Used in figures.*

Acknowledgements

First of all, I would like to thank my supervisors on this project for helping me develop my ideas and produce this piece of work; Bob Holdsworth for presenting the project idea, and for his extensive knowledge of NW Scotland, attention to detail and honest feedback, Jonny Imber for always listening to my ideas and offering advice, and Eddie Dempsey for his enthusiasm and positive outlook. Thanks also goes to Tom Utley for flying the drone over my localities and stitching the resultant images together to provide me with excellent aerial photographs to map onto, and Kit Hardman for allowing me to tag along on his fieldwork in April so that I could get more measurements and share ideas whilst in the field. As my mum (a non-geologist) accompanied me on my initial fieldwork, she deserves thanks for putting up with me getting excited over different fault rocks, and staying in the field with me in all weathers: from 18^{o}C sunshine to sleet showers! Last but not least, I have to thank Jack Lee for his continued support, positive encouragement and always believing in me.

1. Introduction

Dyke swarms are common within basement complexes globally e.g. Canada, Australia, the Falklands (Fig. 1.1) and NW Scotland (this study and references therein), and commonly preserve evidence of emplacement at mid-crustal depths. Evidence for intrusion at depth within the ultramafic Scourie dyke suite of NW Scotland includes metamorphic mineral assemblages typical of amphibolite facies (e.g. primary hornblendes, autometamorphic garnets, two pyroxene metamorphic assemblages) and deformation of the earlier dolerite dykes under amphibolite facies conditions, cross cut by later picrite dykes (Tarney, 1973; Wheeler et al., 2010). It is important to understand reactivation processes within the middle crust, as this is the main load bearing region of the lithosphere, incorporating the brittle-ductile transition (Behr and Platt, 2014) (Fig. 1.2). This is also the main earthquake producing region (e.g. Chen and Molnar, 1983; Sibson, 1983), with the area of study being seismically active >1.4 Ga (e.g. Giletti et al., 1961; Evans and Lambert, 1974).

Aims of this project include documenting the geometry, kinematics, fault rock and mineral vein development associated with the different styles of dyke margin reactivation preserved at a number of key field localities in NW Scotland (Fig. 1.3). This phenomenon is frequently referred to in the literature (e.g. Attfield, 1987; Obst and Katzung, 2006; Fossen and Cavalcante, 2017) but has yet to be described in any detail. The relationships between pre-existing mechanical anisotropies, chemically active fluids and deformation processes across the frictional-viscous transition are studied, looking at how dry and/or hydrothermal events may influence dyke margin reactivation on a local, or regional, scale. Only data from 100% exposed dyke margins (undeformed and reactivated) are used to successfully provide an insight into the reactivation events in the region. Local overprinting relationships are established and representative fault rocks and vein fills sampled for laboratory based microstructural analysis. Microstructural analysis from key samples from the field can provide an insight into the kinematics and overprinting relationships of different stages of

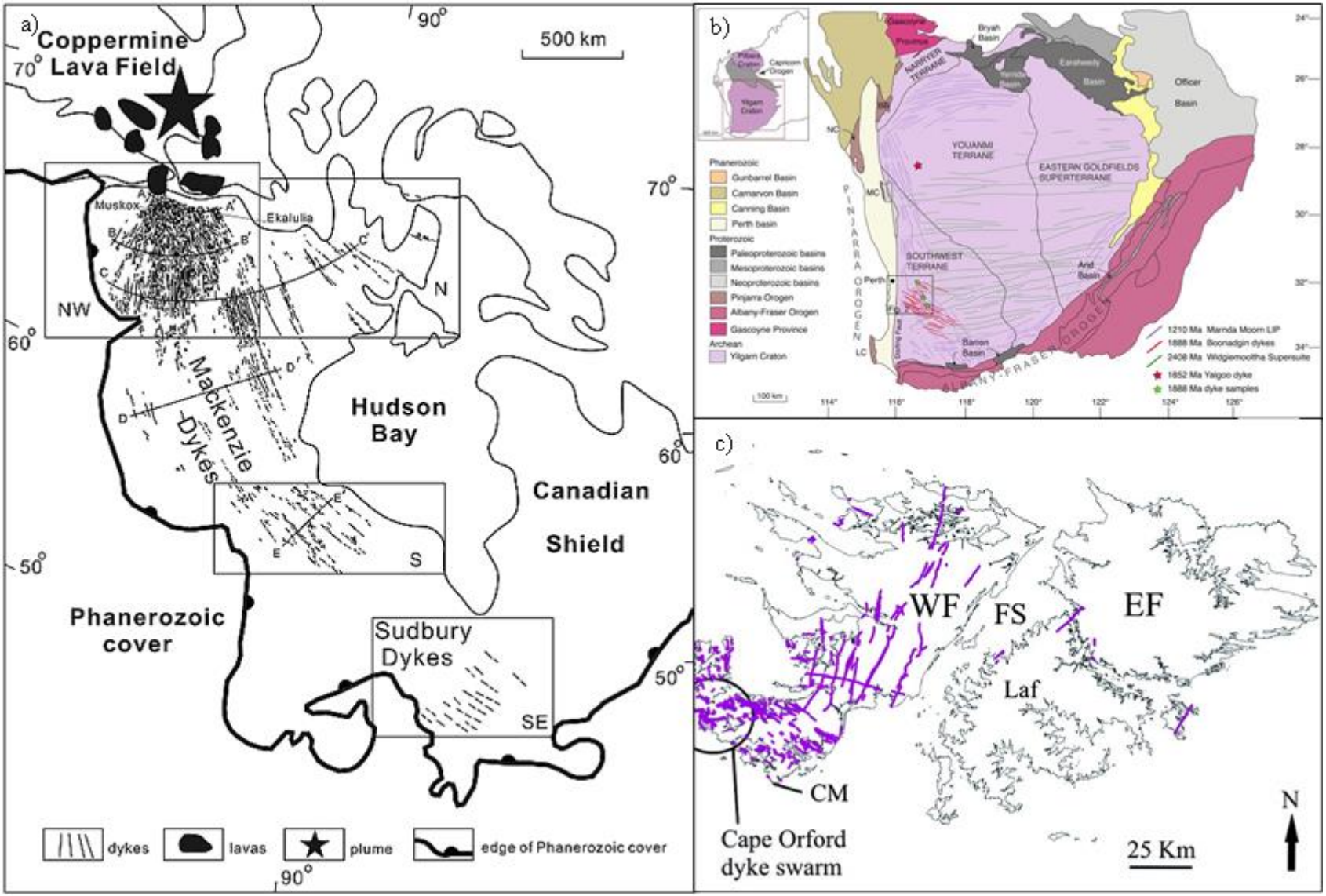
a)
Coppermine
Lava Field
500 km
90°
70°
60°
50°
Muskox
Ekalulia
NW
N
S
SE
Mackenzie
Dykes
Hudson
Bay
Canadian
Shield
Phanerozoic
cover
Sudbury
Dykes
dykes
lavas
plume
edge of Phanerozoic cover
b)
Phanerozoic
Gunbarrel Basin
Carnarvon Basin
Canning Basin
Perth basin
Proterozoic
Paleoproterozoic basins
Mesoproterozoic basins
Neoproterozoic basins
Pinjarra Orogen
Albany-Fraser Orogen
Gascoyne Province
Archean
Yilgarn Craton
NARRYER TERRANE
YOUANMI TERRANE
EASTERN GOLDFIELDS SUPERTERRANE
SOUTHWEST TERRANE
PINJARRA OROGEN
ALBANY-FRASER OROGEN
Bryah Basin
Earaheedy Basin
Officer Basin
Arid Basin
Perth
Barton Basin
1210 Ma Marnda Moorn LIP
1888 Ma Boonadgin dykes
2408 Ma Widgiemooltha Supersuite
1852 Ma Yalgoo dyke
1888 Ma dyke samples
c)
WF
FS
EF
Laf
CM
Cape Orford
dyke swarm
25 Km
N

Fig. 1.1. *(Above) Regional dyke swarms across the globe a) Mackenzie dyke swarm, Canada (Hou et al., 2010) b) Multiple dyke swarms in Australia (Stark et al., 2017) c) Dyke swarms around the Falklands. CM: Cape Meredith; EF: East Falkland; FS: Falkland South; Laf: Ladonia; WF: West Falkland (Stone et al., 2009).*

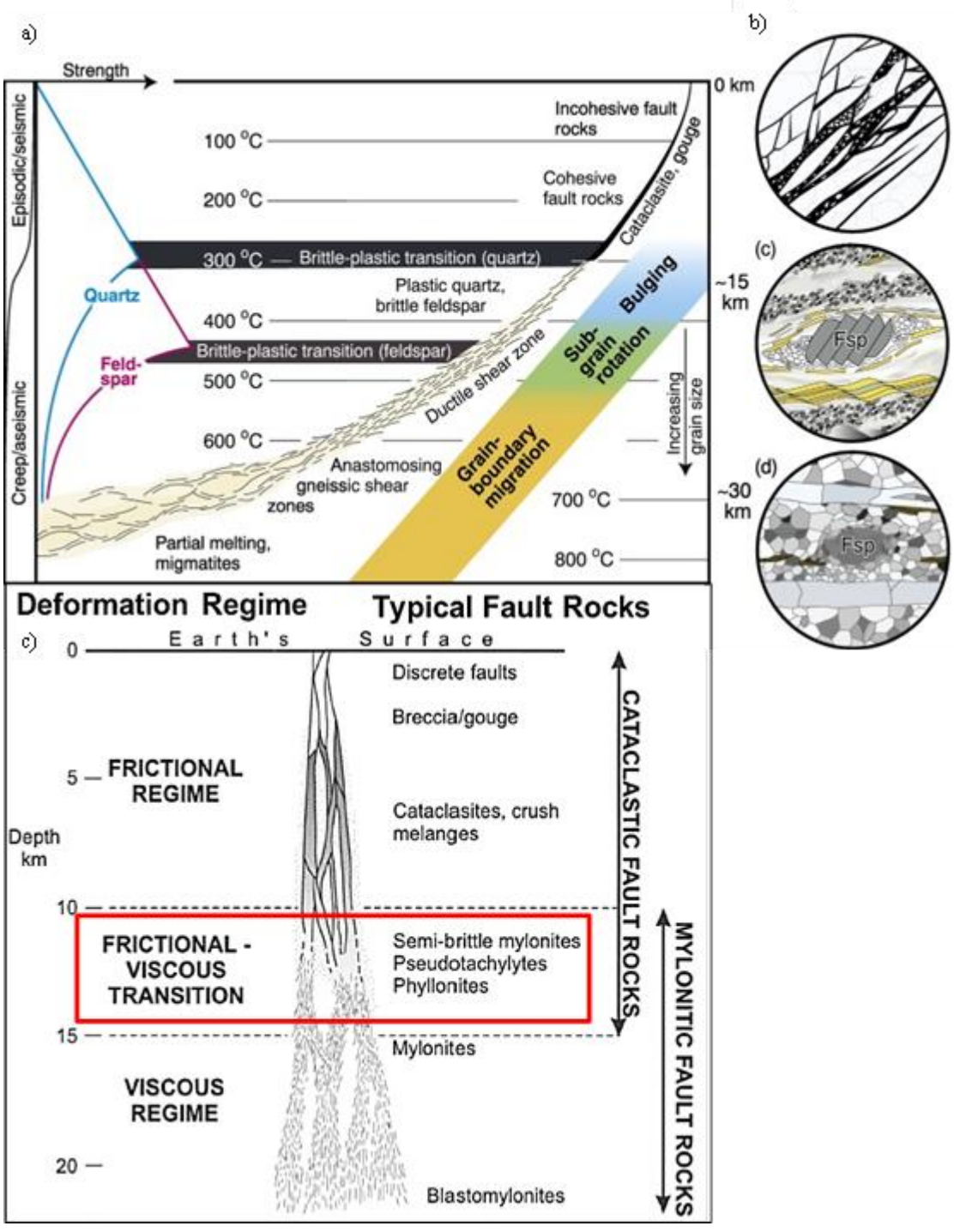

Fig 1.2. *a) Simplified diagram that illustrates vertical variations in shear zones. Quartz and feldspathic brittle-plastic transitions and recrystallisation mechanisms are related to temperature, as well as a dependence on strain rate and amount of fluids present. b-d) Characteristic microfabrics in the three different regimes: b) brittle fracturing c) plastic with brittle feldspar, small recrystallised quartz grains; d) recrystallisation at high temperatures where feldspar and quartz deform plastically, diffusion dominated grain boundary migration is dominant (adapted from Fossen and Cavalcante, 2017) c) Fault rock type with depth within the crust, highlighting the frictional-viscous (also known as brittle ductile, or brittle plastic) transition, the main area of study within this project (adapted from Holdsworth et al. (2001) [adapted from Sibson, 1977]).*

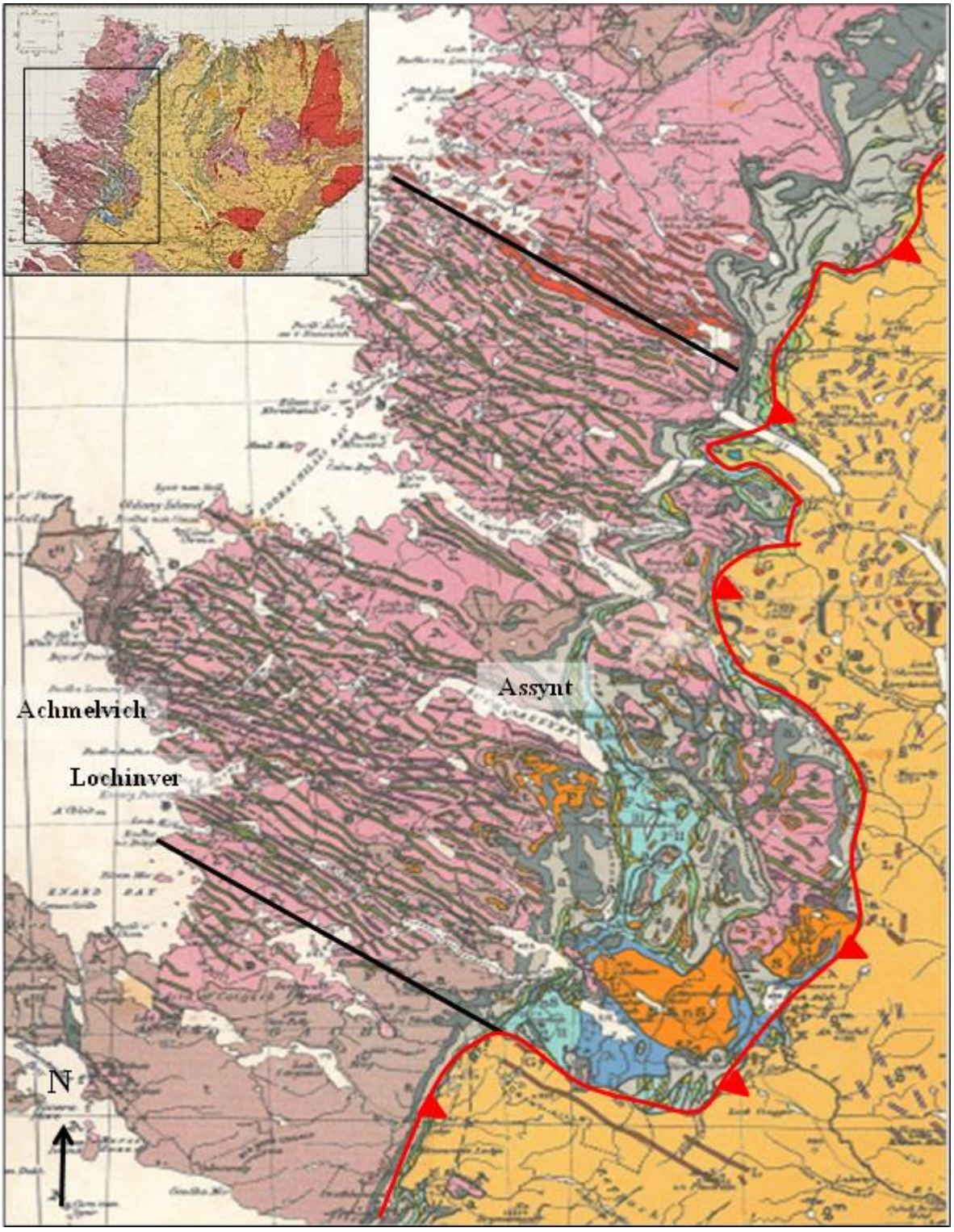

Fig. 1.3. *Geological map encompassing the study area of the Assynt terrane (upper and lower boundaries indicated by thick black lines, Moine Thrust indicated by thick red line). Dark green NW-SE trending structures: Scourie dyke; pink: Lewisian Gneiss. Localities for study marked on. Inset shows location within Sutherland, NW Scotland. Contains British Geological Survey materials © NERC [1972].*

reactivation and/or different reactivation events using optical microscopy. The associations between mineralogical changes, mineral vein development and grain scale deformation mechanisms can be studied in order to assess the influence of fluid influx on deformation styles during reactivation, and the relationship to mechanical weakening. The existing hypothesis that the syn-shearing fluid influx of hydrous fluids can drastically influence the resulting style of deformation can be tested in this research.

Studying an exhumed mid-crustal terrane can give insights into long-term reactivation events, impacting our understanding of when deformation occurs in a brittle or ductile manner. This can be coupled with the relationship between seismic and interseismic periods; pseudotachylytes, and ultramylonites and other fault rocks, respectively (Fig. 1.2c) during long term orogenic cycles. Analysis of fault rocks formed during reactivation can be used to determine what weakening mechanisms lead to reactivation, and if any of these can lead to long term strengthening (e.g. frictional sliding).

2. Regional setting

The basement rocks of the Lewisian Complex of NW Scotland are an example of a typical continental basement terrane. They are Badcallian in age, and lie to the west of the Caledonian age Moine Thrust (Figs. 1.3, 2.1), with major regional scale Palaeoproterozoic and Archean deformation events affecting the Complex in this area. They are not, however, much affected by post-Archaean deformation events (e.g. the Caledonian), and therefore preserve older structures. Single vs multiple terrane models have been inferred from the geology, metamorphism and, more recently, geochronology. Traditionally, the Lewisian Complex was viewed as a single late Archaean crustal block that underwent metamorphism and later deformation, with equivalent age gneisses in all regions (e.g. Peach et al., 1907;

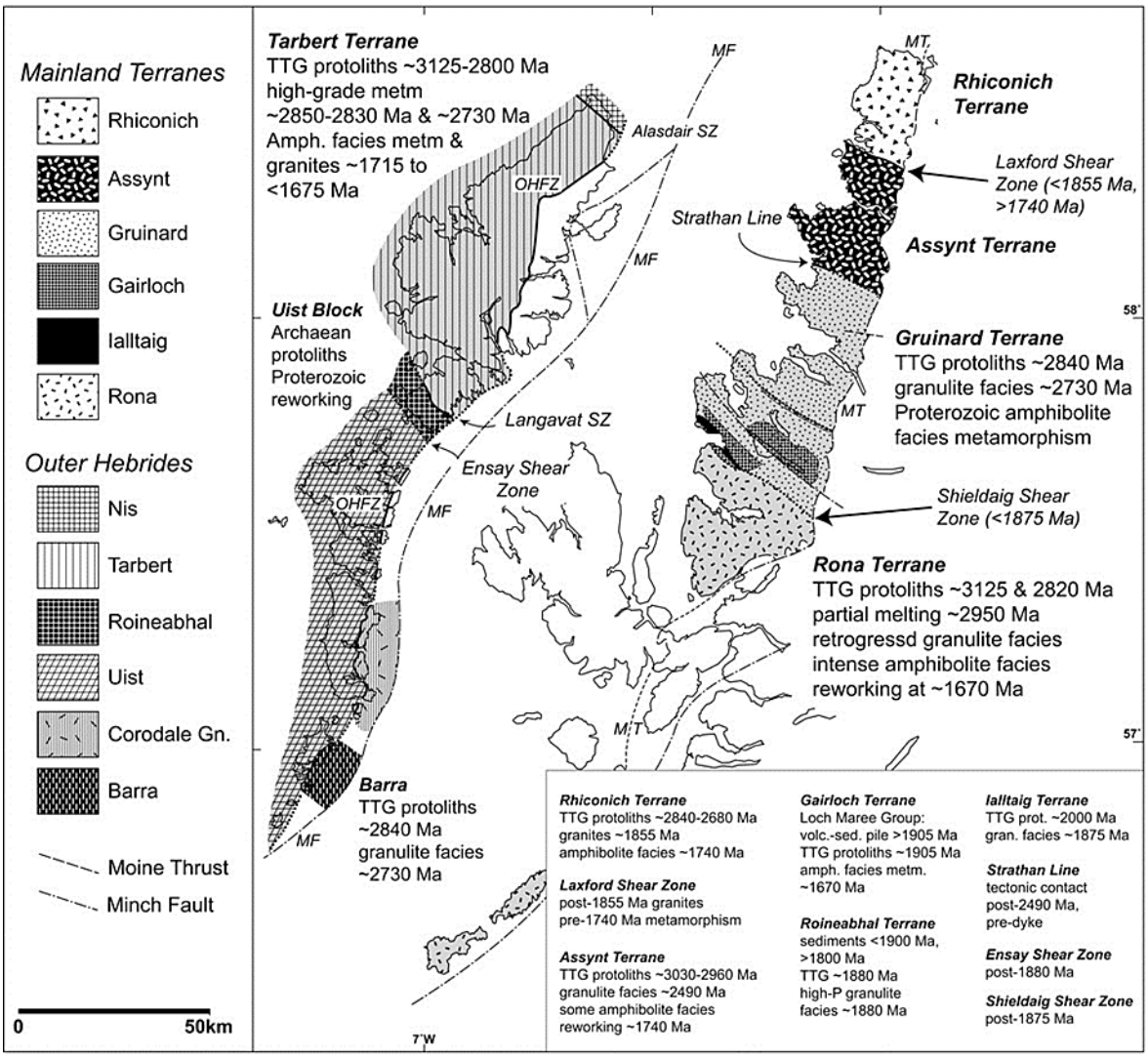

Fig. 2.2. *Early (Nagssugtoquidian) and Late (Labradorian) orogens in the Lewisian complex. Early Laxfordian suturing of Archaean plates surrounding a previously active continental margin, followed by extreme contraction within Late Laxfordian nappes. Well preserved gneisses of the central region are outside of both belts. Area of focus (central mainland) within this study highlighted (adapted from Mason, 2016).*

ages to show magmatism and metamorphism ca. 2.85-2.73 Ga in the Outer Hebrides equivalent to events of the mainland terranes (e.g. Tarbert, Gruinard) (Mason et al., 2004), suggesting these terranes were contiguous (Fig. 2.2). The rationale of a multiple terrane model was analysed by Friend and Kinny (2001). Using U-Pb single-zircon geochronology, they proposed 9 separate terranes which amalgamated in the Palaeoproterozoic. They proposed different ages for the gneisses in Harris (3.215 Ga), and the Leverburgh and Langvat belts (2.78-1.88 Ga), and noted the absence of some metamorphic events in some terranes. The terranes are bounded by crustal scale shear zones (e.g. the Laxford shear zone), which act as continental sutures. The absence of pervasive Laxfordian reworking within the Assynt terrane was suggested to be due to its higher structural level compared to the Gruinard or Rhiconich terranes (Park, 2005; Mason, 2012, 2016), providing evidence for the existence of an early Laxfordian suture in this region (Fig. 2.2) (Mason, 2016).

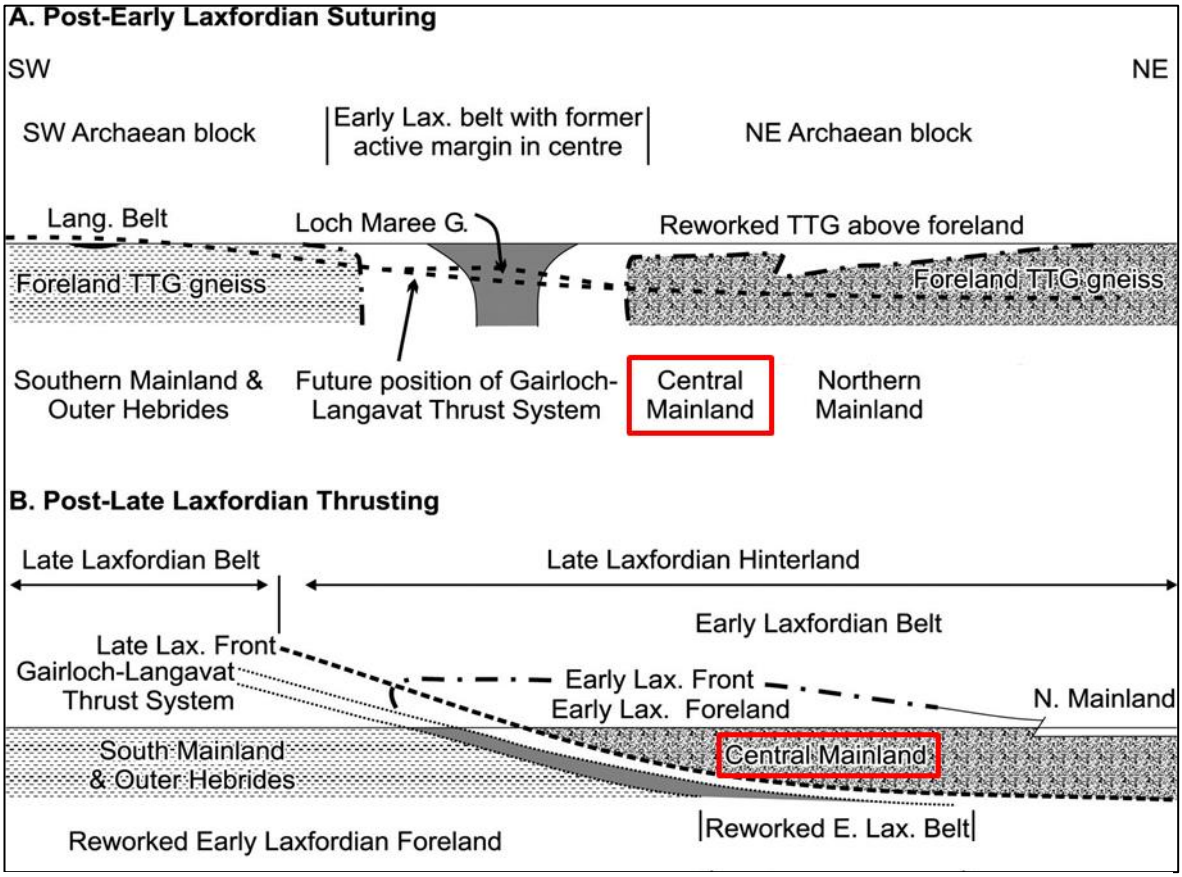

Fig. 2.2. *Early (Nagssugtoquidian) and Late (Labradorian) orogens in the Lewisian complex. Early Laxfordian suturing of Archaean plates surrounding a previously active continental margin, followed by extreme contraction within Late Laxfordian nappes. Well preserved gneisses of the central region are outside of both belts. Area of focus (central mainland) within this study highlighted (adapted from Mason, 2016).*

The Central terrane, referred to by Sutton and Watson (1950), is more commonly known as the Assynt Terrane (Figs. 1.3, 2.1), comprising of highly variable grey, banded tonalite-trondjemite-granodiorite (TTG) orthogneisses (Sheraton et al., 1973) originating from an igneous pluton. U-Pb and Sm-Nd geochronology have provided dates of intrusion 3.03-2.96 Ga (Hamilton et al., 1979; Friend and Kinny, 1995). The Badcallian tectonometamorphic event, initially referred to as the Scourian (Giletti et al., 1961; Sheraton et al., 1973), or early Scourian (Park, 1970), saw the deformation and high grade metamorphism of the TTG gneisses (Evans and Lambert, 1974; Attfield, 1987), which is more widespread in the Assynt terrane (Kinny et al., 2005). U-Pb zircon analysis suggests peak Badcallian metamorphism occurred ca. 2.8-2.7 Ga (Corfu et al., 1994; Love et al., 2004), with minimum temperatures of 710-834^{o}C (Ti-in-zircon thermometry [MacDonald et al., 2015]) and pressures of 850-1150 MPa (mineral equilibria calculations [Johnson and White, 2011]), placing the event within a granulite facies regime. NE-SW structures are preserved, along with sub-horizontal folding and banding within the gneiss (Park, 1970; Sheraton et al., 1973).

The Inverian (referred to as the Late Scourian by Park [1970]) shows the hydrous retrogression of dry Badcallian rocks at amphibolite facies in the middle crust (Park, 1970; Sheraton et al., 1973). Kinny et al (2005) presented the idea that the Inverian tectonometamophic event was due to the suturing of the Assynt and Gruinard terranes, explaining the differing (~100 Myr) protolith ages of the gneiss in each of these terranes, highlighted by Love et al (2004). Mainland Inverian structures can be split into: broad (>4km) shear zones unaffected by Laxfordian reworking; narrow (<1.5km) shear zones cutting through Archaean rocks in the central region and; regions that experienced high strain in the Inverian that were intensively reworked during the subsequent Laxfordian event (Park and Tarney, 1987). Lower crustal deformation produced major NW-SE trending structures, for example the Laxford Shear Zone. This is the boundary between the northern Rhichonich and central Assynt terranes, suggested by Goodenough et al (2010; 2013) to accommodate

the suturing of the two terranes during the Inverian. The ≤1.5km wide Canisp shear Zone (CSZ) is a steeply dipping transpressional shear zone in the centre of the Assynt terrane, first activated within the Inverian (Attfield, 1987). The Lochinver monocline represents the southern margin of the CSZ, with ductile fabrics preserved (i.e. plastic folding) (Bowes and Bhattacharjee, 1967; Attfield, 1987). The Badcallian gneisses are cut by many similar steeply dipping NW-SE shear zones, many of which initially developed during this period (Park and Tarney, 1987). The Inverian is associated with a steeply-inclined foliation, with the associated lineation plunging steeply to the SE along the exposed fault planes, indicating mostly dip-slip movement with a small component of dextral strike slip (Attfield, 1987). The majority of studies conclude the age of the Inverian to be ca. 2.49-2.48 Ga (U-Pb zircon analysis [e.g. Corfu et al., 1994; Love et al., 2004; Goodenough et al., 2013]), however some studies (Friend and Kinny, 1995) suggest ages younger than ca. 2.48 Ga, but that still predate Scourie dyke emplacement. Mineral equilibria modelling of metasedimentary rocks suggest temperatures of 520-550^{o}C (Zirkler et al., 2012), however this may not be peak metamorphism. Ion-exchange thermometers studies with TTG gneisses give temperatures closer to 600^{o}C (Sills, 1983).

The ultramafic Scourie dykes are prominent within the Assynt terrane (Fig. 1.3). These were dated as being emplaced ca. 2.4-2.0 Ga by U-Pb geochronology and Rb-Sr whole rock analysis (Chapman, 1979; Heaman and Tarney, 1989). This intrusion is thought to represent a syn-metamorphic (rather than syn-tectonic) phenomenon relating to the relaxation and closure of Inverian deformation during crustal extension (Tarney, 1973; Evans and Lambert, 1974). Dykes range from a few millimetres to tens of metres in width, and were emplaced roughly parallel to the pre-existing NW-SE trending Inverian shear zones (Fig. 1.3). They are seen to cross cut local Inverian fabrics and show mineralogical evidence of being emplaced under amphibolite facies conditions (O'Hara, 1961; Tarney, 1973; Wheeler et al., 2010), as well as under a dextral transtensional regime (Park et al., 1987). Further

exhumation occurred during dyke emplacement, with two main stages of intrusion (Fig. 2.3) encompassing four variations in composition suggested from geochemical studies by Tarney and Weaver, (1987) and Heaman and Tarney, (1989).

Much of the Lewisian Complex contains evidence of a later shearing event affecting the Scourie dykes at retrogressive lower amphibolite to upper greenschist facies conditions: the Laxfordian. The Laxfordian event started with subduction related magmatism documented ca. 1.9 Ga, forming the Loch Maree complex (marking the boundary between the Central and Southern terranes). This was then terminated by a continent-continent collision that initiated crustal thickening, 1.79-1.66 Ma (Fig. 2.2) (Goodenough et al., 2013; Mason, 2016), with temperatures of 530-630^{o}C and pressures of 650 MPa at depths of ca. 24 ± 5km (Droop et al., 1999) interpreted from ion exchange thermometry of the Loch Maree Group, however these studies were not conducted in the Assynt terrane. The crustal thickening marked the start of a prolonged period of subduction related crustal

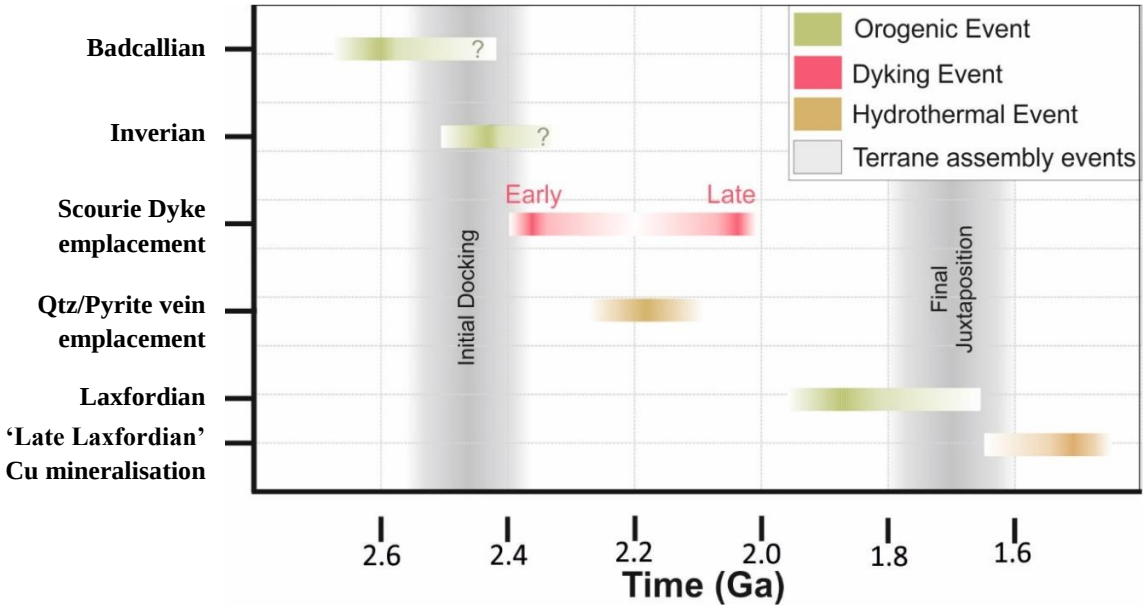

Fig. 2.3 *Chronology of Precambrian events recorded in NW Scotland focussing on the Assynt terrane, including potential dates for the 'Late Laxfordian' (adapted from Vernon et al., 2014).*

accretion that only terminated at the Grenville orogeny, ca. 1 Ga (Spencer et al., 2015 and references therein). Nearing the end of the Laxfordian ca. 1.7 Ga, there was a hypothesised thickening of the continental crust with a minor amount of strike slip resulting from a collisional event (Fig. 2.2) (Mason, 2016). The main episode of Laxfordian deformation has been concluded to lie 1.79-1.67 Ga (U-Pb dating of zircon and titanite in TTG gneisses [Corfu et al., 1994; Kinny et al., 2005]). Within the Assynt terrane, the Laxfordian is generally restricted to the central part of the Canisp and other major shear zones, as well as the NW-SE trending Scourie dyke margins. This made it a highly localised event that reactivated pre-existing Inverian structures. Within the CSZ, Scourie dykes have been strongly affected by the Laxfordian shearing; this is particularly concentrated around the dyke margins, with a lot of dykes sheared to lie parallel to the foliation (Sheraton et al., 1973). Outside of the main shear zones, the dykes only appear sheared along the margins on a scale of a few centimetres to a metre (Attfield, 1987), with the shearing producing mylonitic and blastomylonitic fault rocks (Park et al., 1994). Strong dextral strike slip indicators are present within discrete shear zones, along with a strong lineation plunging 10-30^{o} ESE (Attfield, 1987).

A younger set of 'Late Laxfordian' sinistral structures are present within the Assynt and Gruinard terranes, with Coward (1990) expressing this post-Laxfordian deformation as a crustal extension event, reactivating earlier compressional (Inverian and Laxfordian) structures. Low-greenschist facies sinistral mylonitic shear zones, and other localised ductile fabrics, along with brittle faults (including the Loch Assynt fault) were produced (Beacom et al., 2001). Crush belts, pseudotachylytes and shallowly plunging lineations are present, along with the formation of chlorite and epidote (O'Hara, 1961; Park and Cresswell, 1973), with pseudotachylyte pods along the brecciated dyke margin at the southern side of Achmelvich Bay (visited in this study) (Attfield, 1987). The precise age of this event is unconstrained within the literature, but the sinistral structures have an unconformable

contact with the younger unmetamorphosed ca. 1.2 Ga Stoer Group; both of which are unconformably overlain by Torridonian sequences <1.1 Ga (Park et al., 1994). There is discontinuity with which the term 'Late Laxfordian' is used in the literature, with some authors (e.g. Mason, 2016) using the term to refer to events occurring late in the Laxfordian orogenic cycle (>1.6 Ga), whereas others (e.g. Beacom et al., 2001; Vernon et al., 2014) refer to the 'Late Laxfordian' as a post-Laxfordian sinistral shearing event.

2.1 Small scale Lewisian structures

Average compositions of Badcallian gneisses around the Assynt region are 30% quartz, 30% clinopyroxene, 20% plagioclase, 10% microcline and 10% orthopyroxene. Felsic (plagioclase and quartz) and mafic (pyroxene, hornblende, biotite) layers define strong foliations within the gneiss, 0.5-5 cm in thickness (Jensen, 1984). The Inverian event reworked these Badcallian foliations, resulting in a NW-SE trend within dextral reverse shear zones, with bands of highly sheared gneisses enclosing lenses of lower strain material due to the heterogeneity of the shearing (Attfield, 1987). Gneisses deformed by the Inverian show a more diverse composition; 40% feldspar, 20% quartz, 15% hornblende, 15% biotite and chlorite, 5% pyroxene and 5% additional minerals (e.g. epidote), with the new mafic minerals likely to be due to the breakdown and hydration of pyroxenes (Beach, 1976). On a microscale, quartz crystals in these gneisses contain subgrains (0.25-1 mm), with a smaller crystal size than Badcallian gneisses due to syn-tectonic recrystallisation processes (Jensen, 1984).

Amphibolite facies metamorphism of the dykes around the time of their emplacement sometimes resulted in the loss of chilled margins (not the case at Lochinver, this study) and the alteration of the originally doleritic composition. Metamorphic mineral alteration resulted in the replacement of pyroxenes with fibrous amphibole, containing sieve-like quartz inclusions (Sutton and Watson, 1950; Tarney, 1973). The post-dyke dextral Laxfordian event produced finer foliations within the gneiss, especially in the CSZ (Sheraton

et al., 1973; Attfield, 1987), with typical deformed gneisses showing a more felsic composition than their Badcallian and Inverian counterparts. Mineralogically, compositions are 55% quartz, 10% hornblende, 10% biotite and muscovite, and 5% feldspar (porphyroblasts ~1 mm). There are millimetre scale alternating bands of smaller (<100 μm) and larger (500–1000μm) quartz grains; these form part of the schistose foliation, with pinning of the quartz grains common (Jensen, 1984). Pyroxene is replaced with hornblende followed by biotite with increasing deformation in the most intensely deformed gneisses, with deformed rocks within shear zones showing alteration by synkinematic metasomatism (Beach, 1976).

3. Methodology

3.1 Fieldwork

Fieldwork was undertaken at 100% exposed dyke margins within the Assynt terrane (see Fig. 3). Structural data was collected from four main field localities; Lochinver (NC 087 219), Achmelvich (NC 056 250 and NC 055 248) and Loch Assynt (NC 21 25). Key features were measured at each locality and used to document regional trends for each reactivation event. 21 representative (oriented) samples of key fault rocks at the dyke margins and undeformed dyke material were taken, of which 10 were sectioned for further study. Additional samples and data from earlier fieldwork (by R.E. Holdsworth and E. Dempsey) around Achmelvich and Copper Island (Loch Assynt) were also used during analysis.

3.2 Microstructural analysis

Detailed analysis of the thin sections has been undertaken to document kinematics and overprinting relationships at the microscale using Leica and Nikkon optical microscopes (the Nikkon with the additional 1x lens for broader observations) and an attached camera driver for photomicrographs. Image stitching used the Microsoft Image Composite Editor software to produce larger scale images for analysis.

4. Field relationships of dyke margins and surrounding features

Dyke margin reactivation is a common phenomenon, but little described within the literature; it is noted, for example by Attfield (1987) as occurring, but has not been described in detail. The NW-SE-trending dyke margins at Lochinver, Achmelvich Bay (North and South) and Loch Assynt have been analysed within the present study (Fig. 4.1a) and display a wide range of deformation styles; from undeformed, to viscous, to brittle, along with features related to fluid influx during and after deformation. Lochinver, the type locality for the undeformed dyke margin and associated features, lies ~3km across strike from the centre of the Canisp shear zone (CSZ) and is the furthest south within this study (Fig. 4.1a). Moving northwards, Achmelvich South and Achmelvich North are in close proximity to the CSZ (0.8km and 0.6km across strike respectively), with Achmelvich North lying on the northern margin of the Lochinver monocline (Fig. 4.1b). Moving eastwards and northwards across strike (~7km) to the other side of the Canisp shear zone, the Loch Assynt dyke(s) run sub-parallel to the nearby Loch Assynt fault, with the fault traced to the coastal exposures around Clashnessie Bay (Fig. 4.1a)

4.1. Pre-dyke foliations

The quartzo-feldspathic Lewisian gneisses at the four main localities contain compositional banding averaging 0.5-2cm in width, split into felsic quartz and feldspar bands, and mafic hornblende, biotite and pyroxene bands. These define the gneissose foliation, with average crystal sizes of 1-2mm. Gneisses in the study areas commonly contain mafic (hornblende) pods averaging 20cm in diameter, with crystal sizes larger than those within the gneiss, at 3-5mm; one pod at Lochinver contains acicular crystals ≤3cm in length. In some areas, the gneiss shows a migmatitic texture (e.g. Achmelvich North, NC 05708 25617). Here, crystal sizes vary based on mineralogy; felsic areas contain crystals ~1mm whereas mafic areas reach 3-5mm. The above evidence, as well as the presence of garnet and orthopyroxene (Park, 1964; Pattison et al., 2003), points to a granulite facies metamorphic

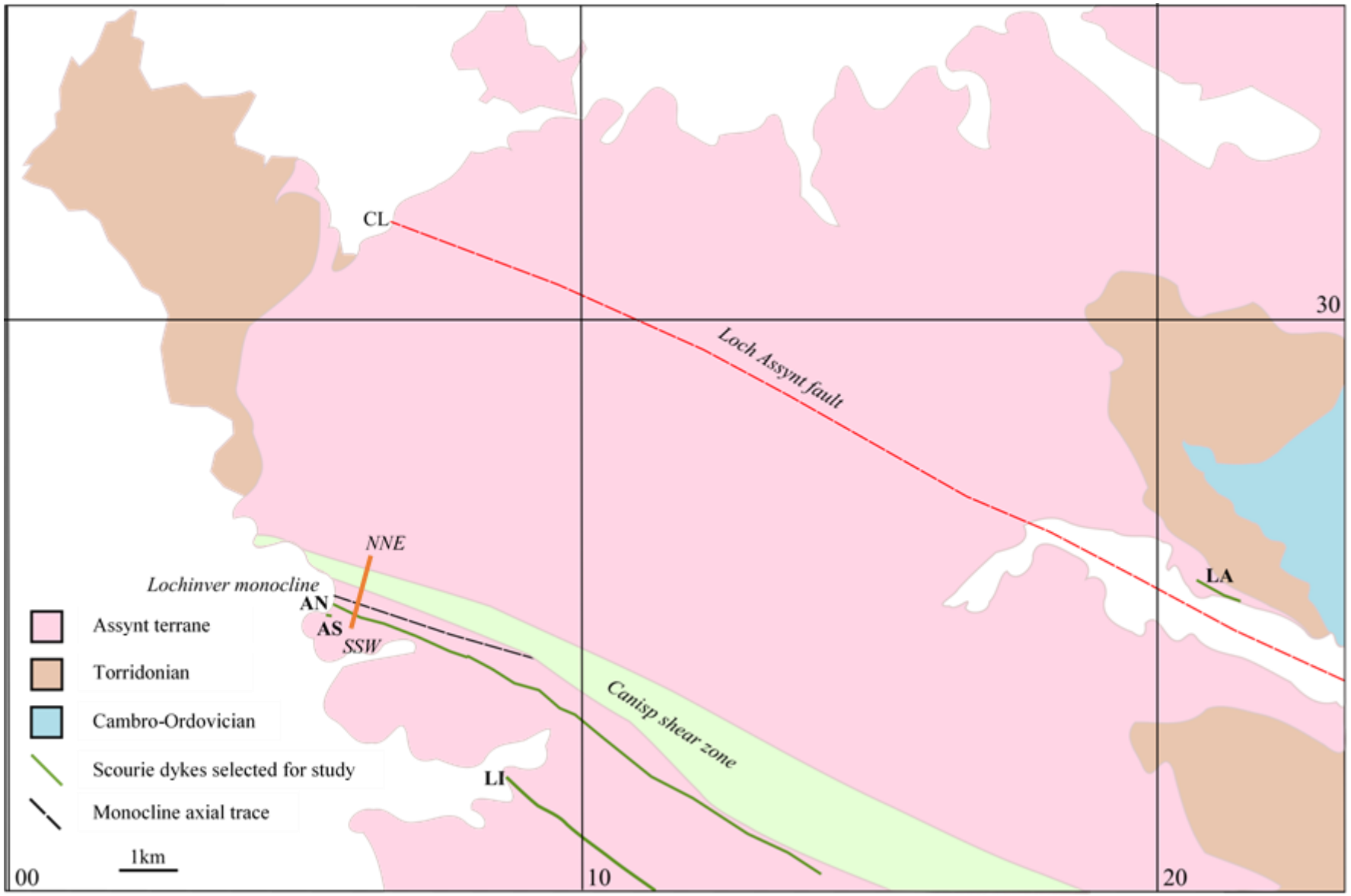
CL
Loch Assynt fault
30
NNE
Lochinver monocline
AN
AS
SSW
LA
Canisp shear zone
LI
Assynt terrane
Torridonian
Cambro-Ordovician
Scourie dykes selected for study
Monocline axial trace
1km
00
10
20

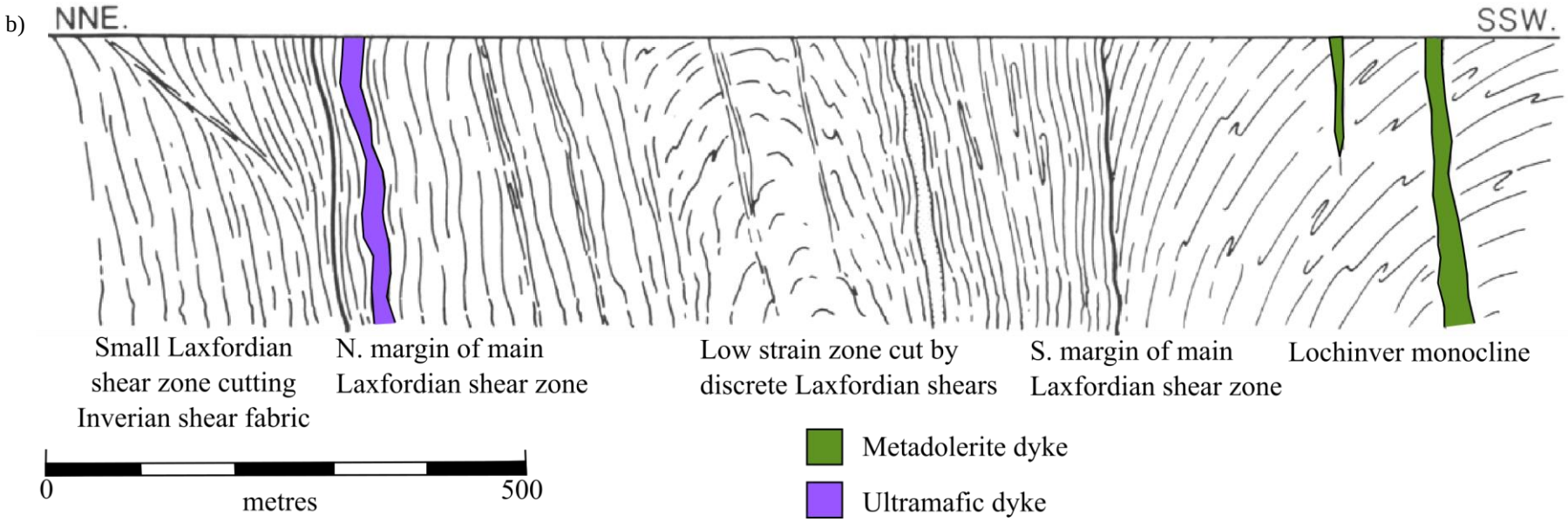

Fig 4.1. *a) Simplified geological map showing the study locations within the Assynt terrane, LA: Loch Assynt; LI: Lochinver; AS: Achmelvich South; AN: Achmelvich North; CL: Clashnessie. Individual Scourie dykes from study locations mapped along with the main structural features affecting the region. Orange line represents the approximate line of section in the cross section (b). A more detailed geological map can be found in Figure 1.3. b) Schematic cross section of the extreme western end of the Canisp shear zone (after Attfield, 1987).*

grade for the origin of these gneisses during the Badcallian event, ca. 2.8-2.7 Ga.

At Loch Assynt, the gneissose foliations dip moderately to the NW (average 067/49 NW), with little evidence for anything other than isolated minor folding in this area. Stereonet analysis shows a spread of poles along a great circle consistent with open folding around a moderately WNW plunging ß axis (Fig. 4.2a). Moderately SW dipping gneissose foliations at Lochinver (average 097/29 SW) show some variations in strike within the field (NW-SE to ENE-WNW), with stereonet analysis appearing consistent with folding around a shallowly SW plunging beta-axis (Fig. 4.2b). The foliations and folding in both areas pre-date the emplacement of the dykes, which cross-cut the foliation at high angles. Similarly, the dykes show no evidence for folding. The locality at the southern end of Achmelvich Bay (herein referred to as Achmelvich South) preserves gneissose foliations that mainly dip moderately to the NW (average 066/43 NW), folded around NE-SW trending fold axes with the fold hinge plunging to the NE (Fig. 4.2c). Smaller scale (<50cm) folds within the gneiss also show similarly oriented fold axes (NNE-SSW), with the NE-SW trending fold limbs indicating dextral vergence within these folds. Once again, these folds pre-date the dyke. Gneissose foliations at the northern end of the beach at

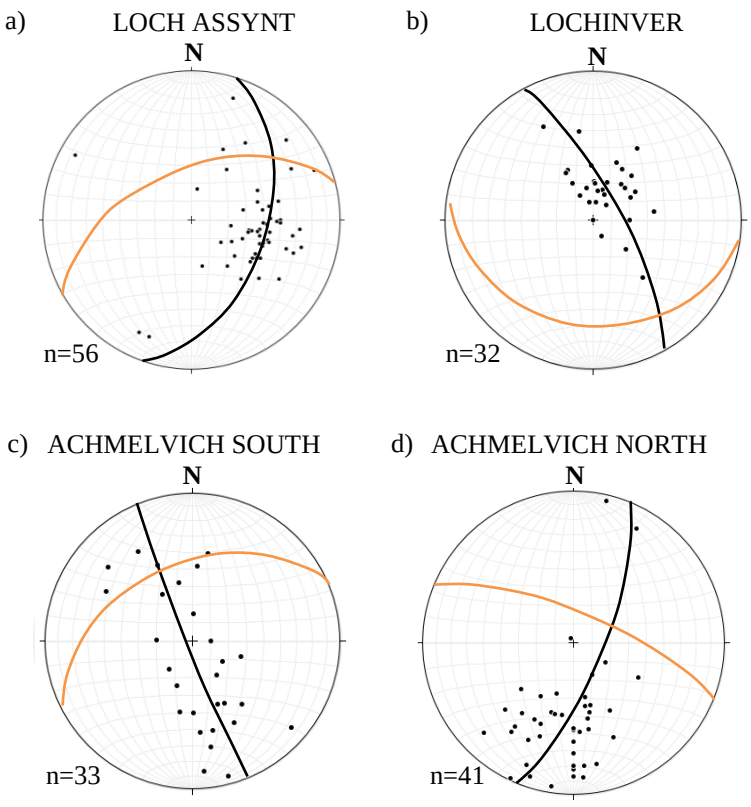

***Fig 4.2**. Poles to planes of gneissose foliations at the four main localities, orange plane; mean plane, black plane; best fit girdle a) Loch Assynt, n=56 b) Lochinver, N=32 c) Achmelvich South, n=33 d) Achmelvich North, n=41*

Achmelvich Bay (herein referred to as Achmelvich North) dip moderately to the NNE (average 083/45 NNE), with the changing strike of some foliations showing some evidence of folding (trending ESE-WNW) (Fig. 4.2d). Steep dips (~70^{o}) are preserved close to the dyke margin. The opposing dip of the foliations here compared to other localities is likely due to the proximity of the Lochinver monocline, tilting the foliation to the NNE. This folding is likely to be due to Inverian deformation (e.g. Attfield, 1987) and therefore also predates the dyke.

4.2. Original intrusive relationships

Lochinver: Sharp, little modified contacts are present at the ~25m wide dyke at Lochinver; these cross-cut the gneissose banding at variable, but often high angles (Figs. 4.3a, 4.5a-b). Here the dyke margin has a shallower dip (average 124/68 NE) than at other localities (Figs. 4.3b, 4.5a). An undeformed dilational jog along the dyke margin (Fig. 4.5b) suggests a component of top-to-the-NE extension during emplacement.

Fresh surfaces of the dyke are green-grey weathering dark green-black. Lithologically, the dyke is composed of predominately 1-2mm anhedral hornblende crystals (70-80%) with subsidiary minerals including some feldspars; little lithological variation occurs across the dyke. A 1.5cm thick chilled margin along the dyke margin shows an obvious upper boundary within the field defining the upper limit of sub-mm crystal sizes (Figs. 4.5c-d). Crystal sizes are on a sub-mm scale at the dyke margins within the chilled margin, which also preserves an orthogonal texture defined by less weathered bands (Fig. 4.5c). Figure 4.5d shows injections of dyke material into the gneiss along the contact, also exhibiting the orthogonal texture. This is possibly indicative of a spinifex-like texture along the dyke margin, indicating a large degree of undercooling during dyke emplacement (Lowrey et al., 2017). Crystal sizes increase to 1-2mm on fresh surfaces at the centre of the dyke.

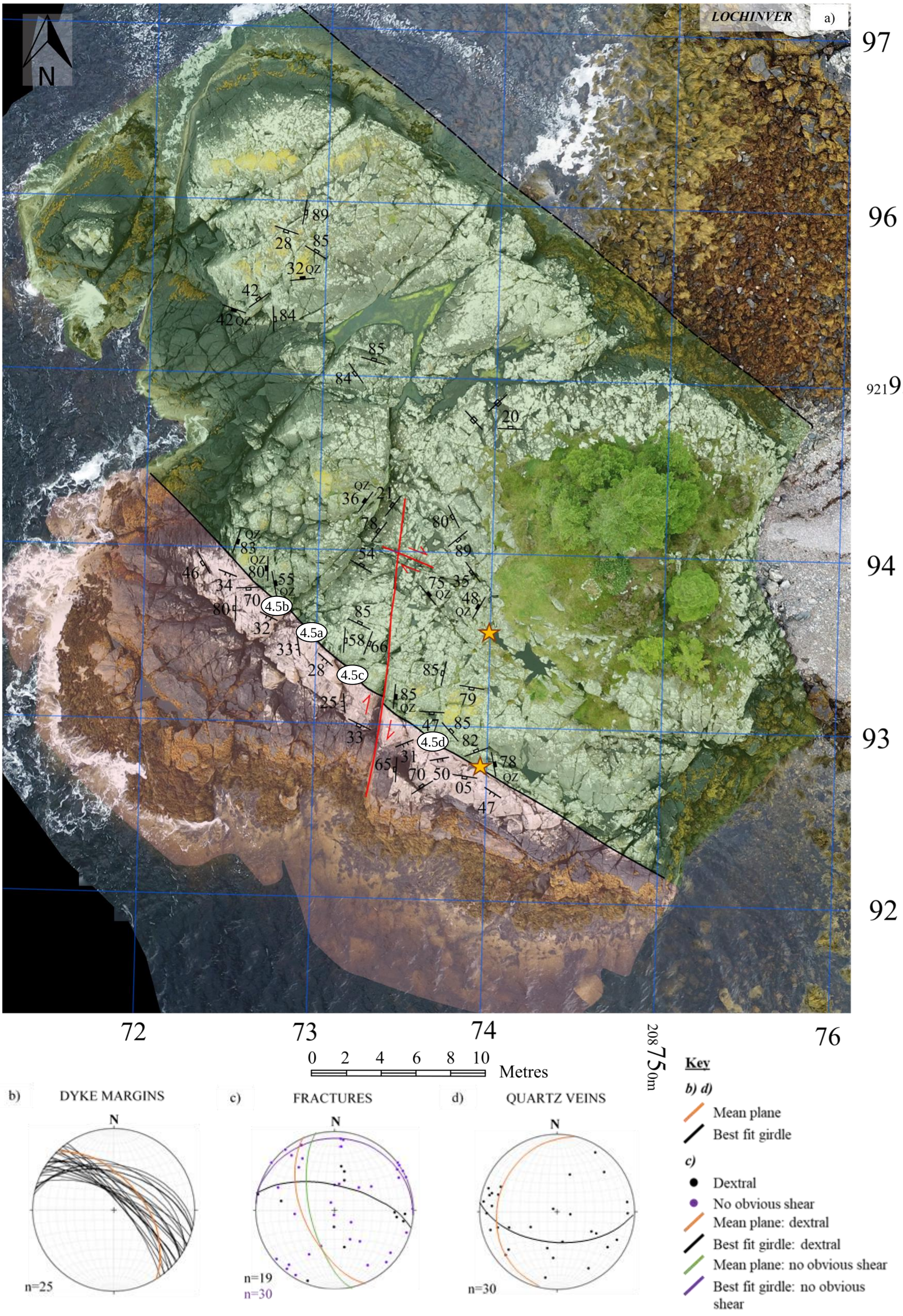

Fig 4.3. *Lochinver a) Geological map of the undeformed dyke margin, for key see Figure 4.4. Sample and photograph locations indicated. b) Stereonet of dyke margins, n=25, orange plane: mean plane c) Stereonet of poles to planes of fractures d) Stereonet of poles to planes of quartz veins.*

Key

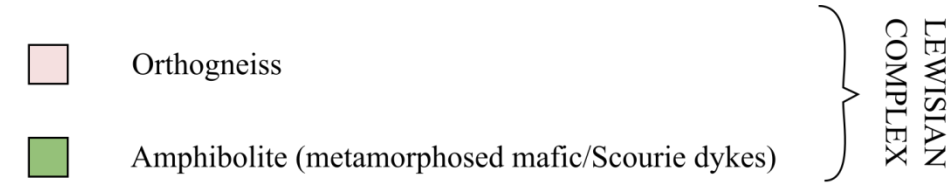


Geological boundary, known


Geological boundary, inferred


Strike Slip Fault, known - offset indicated


Strike Slip Fault, unknown - offset indicated


Normal Fault - downthrow indicated where known


Fault, unknown - unknown offset

Inclined Fracture/Joint, dip in degrees


Vertical Fracture/Joint

Inclined Foliation, dip in degrees

Vertical Foliation

Inclined Schistosity, dip in degrees

Vein, mineralisation indicated, dip in degrees, QZ, Quartz; EP, Epidote; Z, Zeolite

Vertical Vein, mineralisation indicated, QZ, Quartz; EP, Epidote; Z, Zeolite

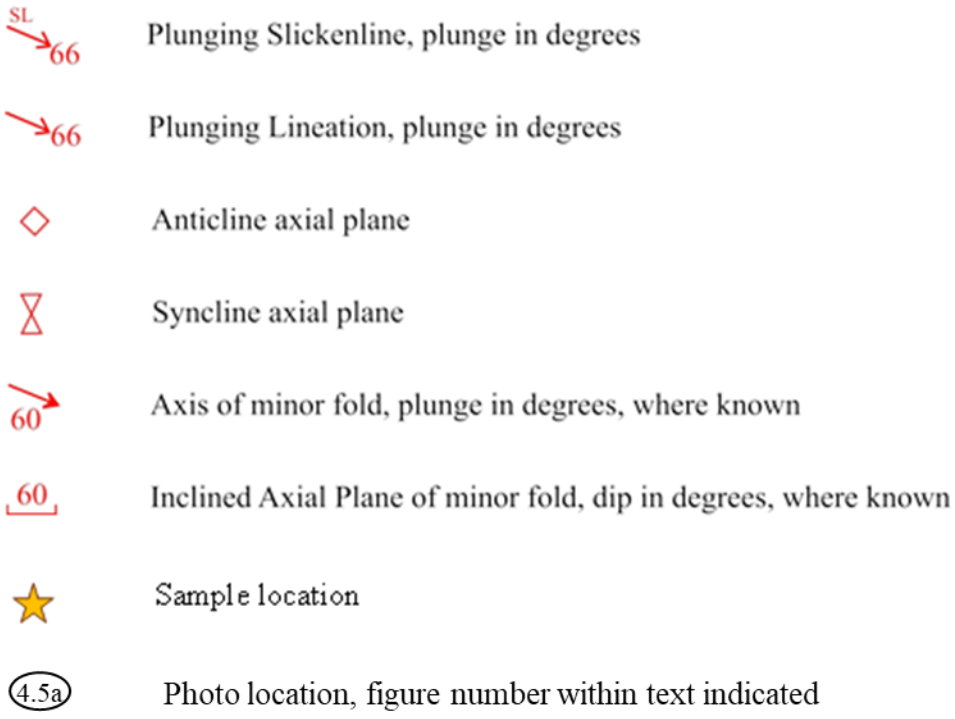

Fig 4.4. *Key for the geological maps in Figures. 4.3, 4.6, 4.8, 4.10.*

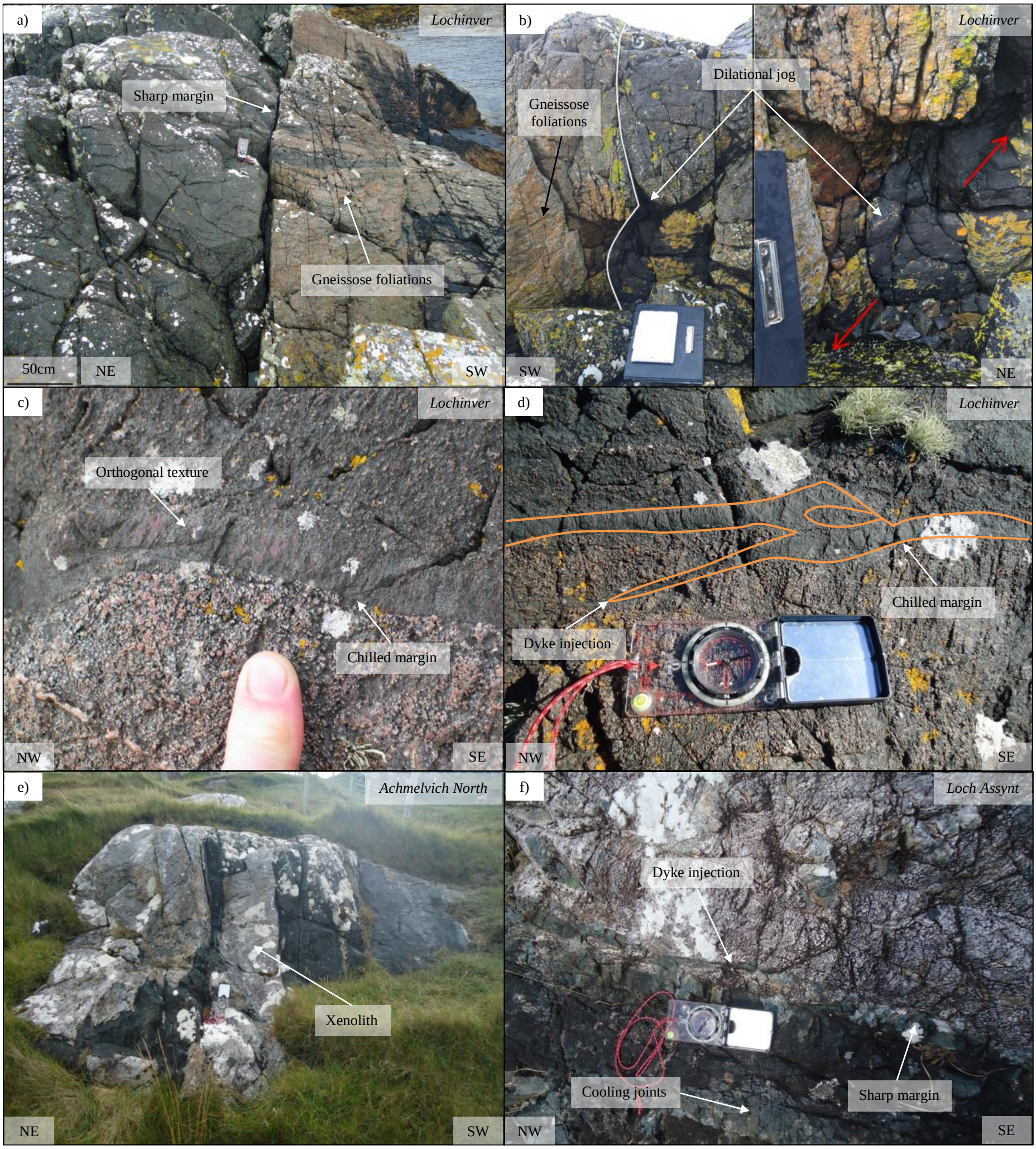

Fig 4.5. *Undeformed intrusive features a) Lochinver; dyke margin trending NW-SE, dipping to the NE, cross sectional view b) Lochinver; small syn-tectonic dextral pull apart along the dyke margin, cross sectional view, weather writer for scale c) Lochinver; spinifex-like texture in the chill margin along the dyke margin, plan view, finger for scale d) Lochinver; injections of the dyke into the gneiss, boundaries of chilled margin indicated, plan view, compass clinometer for scale d) Achmelvich North; xenoliths along the dyke margin, cross sectional view, compass clinometer for scale f)Loch Assynt; igneous textures preserved at the northern margin, plan view, compass clinometer for scale.*

Later brittle N-S and NE-SW trending small-scale faults (Fig. 4.3a) offset the dyke margin dextrally by 30cm and 6cm respectively, with no observable fault rock or mineral fills present. The larger N-S trending fault preserves two sets of lineations on the main fault plane: one plunging 62^{o} (S), and the other with a sub-horizontal plunge. Overall, most other fractures within the dyke lack a systematic arrangement in terms of orientation (Fig. 4.3c).

Achmelvich and Assynt: Some original igneous features are also preserved at Achmelvich North, as xenoliths of the gneiss (maximum 170cm long, 40cm wide) seen close to the northern dyke margin (Fig. 4.5e). A lack of deformation at some outcrops at Loch Assynt has resulted in the conservation of igneous textures: small injections of the dyke into the gneiss, baked gneiss at the dyke margin and systematic N-S trending jointing only present at the dyke margin, interpreted as cooling joints within the dyke (Fig. 4.5f). In other locations, the original intrusive dyke margins are to varying degrees overprinted by the effects of later ductile overprinting (e.g. Achmelvich North and South) and/or brittle faulting (e.g. Loch Assynt, Achmelvich South) which follow the pre-existing dyke margins.

4.3. Early quartz veins

Quartz veins at Loch Assynt range from a few millimetres to ≤50cm in width, and are commonly traceable for several metres along strike in the case of the larger veins. These are common, particularly within the gneiss, trending NE-SW, perpendicular to the dyke margins (see Vernon et al (2014) for Assynt quartz vein characteristics). The smaller dyke by the Loch is cross-cut by a NE-SW trending shear ~5cm wide, with a sharp lower boundary (Appendix Fig. 1.1a-b). This is associated with NNE-SSW trending dilational jogs of quartz mineralisation, the orientation of which indicate sinistral transtension during shearing. The shear is also associated with hematite staining. This is in a similar orientation to the ca. 2 Ga quartz veins, with Vernon et al (2014) noting some of the offset

markers in the adjacent wall rock to these veins provides evidence for sinistral offset during vein emplacement. This is in addition to some en-echelon off-shoots, indicating that the brittle NE-SW shear within the smaller dyke could be related to these quartz veins.

1-2mm wide quartz veins are sparsely distributed across the outcrop at Lochinver (<1m in length), mainly trending NNE-SSW within the dyke (Fig. 4.3d). This orientation is consistent with the orientation of the ca. 2 Ga quartz veins found a Loch Assynt (Vernon et al., 2014).

4.4. Ductile post-dyke deformation

Achmelvich North: The 15-23m wide dyke at Achmelvich North (Fig. 4.6a) preserves steeply dipping dyke margins (average 120/77 SW, Fig 4.6b), with evidence for the local development of schistose viscous mylonites either side of the pre-existing intrusive contacts (Fig. 4.6c). Biotite-muscovite schist (derived from the quartzo-feldspathic gneissic protolith) and hornblende schist (derived from the doleritic dyke protolith) are found along the contact, reaching up to 1.10m in width in the biotite-muscovite schist at the northern margin. However on average, the width of the schistose region is 11cm and 15cm within the gneiss and dyke respectively at both northern and southern dyke margins. S-C banding and asymmetric wrapping of lower strain pods in the mylonites give consistent dextral shear senses (Fig. 4.7). This fabric has reworked most of the original igneous features, such as chilled margins, at the contact. It is also associated with later foliation-parallel quartz mineralisation along the contact (Figs. 4.6d, 4.7a, Appendix Fig. 1.2a), which is sheared into parallelism with the schistose fabric in localised areas (<30cm in length) of the dyke margin. This implies a syn-tectonic origin of the quartz mineralisation along the dyke margins. Quartz is also present here in the form of veins (<5mm), mainly located around the dyke margin or within the centre of the dyke. The majority of these are parallel to the NW-SE trending dyke margin (Fig. 4.6d), with some oriented NNW-SSE; a clockwise rotation from the margin. Pre-existing compositional

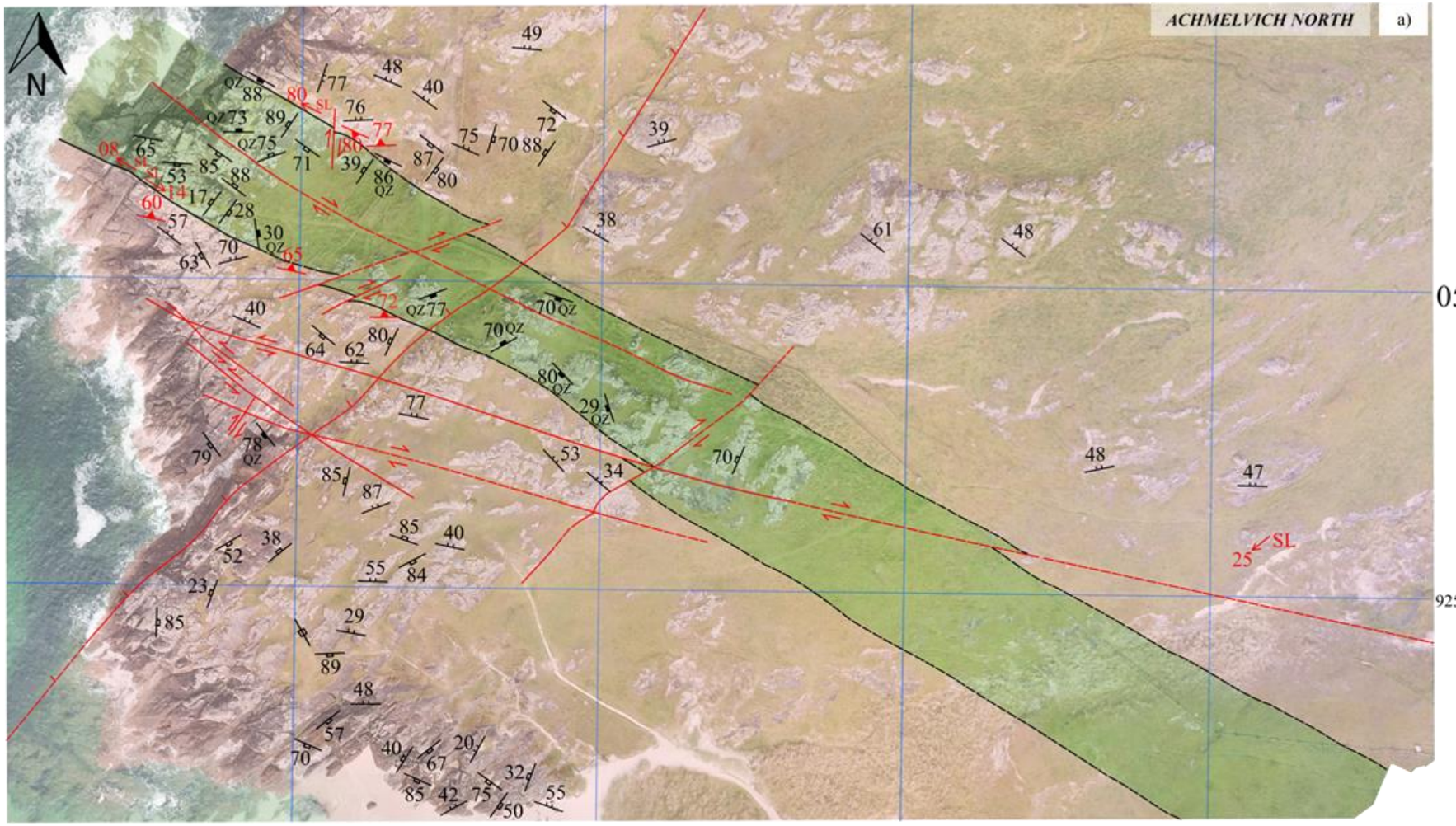

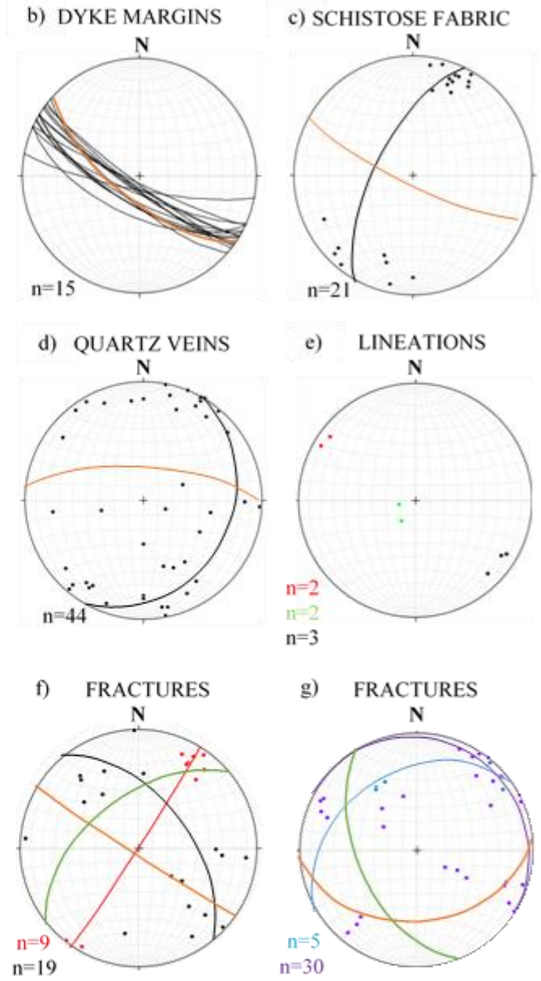

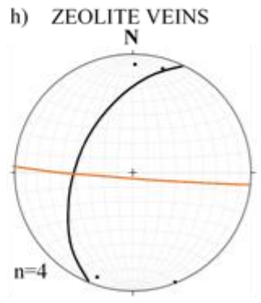

Key

b)
- Mean plane

c) d) h)
- Mean plane
- Best fit girdle

e)
- Dextral oblique shearing
- Sinistral oblique shearing
- Dip-slip, some dextral component

f)
- Dextral
- Sinistral
- Mean plane: sinistral
- Best fit girdle: sinistral
- Mean plane: dextral
- Best fit girdle: dextral

g)
- Tensile
- No obvious shear
- Mean plane: tensile
- Best fit girdle: tensile
- Mean plane: no obvious shear
- Best fit girdle: no obvious shear

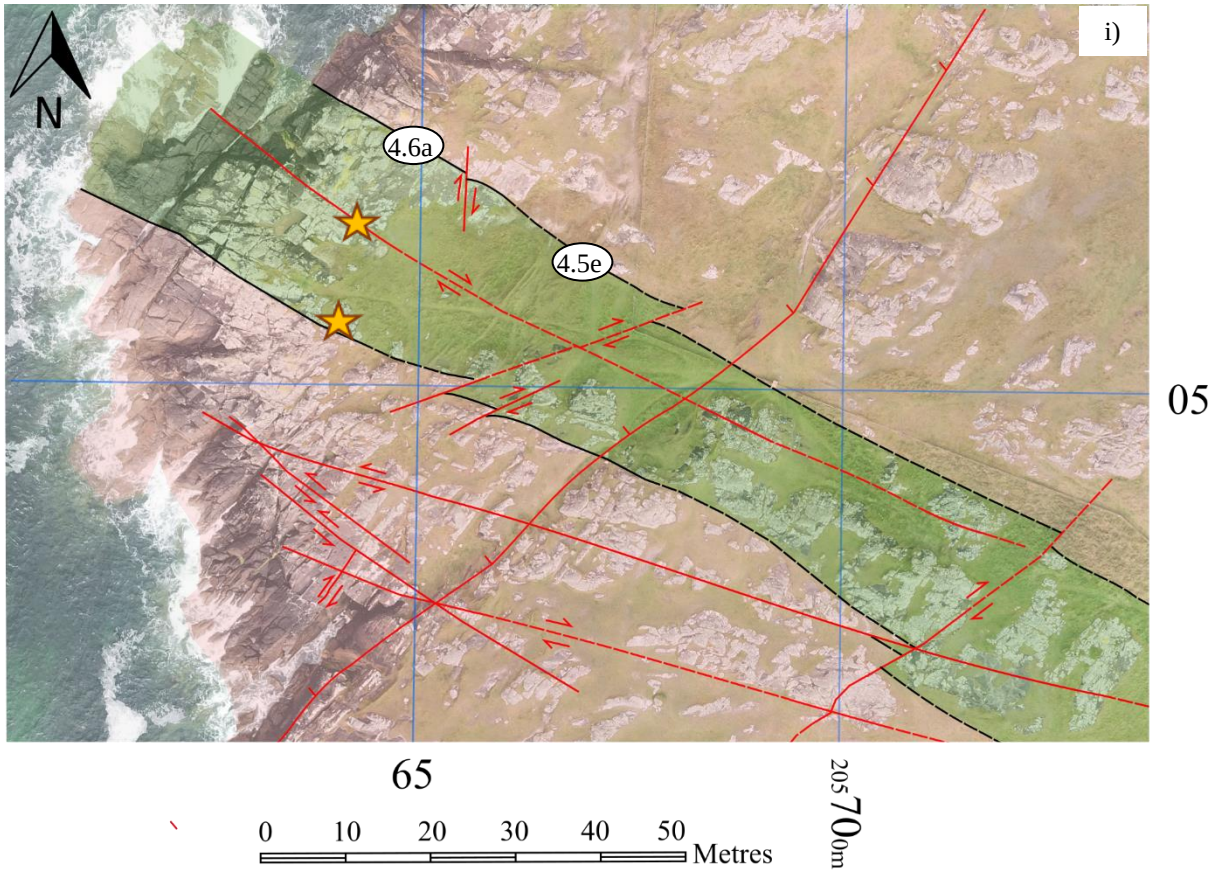

Fig 4.6. *Achmelvich North a) Geological map of the dyke at Achmelvich North and surrounding features, for key see Fig. 4.4 b) Stereonet of dyke margins c) Stereonet of poles to planes of schistose fabric at the dyke margins d) Stereonet of poles to planes of quartz veins e) Lineation data from NW-SE trending (faulted) dyke margins f-g) Stereonet of poles to planes of fractures h) Stereonet of poles to planes of zeolite veins i) Map indicating sample and photograph locations in relation to the geology.*

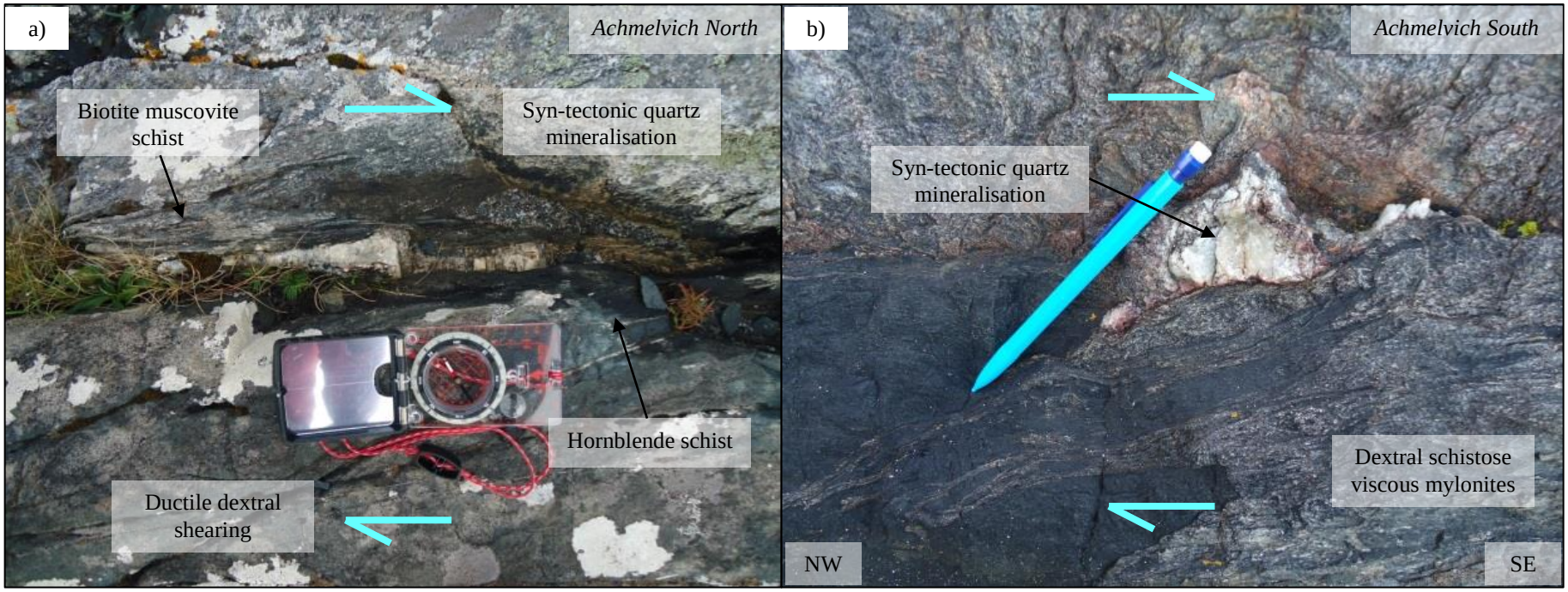

Fig 4.7. *Quartz mineralisation and schistose fabric along the dyke margins at Achmelvich, both plan view a) Syn-tectonic quartz mineralisation along with the schistose fabric at Achmelvich North b) Syn-tectonic quartz mineralisation and schistose fabric along the southern dyke margin of Achmelvich South.*

foliations in the quartzo-feldspathic gneisses are also rotated (~15º clockwise) approaching the contact (see foliation measurements on map at northern margin, Fig. 4.6a), indicative of drag during dextral shearing along the dyke margins.

Within the field, steeply plunging lineations are found on the dyke margins at Achmelvich North average 86→306 (Fig. 4.6e). Slickenline identification criteria such as feeling for the 'smooth side' (fault movement direction) vs 'rough side of the lineation has been used to identify these lineations as slickenlines in accordance with the 'smoothness-roughness hand' technique of Billings (1942) (discussed by Doblas, 1998). These are dip-slip with small dextral component. Shallowly plunging ESE lineations (average 14→120) are present along both the northern and southern dyke margins, overprinting the aforementioned steeply plunging lineations. These were identified as slickenlines associated with dextral shearing (Fig. 4.6e). The structural evidence presented indicates dextral strike slip transtension and viscous shearing during this event; this is the same age as the CSZ, with which is it collinear and coplanar (Beacom et al., 2001; Beacom, 1999).

A shear zone cuts through the centre of the dyke sub-parallel to the dyke margins, sharply offsetting a pair of cross-cutting quartz veins by ~8cm dextrally along the main fault plane. At the coast, the shear zone is narrow (~1cm wide), compared to further inland where it widens to 50-100cm and is defined by a strong mineral stretching lineation within the rock (60→272). Mafic pods (3-5mm) within the gneiss to the south of the southern dyke margin (e.g. NC 05636 25043) preserve obvious asymmetric strain shadows, which are ≤50cm in length to the left of the pod. These other brittle-ductile dextral shears are evidence that the ductile shearing was not purely restricted to the dyke margins at this locality.

Achmelvich South: Two dykes, 5m wide, are present at Achmelvich South, segmented with a staggered arrangement and no evidence for any tectonic offset along the adjoining tips (see map, Fig. 4.8a). This arrangement suggests an en-echelon style of dyke emplacement.

Dyke margins here are steeper than those at Achmelvich North (average 111/85 NE, Fig. 4.8b). Pre-existing folds with shallowly dipping axes (section 4.1) are dextrally offset across the dyke margins, however the offset should not be taken as a typical offset during Laxfordian shearing, as the dyke margins have also been affected by later shearing (section 4.5). The southern dyke margin preserves schistose mylonites (<20cm) with dextral S-C banding, as at Achmelvich North (Figs. 4.7b, 4.8c). This behaviour locally extends to the centre of the dyke, with dyke material showing dextral S-C banding on both metre and centimetre scales, but lacking a pervasive schistose foliation. Some relict schistose material ~20cm in length and 5cm in width is present at the northern margin, but otherwise appears to have been overprinted by the effects of later brittle shearing (see section 4.5). Similar style quartz mineralisation to Achmelvich North is seen along the dyke margins (Figs. 4.7b, 4.8d Appendix Fig. 1.2b); this implies that localised syn-tectonic quartz mineralisation was widespread around Achmelvich Bay and that it was directly associated with, and possibly controlled by, the development of ductile dextral shear zones . ~1mm wide quartz veins were frequent at the dyke margins, and more sporadic within the dyke, occasionally appearing within the gneiss. Quartz veins have an average orientation of 131/64 NE (Fig. 4.8d), which is a clockwise rotation from the dyke margin; there were fewer contact parallel veins here than at Achmelvich North. This would once again indicate a dextral shear sense in order to facilitate the vein formation in oblique tensile fractures.

The faulted dyke margin preserves a set of steeply plunging lineations (average 82→146) with downward throw to the north associated with tensile fractures, and an overprinting shallowly ESE plunging lineation (average 116→16) (Figs. 4.8e, 4.9). Steps sub-perpendicular to the lineations were used to identify these as slickenlines (Doblas, 1998). These indicate dip slip movement, followed by dominantly dextral strike-slip movement, also with downward throw to the north; this is similar to Achmelvich North.

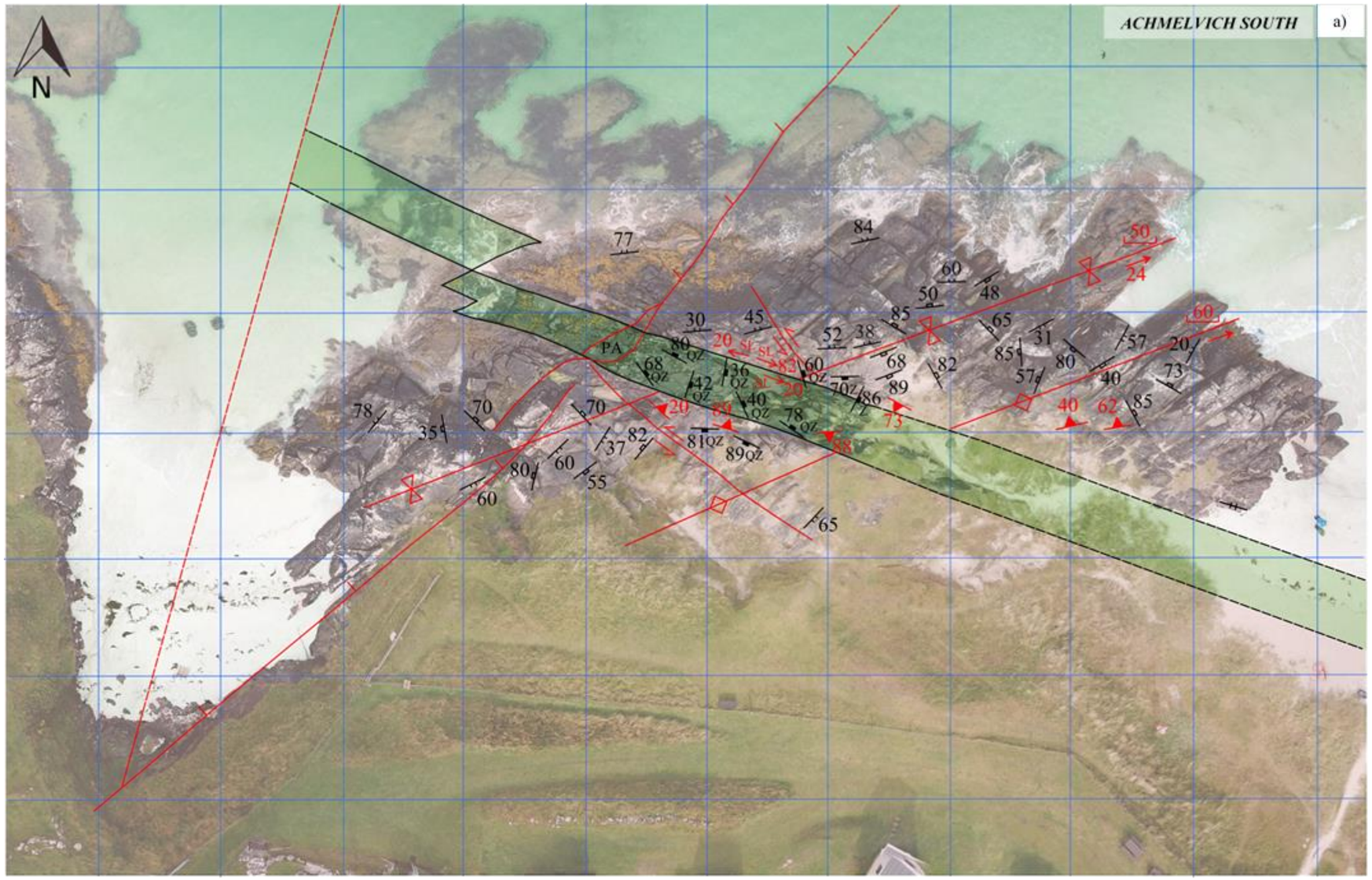

b) DYKE MARGINS
N
n=24

c) SCHISTOSE FABRIC
N
n=17

d) QUARTZ VEINS
N
n=29

e) LINEATIONS
N
n=12
n=10
n=18

f) FRACTURES
N
n=17
n=5

g) FRACTURES
N
n=7
n=41

h) ZEOLITE VEINS
N
n=38

Key

b)
- Mean plane

c) d) h)
- Mean plane
- Best fit girdle

e)
- Dextral oblique shearing
- Sinistral oblique shearing
- Dip-slip, some dextral component

f)
- Dextral
- Sinistral
- Mean plane: sinistral
- Best fit girdle: sinistral
- Mean plane: dextral
- Best fit girdle: dextral

g)
- Tensile
- No obvious shear
- Mean plane: tensile
- Best fit girdle: tensile
- Mean plane: no obvious shear
- Best fit girdle: no obvious shear

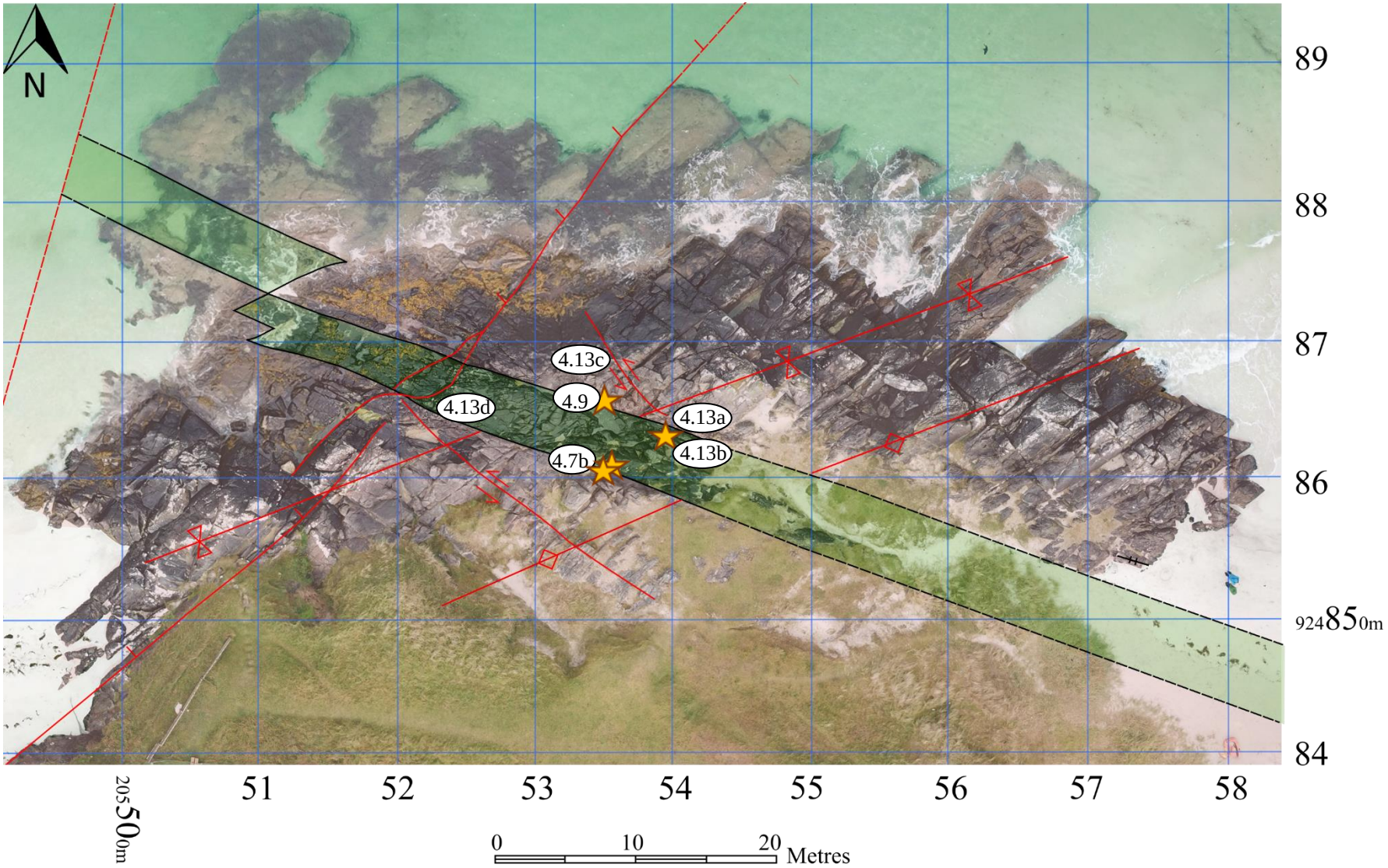

Fig 4.8. *Achmelvich South, a) Geological map of the dyke at Achmelvich South and surrounding features, PA; Pull apart, for key see Figure 4.4 b) Stereonet of dyke margins c) Stereonet of poles to planes of schistose foliations d) Stereonet of poles to planes of quartz veins, e) Lineation data from NW-SE trending (faulted) dyke margins f-g) Stereonet of poles to planes of fractures h) Stereonet of poles to planes of zeolite veins i) Map indicating sample and photograph locations in relation to the geology.*

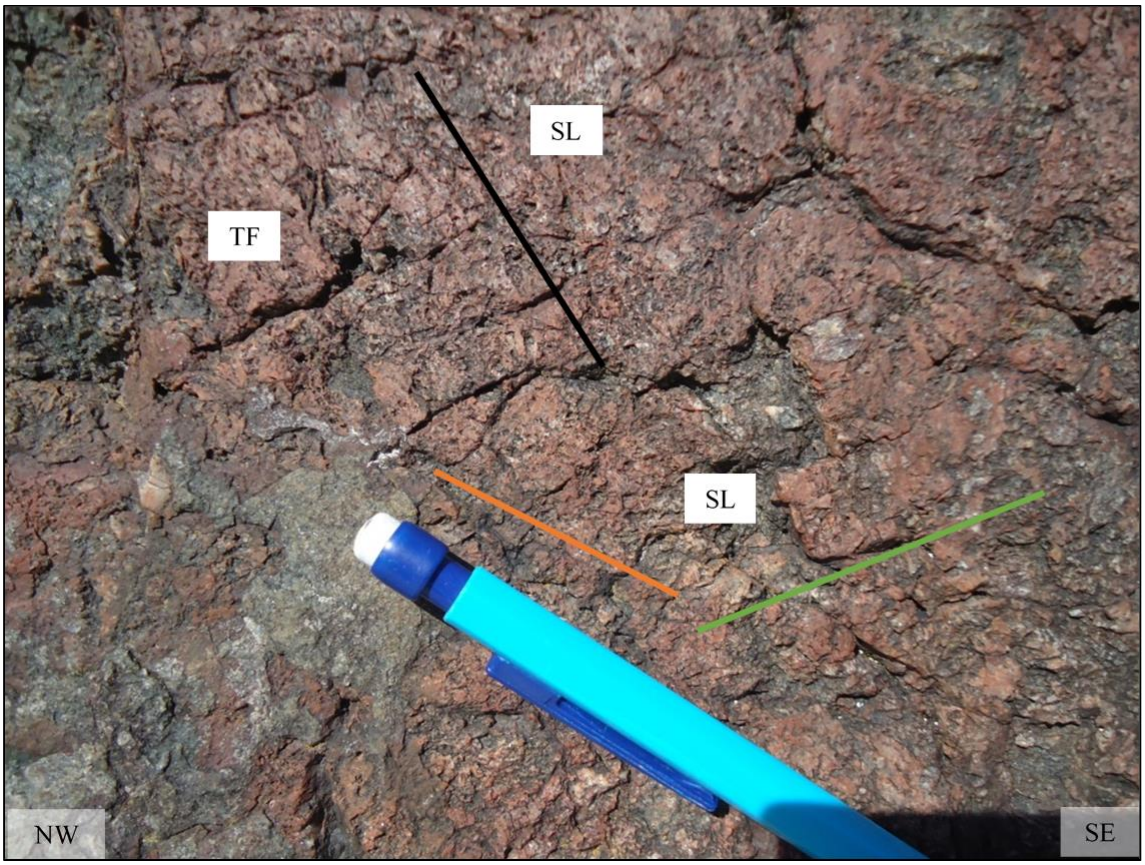

Fig 4.9. *Field photograph of lineations on the faulted northern dyke margin, cross section view. TF: tensile fracture; SL: slickenline; black; dip-slip with some dextral component; orange: dextral strike-slip; green: sinistral strike slip. Pencil for scale.*

The dextral viscous shearing event described cross cuts pre-existing Badcallian and Inverian structures, affecting both the dyke margins and the gneiss. It also post-dates the ca. 2 Ga quartz veins described and dated by Vernon et al. (2014), however, as the schistose viscous fabric is not preserved at Loch Assynt, there is no clear field evidence for relative age relationships at this locality. Post-dating the quartz veins would place the viscous shearing as being younger than 2 Ga, most likely related to the Laxfordian shearing recognised in the central part of the CSZ according to the literature (e.g. Attfield, 1987). Laxfordian fabrics within the CSZ affect the Scourie dykes, both inside and outside of the shear zone, with characteristic deformation including discrete shear zones accommodating strain within anastomosing networks within the dykes and at their margins. Findings by Attfield (1987) of a strong lineation plunging 10-30^{o} ESE, indicating a predominantly dextral strike slip regime, are in agreement with this study.

4.5. Brittle 'Late Laxfordian' structures

Loch Assynt: Loch Assynt preserves brittle, steeply dipping dyke margins (average 115/83 NNE) (Fig. 4.10a-b), sharply cross cutting the pre-existing gneissose foliation at high angles (Fig. 4.5f). Exposure is limited to three good sized (100% exposure) outcrops locally inland at various points along the dyke margins (e.g. NC 20950 25253, NC 21045 25192, and NC 21152 25183), and one by the loch shore (NC 21489 25025). The larger dyke is 40-45m in width, whereas the smaller dyke, which is only exposed by the loch shore (NC 22128 92505), is narrower at 10m; both are cut by early quartz mineralisation (Fig. 4.10c, see section 4.3). Brittle shears are present at the dyke margin and within the gneiss; at the best exposure of these at NC 21405 25050, these comprise a main shear plane, e.g. 119/81 SW (dyke margin parallel), and two main subsidiary shears; e.g. 095/80 W, 042/88 SW, the former at an angle of 24^{o} anticlockwise, and the latter at 77^{o} anticlockwise from the main shear plane. These appear to be Riedel shears (M, R and R' respectively), arranged in a sinistral arrangement (e.g. Fig. 4.11a), however no obvious associated slickenlines were observable within the field. Across the locality, dominantly NW-SE trending fractures with some sinistral offsets on a centimetre scale, and associated tensile fractures are present, with some dextral R' fractures additional to this (Fig. 4.10d-e). At most dyke margin outcrops, further evidence of reactivation is preserved in the form of 1-5cm thick bands of dark foliated fault rock. Intense grain size reduction has occurred within the gneiss (NC 21045 25192) and dyke (NC 21489 25025) at the dyke margin, and is associated with S-C banding indicative of sinistral shear (Fig. 4.11b-c). This sinistral ultramylonite is sometimes associated with narrow (<1mm) bands of dark brown/red, hard, fault rock interpreted in the field to be potential pseudotachylytes (see microstructures section 5.7.2 for further evidence). Ultramylonites along the dyke margin are also frequently associated with quartz-epidote mineralisation (≤1mm crystals) (Fig. 4.10f). Veins are commonly ~1mm wide, and traceable for ≤1m (e.g. NC 21105 25226) and commonly strike parallel to the dyke contacts (Fig. 4.10d, Fig. 4.11c insert). Slickenfibres

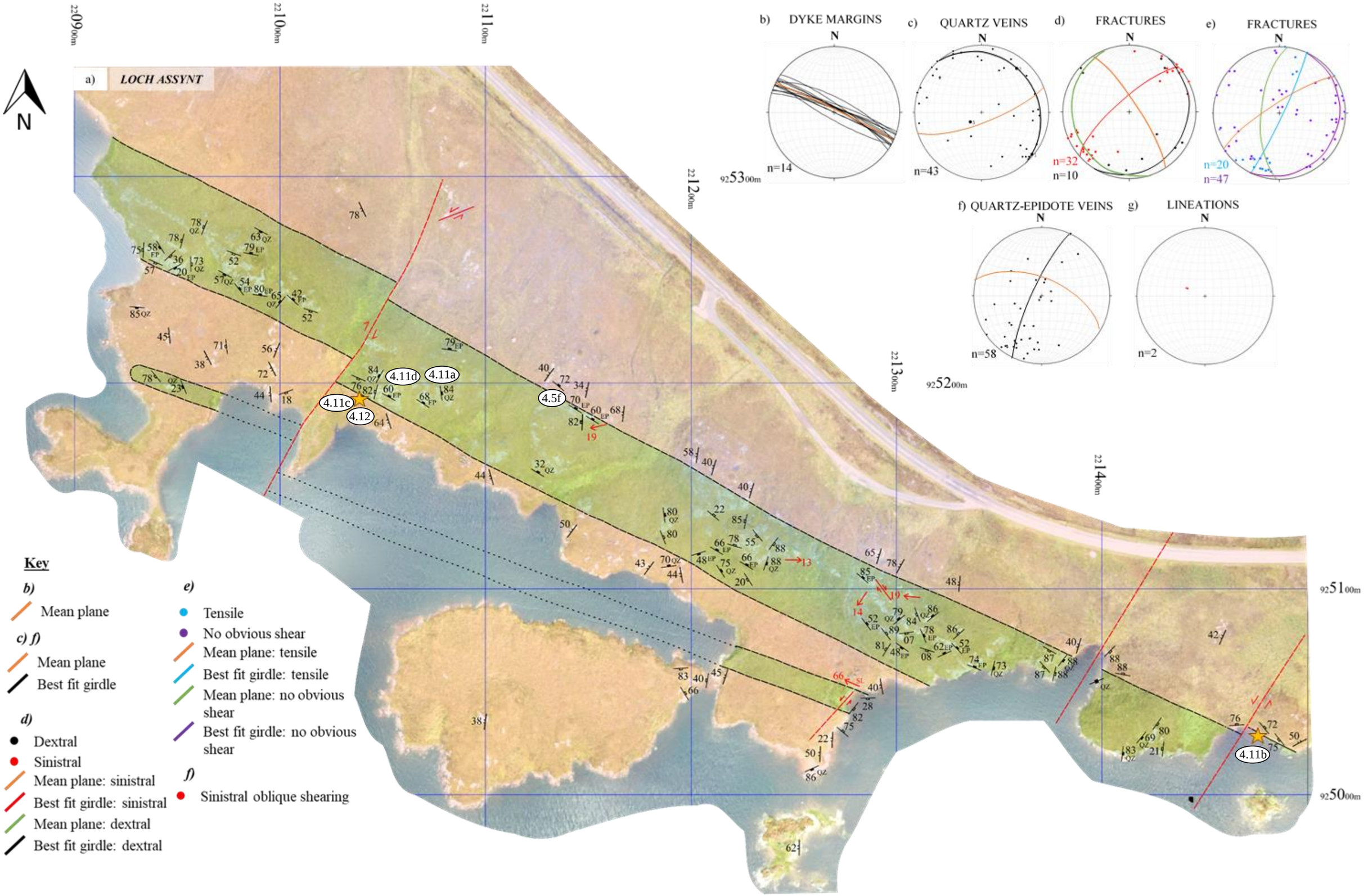
a) LOCH ASSYNT
N
b) DYKE MARGINS
c) QUARTZ VEINS
d) FRACTURES
e) FRACTURES
f) QUARTZ-EPIDOTE VEINS
g) LINEATIONS
n=14
n=43
n=32
n=10
n=20
n=47
n=58
n=2
4.11a
4.11b
4.11c
4.11d
4.12
4.5f
Key
b) Mean plane
c) f) Mean plane
Best fit girdle
d) Dextral
Sinistral
Mean plane: sinistral
Best fit girdle: sinistral
Mean plane: dextral
Best fit girdle: dextral
e) Tensile
No obvious shear
Mean plane: tensile
Best fit girdle: tensile
Mean plane: no obvious shear
Best fit girdle: no obvious shear
f) Sinistral oblique shearing
0 20 40 60 80 100
Metres

Fig 4.10. *(above) Loch Assynt a) Geological map of the dyke and surrounding features, for key see Figure 4.4. Sample and photograph locations indicated b) Stereonet of dyke margins c) Stereonet of poles to planes of quartz veins d-e) Stereonet of poles to planes of fractures, f) Stereonet of poles to planes of quartz-epidote veins g) Lineation data from NW-SE trending (faulted) dyke margins.*

are associated with the quartz-epidote mineralization; the hand specimen (field locality NC 21045 25192) contains evidence of polished slickensides with two sets of slickenlines plunging at 66^{o} and 50^{o}. Epidote slickenfibres are visible on the slickenside surface Fig. 4.12), with the steps indicative of sinistral shear (see Fig. 13.9, Fossen, 2010, p. 264). This indicates epidote mineralization was syn-tectonic. Quartz-epidote veins across the locality are more common within the dyke compared to the gneiss, cross cutting examples of the earlier ca. 2 Ga quartz veins. The quartz-epidote veins show strikes that are rotated anticlockwise from the strike of the dyke margin, and are also found in dilational jogs that locally rotate the vein anticlockwise (Fig. 4.11d). This indicates sinistral shear during the vein emplacement, and as the dyke margins show abundant contact parallel veins, this suggests that fluid influx occurred during sinistral reactivation of the dyke margins. Epidote was also present at the smaller dyke by the Loch, in a 1cm wide, 40cm long epidote vein within the dyke at an angle of 70^{o} clockwise to, and terminating at, the central shear perpendicular to the dyke margin. The epidote was fibrous, with the fibres oriented perpendicular to the vein margins (Appendix Fig. 1.1c). Two sets of moderately plunging lineations were found on the northern margin of the smaller dyke at the loch shore (NC 25050 21280), and associated with epidote mineralization (NC 21045 25192) (Figs. 4.10g, 4.12). These were identified as slickenlines (66→311, and 50→314) with sinistral kinematic indicators (Billings, 1942; Doblas, 1998).

Cross cutting the dykes are large-scale ~NE-SW trending faults, offsetting the dyke margin by <20m; the fault planes were not seen directly, but were inferred from displacement of the dyke margins. Of the three main faults, one shows dextral offset of the dyke margins, one is unknown (fault extends from the road section), and the third is sinistral. The second fault in particular cutting through the younger Torridonian sequences implies that some (if

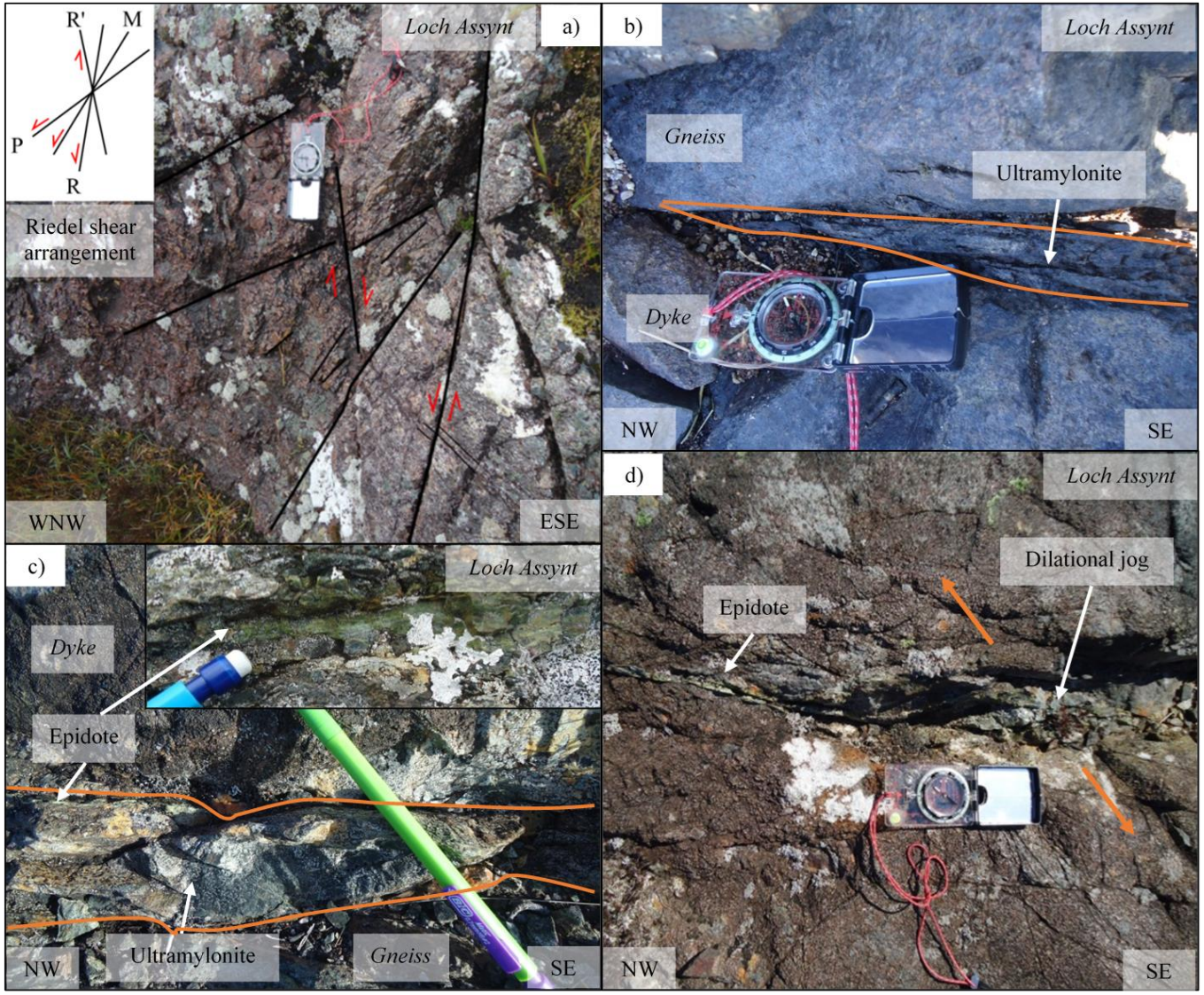

Fig 4.11. *– Field photographs of features associated with sinistral shearing at Scourie dyke margins and within the surrounding Lewisian gneiss at Loch Assynt, all plan view a) Sinistral riedel shears within the gneiss, compass clinometer for scale, shear directions indicated b) Ultramylonite at the southern dyke margin, outlined, some thin pseudotachylytes seen here in the field, compass clinometer for scale c) Ultramylonite associated with epidote at the dyke margin, outlined, inset: epidote smeared parallel to the contact, pencil for scale d) Sinistral dilational jog in a quartz epidote vein in the centre of the dyke, compass clinometer for scale, opening direction indicated.*

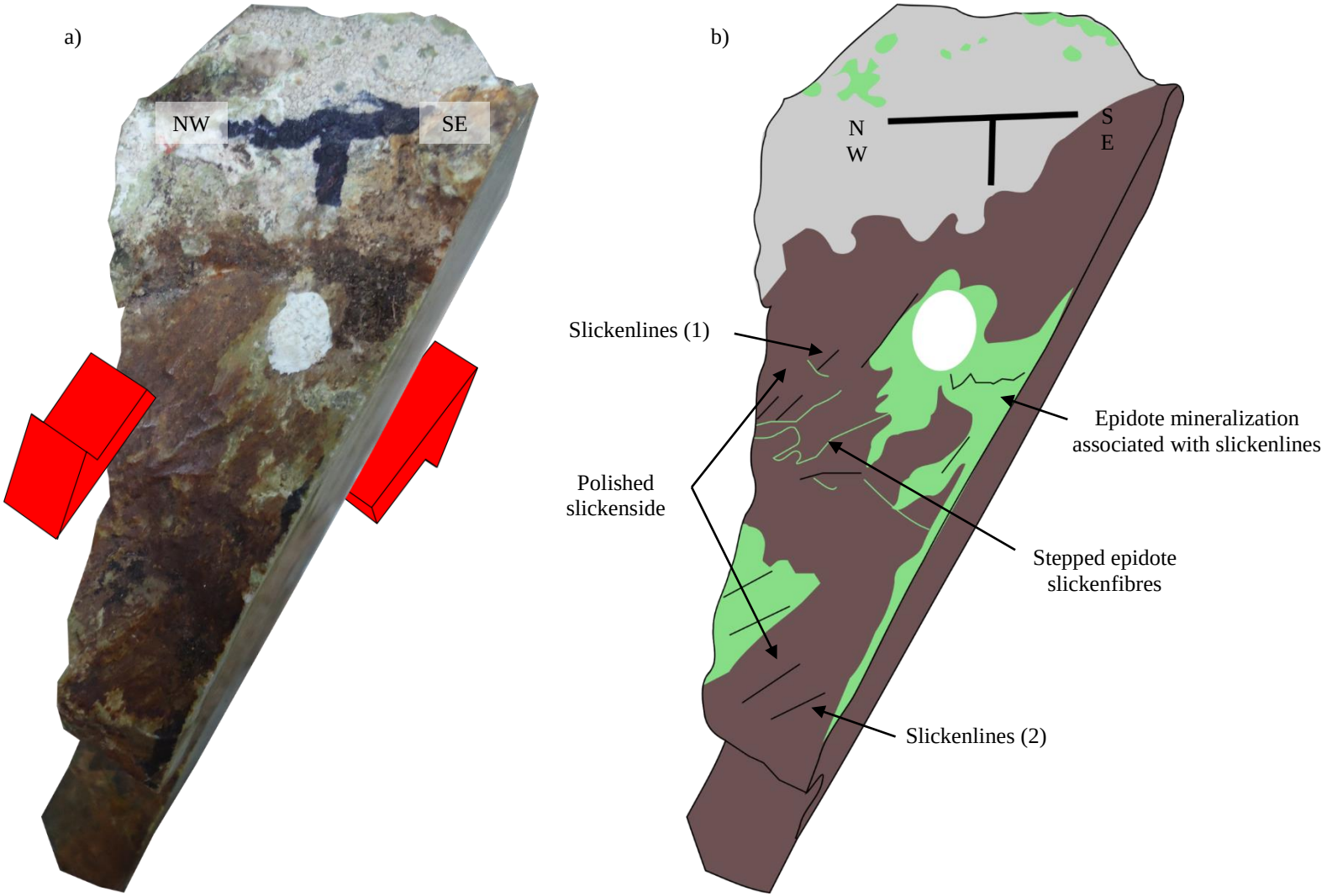

Fig 4.12. *Oriented hand specimen from Loch Assynt (NC 21045 25192), sample dips at 70º into the page. Slickensides with slickenlines and epidote slickenfibres associated with the dyke margin at this locality a) Hand specimen photograph, shear sense indicated b) Annotated line drawing.*

not all) of these faults are much younger than the dyke margin reactivations in this area, likely associated with the Mesozoic dextral normal faults cross cutting the Torridonian and Lewisian (R.E. Holdsworth, 2018 personal communication).

A small island to the south of the Loch shore where the smaller dyke outcrops is herein referred to as 'Copper Island' (NC 21255 24980). Copper mineralisation and associated sulphides are found here along steep fracture sets cutting the gneisses (data here collected by R.E Holdsworth and E. Dempsey). NW-SE fractures show left lateral offset markers, including of the ca. 2 Ga quartz veins, and are also associated with shallowly plunging slickenlines and WNW-ESE en-echelon tensile fractures consistent with sinistral shear (Appendix Fig. 1.3a-b). These tensile fractures contain infills of quartz-epidote-chlorite, very similar to that seen widely at the dyke margins (Appendix Fig. 1.3c-d). Subordinate E-W shears give right lateral offsets of markers with associated NW-SE en-echelon quartz-epidote filled tensile fractures and shallowly plunging slickenlines consistent with dextral shearing. The copper mineralization is hosted in one of these dextral E-W shears, but since they are seen to form demonstrable conjugate sets with the NW-SE sinistral fractures (Appendix Fig. 1.3d-e), it is thought that all of the steep fractures are the same age and that they are related to the sinistral ‘Late Laxfordian’ Loch Assynt fault which lies in the centre of Loch Assynt a few tens of metres to the SW (Krabbendam and Leslie, 2010; Vernon et al., 2014). An as yet unpublished Re-Os age of ca. 1.55 Ga has been obtained for this copper mineralization (R.E. Holdsworth, 2018 personal communication) and this is thought to date the age of the ‘Late Laxfordian’ sinistral shearing along NW-SE (and subordinate conjugate E-W dextral) faults in the region.

The Loch Assynt fault can be traced along strike northewestwards to the coast near Clashnessie Bay (NC 06783 31686), and along the track to Lagg Fishery (e.g. NC 16350 30700), however this does not cross-cut the Stoer Group across the bay (Fig. 1.3). Gneissose foliations at the coast either side of the fault are moderately dipping, and in the

opposite direction to those at Loch Assynt itself (average 000/61 E). There is a ~10m wide region of 1-2m angular blocks of gneiss running parallel to the cliff face, showing irregular foliation orientations compared to the cliff faces on either side of the tidal inlet at this locality. This large-scale fault breccia shows abundant chlorite mineralization with occasional pyrites, both at this locality and along the Lagg Fishery track (Appendix Fig. 1.4), especially on NW-SE trending, fault-parallel fracture surfaces, sometimes associated with shallowly plunging (05→169) or horizontal slickenline lineations. Quartz-epidote mineralisation is also present in association with the chlorite, with veins trending WNW-ESE (Appendix Fig. 1.4a). This orientation is reminiscent of the sinistral tensile quartz-epidote veins on 'Copper Island' thought to be associated with the inland section of the Loch Assynt fault.

Achmelvich South: The northern dyke margin at Achmelvich South preserves widespread evidence of brittle behaviour; this overprints the schistose Laxfordian fabric (section 4.4), which is only sparsely preserved at this margin, compared to the southern margin and at Achmelvich North. Two main fracture sets dominate the locality (obvious from the map, Fig. 4.8a); NW-SE and NE-SW trending. Fractures displaying sinistral offsets of gneissose foliations on a centimetre scale are generally associated with the NW-SE trending fracture set (Fig. 4.8e-f). On a smaller scale, tensile fractures within the gneiss at the SE end of the northern margin trend NE-SW (e.g. 069/89 NE), but do not cut across the faulted dyke margin (Fig. 4.13a). 1-2.5cm bands of dark brown/red aphanitic fault rock lines the northern dyke margin (Fig. 4.13b) which, upon close inspection, contains ~1mm clasts of wall rock. There are en-echelon off-shoots of the fault rock into the gneiss 0.5-1cm wide, traceable for up to several metres from the dyke margin and trending ~ENE-WSW compared to the NW-SE trending dyke margins. These are interpreted as pseudotachylytes and their off-shooting tensile injection veins. Some of the injection veins show brecciation; angular clasts <2cm of pseudotachylyte and gneiss are contained within

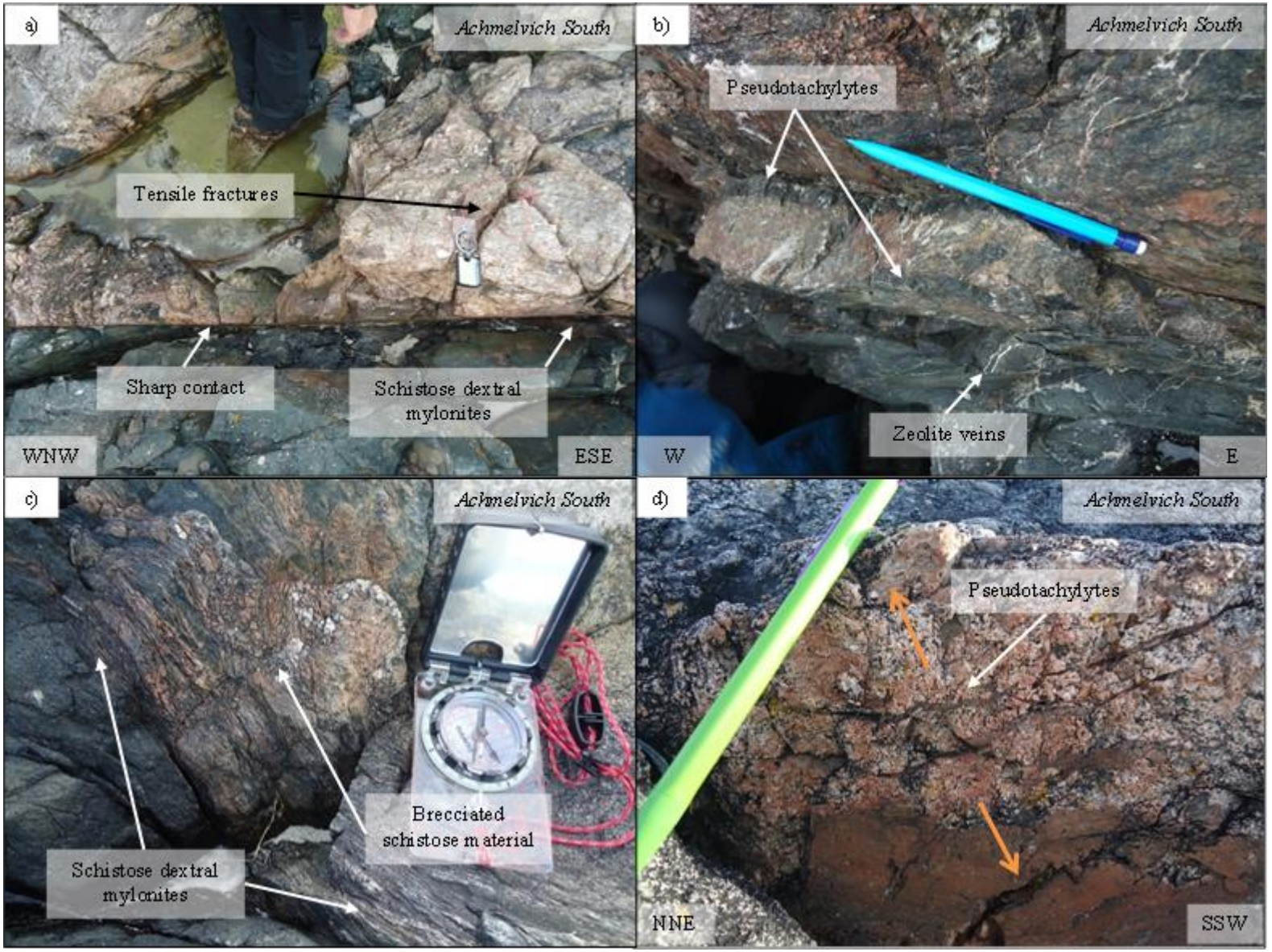

Fig 4.13. *Field photographs of 'Late Laxfordian' features at Achmelvich South, a-c plan view, d cross sectional view a) Tensile fractures within the gneiss along the northern dyke margin, compass clinometer for scale b) Pseudotachylytes and overprinting zeolites at the northern dyke margin, pencil for scale d) Breccia along the southern dyke margin, compass clinometer for scale c) Dilational jogs of pseudotachylyte, opening direction indicated, pencil for scale.*

a pseudotachylyte matrix. Cross cutting the pseudotachylytes are pale coloured veins with a low Mohs hardness and a milky lustre (Fig. 4.13b) which in thin section were found to be zeolite veins. These mostly trend ENE-WSW and lie anticlockwise of the NW-SE trending dyke margins (Fig. 4.8g). Zeolite is also present in a NE-SW trending pull apart in the centre of the dyke (indicated by 'PA' in Figure 4.8a). These brittle features are consistent with sinistral shear during pseudotachylyte generation due to seismogenic shearing along the dyke margin, and later zeolite vein emplacement. The faulted northern dyke margin is stained a prominent red-brown colour (hematite), which reaches up to 3m north of the contact. The southern dyke margin also preserves some (limited) evidence for brittle behaviour, consisting of brecciated schistose material containing 3-5mm clasts of biotite-muscovite schist and quartz (Fig. 4.13c). The northern margin preserves a later set of slickenline lineations which overprint the dip-slip and dextral lineations associated with earlier Laxfordian events. These plunge shallowly to the NW (average 23→284) (Figs. 4.8e, 4.9), and were interpreted as shallowly plunging sinistral slickenlines (Billings, 1942; Doblas, 1998), likely associated with the localised, pseudotachylyte generating, sinistral shearing along the dyke margins.

A NNW-SSE trending fault within the gneiss to the north of the northern dyke margin preserves pseudotachylytes on the exposed fault surface. Dilational jogs (~E-W) on this surface contain pseudotachylyte, as well as lineations plunging ~45^{o} NNW (Fig. 4.13d). This fault therefore appears to be sinistral, the strike of which rotates anticlockwise approaching the dyke margin, and is not traceable upon reaching it. Running sub-parallel to this at the southern dyke margin, another fault sinistrally offsets the margin of a large (>1m in length) amphibolite pod within the gneiss.

Achmelvich North: A complex series of faults and fractures are present, mainly within the gneiss. These show three main orientations, mainly offsetting gneissose foliations and, in some cases, the dyke contact (Fig. 4.6e-f): 1. Sinistral offset, 122^{o} (sub-parallel to the dyke

margins); 2. Sinistral offset, 107º (15º anticlockwise rotation from the dyke margin orientation) and; 3. Dextral offset, ~60º (62º anticlockwise rotation from the dyke margin orientation). This indicates a sinistral Riedel shear arrangement (M, R and R' respectively). These orientations are not dissimilar to those of fracture sets at Loch Assynt (e.g. Fig. 4.11a), indicating a possible association with 'Late Laxfordian' shearing. One NW-SE trending fault offsets the dyke dextrally at NC 05709 25020 (see map, Fig. 4.6a), however lineations are found when tracing the fault plane to the WSW that are interpreted to be sinistral slickenlines ('smooth side' vs 'rough side' method, Billings, 1942). This indicates some later brittle reactivation of this fault. Red hematite staining was also present at both dyke margins at Achmelvich North and along large-scale faults within the gneiss. Slickenlines with sinistral kinematic indicators (Billings, 1942; Doblas, 1998) are present along the southern dyke margin; these are again associated with zeolites (Figs. 4.6g).

4.6 Fieldwork Summary

Badcallian & Inverian: Shallowly dipping Badcallian foliations affected by folding are found at Lochinver, Achmelvich South and Loch Assynt (Table 4.1). However Achmelvich North, located on the northern limit of the Inverian Lochinver monocline, shows foliations that dip steeply to the NNE.

Scourie dyke emplacement: The dyke margin at Lochinver is not affected by later deformation, with sharp, moderately dipping boundaries and a 1.5cm chilled margin containing a spinifex-like texture. Xenoliths of gneiss are found within the dyke at Achmelvich North.

Laxfordian: Dextral schistose viscous mylonites are present at both dyke margins at Achmelvich North, and the southern dyke margin at Achmelvich South. These are associated with syn-tectonic quartz mineralisation (Table 4.1), with deformation consistent with Laxfordian deformation within the CSZ.

'Late Laxfordian': Loch Assynt preserves dyke margins with little evidence of dextral schistose viscous mylonites, as seen at Achmelvich. Instead, they show ductile sinistral ultramylonites, 1-5cm in thickness, overprinted by brittle sinistral shears. Quartz-epidote mineralisation concentrated at the dyke margins (Table 4.1) provides evidence of stepped epidote slickenfibres indicative of sinistral shear. Quartz-epidote mineralisation is also present associated with tensile fractures at 'Copper Island' and to the NW along the Loch Assynt Fault at Clashnessie. Associated sulphides from 'Copper Island' provide ages from Re-Os geochronology of 1.55 Ga (R.E. Holdsworth, 2018, personal communication). The northern margin at Achmelvich South also shows brittle deformation, with 1-2cm thick pseudotachylytes and injection veins, cross cut by zeolite mineralisation. Both of these features have sinistral kinematics, indicating they are synchronous with deformation found at Loch Assynt.

Table 4.1. *Summary table indicating trends of main features across the 4 main localities of the study area.*

Feature	**Locality**			
	Lochinver	***Achmelvich North***	***Achmelvich South***	***Loch Assynt***
Gneissose foliations	E-W trending Moderately dipping Folded around SW plunging axis	NW-SE trending Steeply dipping	NE-SW trending Moderately dipping Folded around NE plunging axis	NE-SW trending Moderately dipping Folded around WNW plunging axis
Dyke margins	NW-SE trending Moderately dipping	NW-SE trending Steeply dipping	NW-SE trending Sub-vertical	NW-SE trending Sub-vertical
Fractures: Dextral	-	NE-SW trending	NW-SE trending	NW-SE
Sinistral	-	NW-SE trending	NW-SE, NNE-SSW trending	NW-SE trending
Tensile	-	E-W trending	NE-SW trending	NE-SW trending
Schistose fabric	-	NW-SE trending	NW-SE trending	-
Quartz veins	(Early) NE-SW trending	NW-SE trending	NNW-SSE trending	(Early) NE-SW trending
Quartz-epidote veins	-	-	-	WNW-ESE trending
Zeolite veins	-	E-W trending	WSW-ENE trending	-
Lineations: Sinistral oblique	-	Shallowly NW plunging	Shallowly NW plunging	Moderately W plunging
Dextral oblique	-	Shallowly SE plunging	Shallowly SE plunging	-
Dip-slip	-	Steeply NW plunging	Steeply SE plunging	-

5. Microstructures

5.1 Microstructural abbreviations

Table 5.1. *List of microstructural abbreviations and definitions. *See Figure 5.1 and Table 5.2.*

Abbreviation	Definition
BLG	Bulging recrystallization.
CPO	Crystal preferred orientation: ascertained using a gypsum plate of the polarizing microscope, which should show a dominance of a single colour for samples with strong CPOs (Fossen, 2016). This is determined by eye.
GBAR*	Grain boundary area reduction.
GBM*	Grain boundary migration recrystallisation .
GBS	Grain boundary sliding.
SGR*	Subgrain rotation recrystallisation: defined by the rotation of subgrains (<20^{o} extinction angle to neighbouring grains) to form new grains (>20^{o} extinction angle to neighbouring grains).
(X)µm	Unless otherwise stated, measurements refer to the long axis grain diameters.

5.2 Microstructural textures

This section presents a microstructural analysis of dyke margins and associated features from the four main field localities, which is used to supplement field observations and further constrain the deformation histories of reactivation (see field maps, section 4, and Appendix 2 for sample locations). In addition to the analysis carried out on these deformed dyke margins from Achmelvich (NC056250 and NC055248) and Loch Assynt (NC2125) comparative microstructural analysis was also performed on samples of an undeformed Scourie dyke and the Lewisian Gneiss from Lochinver (NC087219). These show differing levels and complexities of inferred overprinting relationships of deformation, indicated by the fault rocks and microscale deformation within the samples.

Microstructural classifications from experimentally deformed quartzite by Hirth and Tullis (1992) and Passchier and Trouw (2005) are used throughout to indicate the separate regimes of dislocation creep. Distinct microstructures are produced within each regime due to the dominant dynamic recrystallisation mechanisms. During deformation, mechanisms to produce and annihilate dislocations within grains are in competition, which

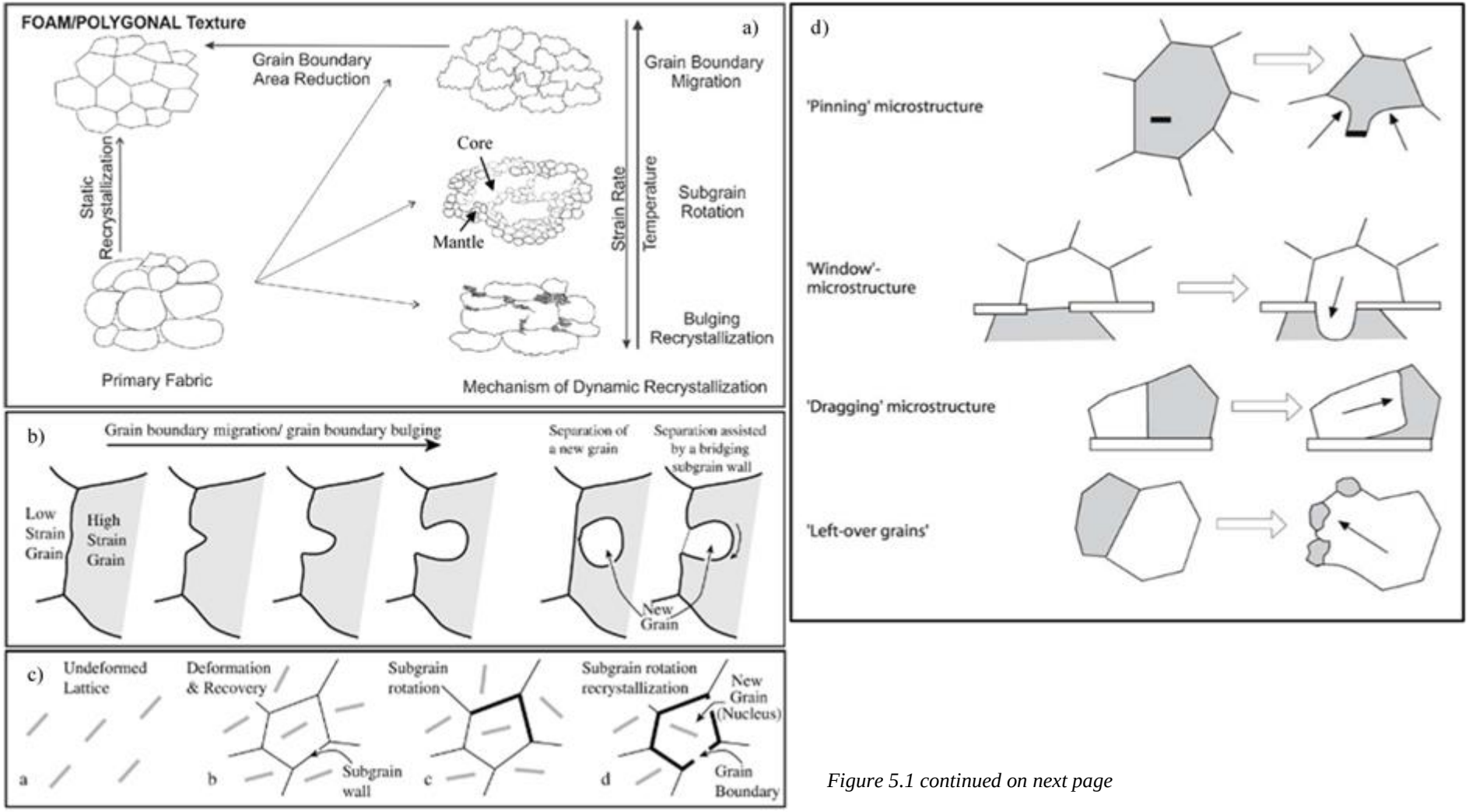

Figure 5.1 continued on next page

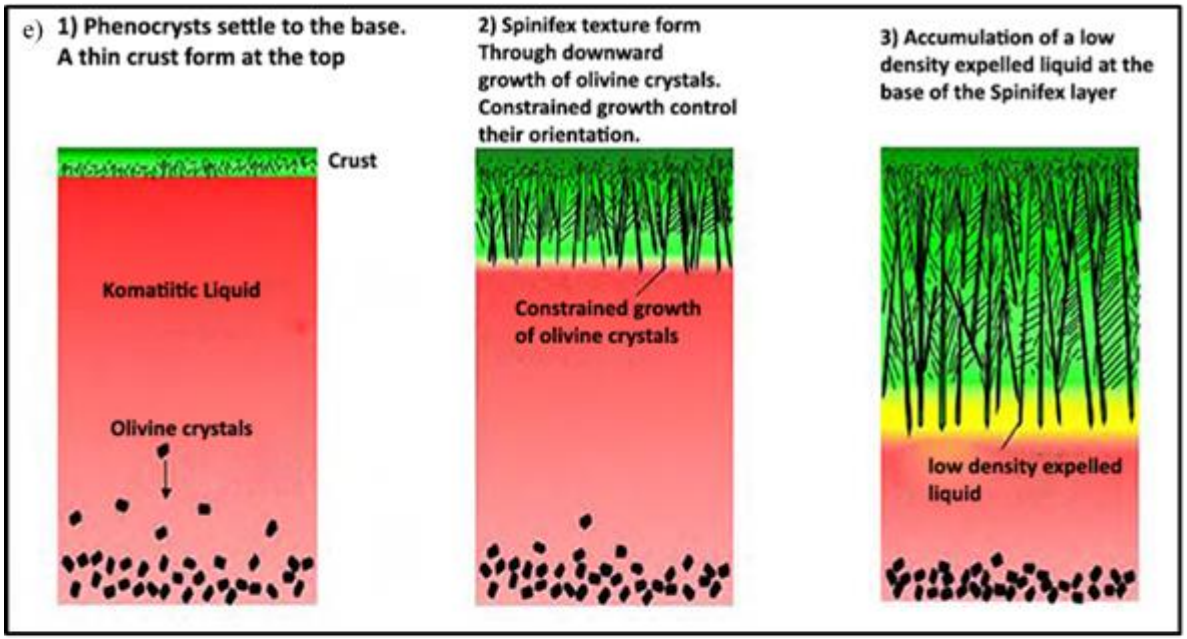

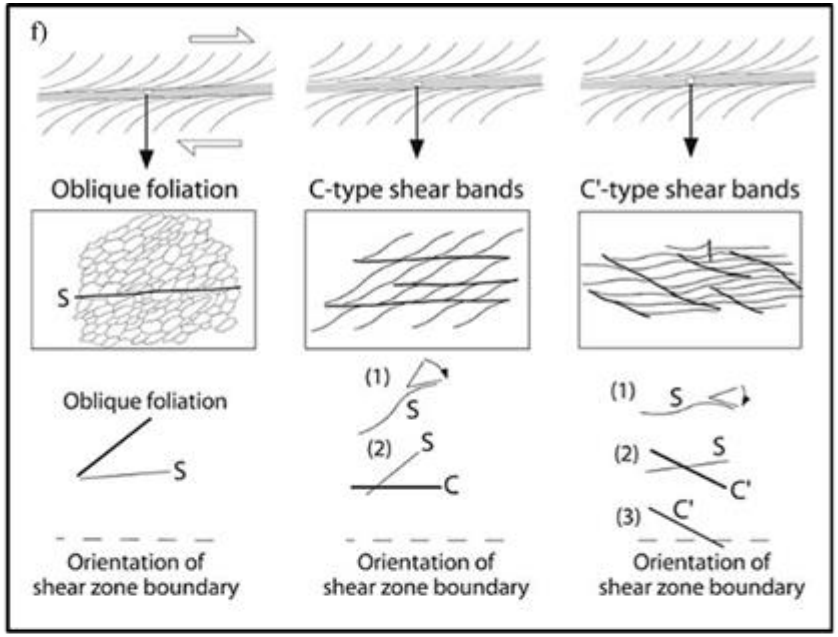

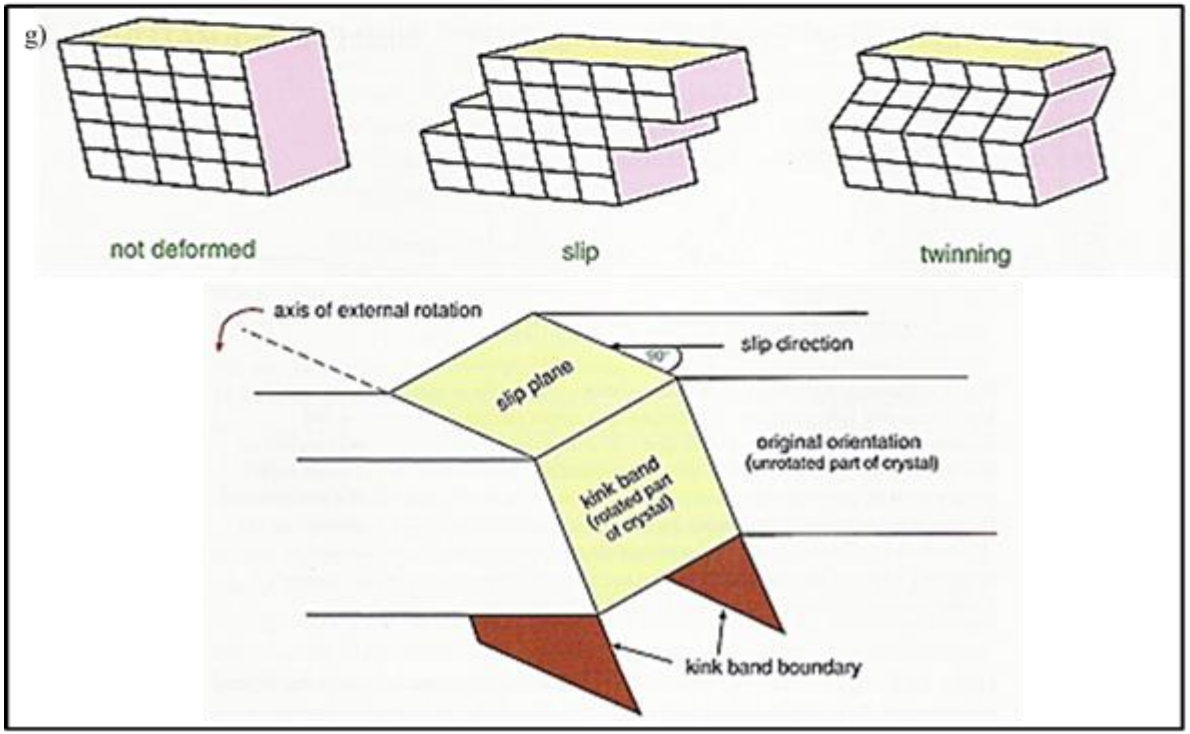

Fig 5.1. *a) Different mechanisms in deforming quartz producing characteristic microstructures (Tandon et al., 2015) b) Basic processes involved in new grain development: bulging nucleation, bulge separated from parent grain dye to formation of a bridging subgrain wall (adapted from Halfpenny et al., 2006) c) High angle grain boundaries and new grains from progressive subgrain rotation (adapted from Halfpenny et al., 2006) d) Microstructures indicating movement direction of migrating grain boundary during GBM recrystallisation (adapted from Passchier and Trouw, 2005) e) Mechanism for 'spinifex texture' formation (Arndt and Fowler, 2004) f) Foliation pairs common in ductile shear zones: shear zone is shown (top), with typical curvature of the foliation, main differences are shown in the centre, with elements used to determine shear sense shown at the bottom (Passchier and Trouw, 2005) g) Kink band formation (Vernon, 2004). Top: general slip processes and deformation twinning. Bottom: Geometry of a kink band*

Table 5.2. *Summary of microstructural characteristics and deformation conditions associated with regimes of dislocation creep first recognized by Hirth and Tullis (1992) (adapted from Smith et al., 2007).*

Dislocation Creep Regime	**Dominant Recrystallisation Mechanism**	**Favoured conditions**	**Common Microstructural Characteristics**
Regime 1	Strain-induced grain-boundary migration recrystallisation.	Low T, high strain rates. Lower greenschist facies.	Irregular and patchy undulose extinction, very fine recrystallised grain size, absence of aligned grains.
Regime 2	Subgrain rotation recrystallisation (SGR).	Moderate T, moderate strain rates. Upper greenschist facies.	Homogeneously flattened original grains, sweeping undulose extinction, optically visible subgrains often with strong crystallographic-preferred orientation (CPO) and/or shape preferred orientation (SPO), sub-basal deformation lamellae, core/mantle structures.
Regime 3	Grain-boundary migration recrystallisation (GBM).	High T, low strain rates. Amphibolite facies.	Large recrystallised grain size with lobate or sutured grain boundaries, high percentage of recrystallised grains, weak crystallographic-preferred orientation (CPO) and shape-preferred orientation (SPO) of recrystallised grains.

changes their internal strain energy. Post-deformation, annihilation predominates, reducing the length of dislocations. With increasing temperature and decreasing strain, these are bulging (BLG), subgrain rotation (SGR), and grain boundary migration (GBM) recrystallisation. High temperature deformation can result in grain boundary area reduction (GBAR); decreasing the surface area of grain boundaries results in a decrease in internal free energy. A summary of these are presented in Figure 5.1a-d and Table 5.2, and Passchier and Trouw (2005). When brittle deformation is predominant, fracturing and cataclasis are the prevalent microstructures. In the presence of fluids, dissolution-precipitation at grain boundaries is common, with diffusion dominated creep dominant.

5.3. Badcallian Gneisses

Basement quartzo-feldspathic gneisses are visible across the four main field localities, showing original gneissose fabrics. Gneisses at Lochinver, in particular, are sampled due to the lack of Laxfordian (and later) deformation at the locality. The gneiss contains the assemblage: 30% quartz (150-350µm), 50% hornblende (<500µm) 20% plagioclase feldspar (albite, 150µm), and accessory chlorite (200µm) occurring as a product of retrogression. Compositional bands >5mm thick within the sample from Lochinver are defined by variations in the proportions and grain size of quartz and feldspar; ranging from 40% quartz and feldspar with a grain size of ~500µm, to 70% quartz and feldspar with a grain size of ~100µm (Fig. 5.2a). Variations in the quartz and feldspar are accompanied by variations in the amphibole content; 60% to 30% in mafic and felsic bands respectively.

Grain aggregates within the gneiss show heterogeneous grain sizes, generally with lobate grain boundaries at all contacts (Fig. 5.2). 20% of the quartz grain aggregates are polygonal, with the majority showing grain sizes of ~200-300µm. The quartz shows regular extinction, with little intracrystalline deformation (Fig. 5.2b). The characteristics of these grain aggregates are consistent with grain boundary area reduction (GBAR). Lobate quartz grain boundaries are common (Fig. 5.2b-c), with some crystals containing subgrains (<20^{o} extinction angle, ≤150µm), further deforming by SGR recrystallisation. Hornblende preserves small amounts of BLG recrystallisation (Fig. 5.2c). These deformation microstructures overprint the GBAR within the quartz, which is consistent with initially high-grade metamorphism (>700^{o}C), followed by a retrogressive deformation history of the gneiss, from granulite facies to greenschist facies.

5.4. Scourie dykes

Samples 15 and 16 were collected from the undeformed Scourie dyke margin (NC 08740 21927), and central dyke (NC 08740 21935) respectively. This locality, near to the town of Lochinver, provides an example of an undeformed Scourie dyke margin. The dyke contains the assemblage: 75% hornblende (≤1mm), 10% plagioclase feldspar (500µm),

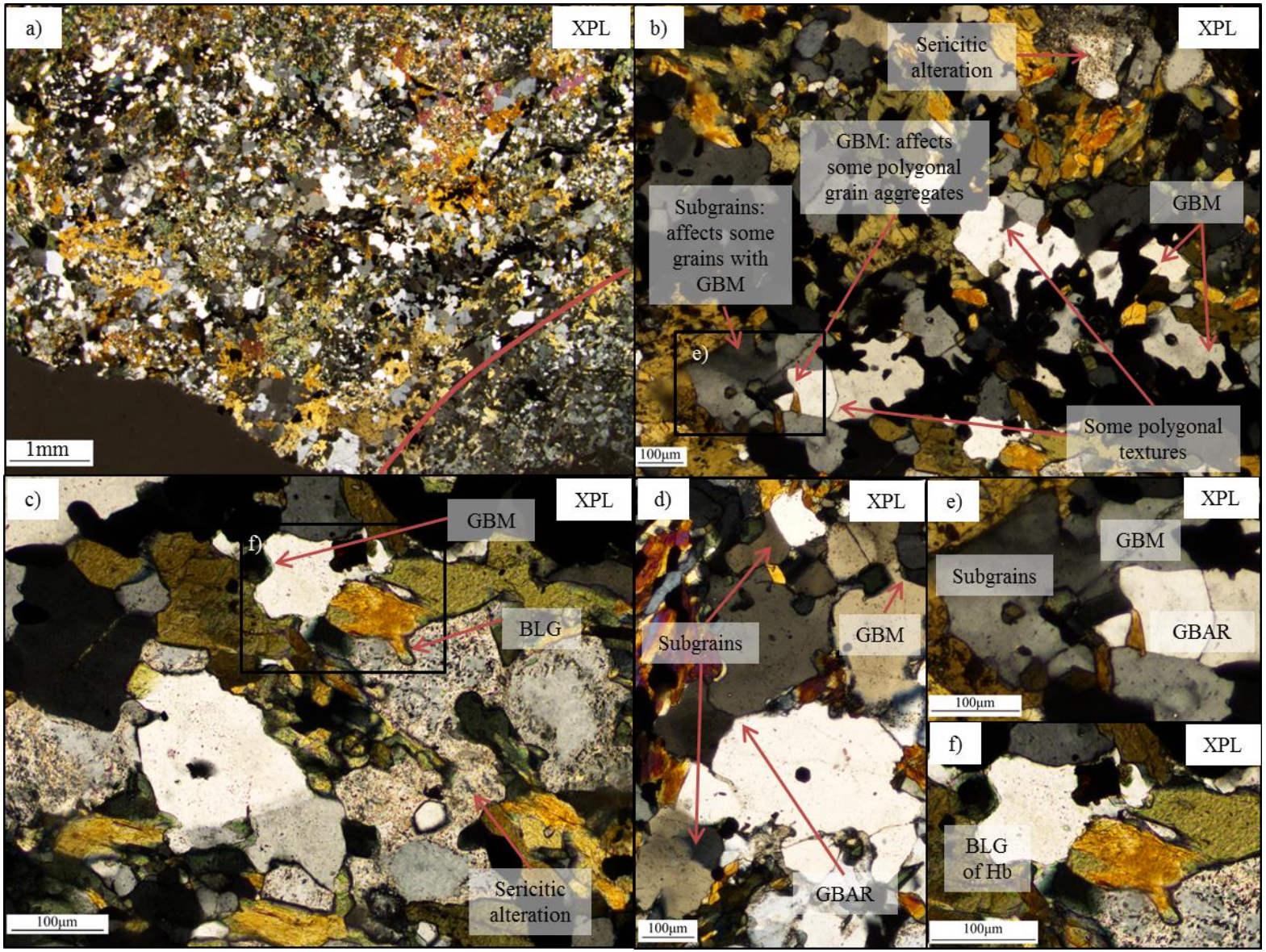

Fig 5.2. *Badcallian gneiss at the dyke margin at Lochinver, a) Compositional banding, red line separates mafic band (above) and felsic band (below) b-d) Deformation microstructures e-f) Zoomed in sections from b and c, see Figure 5.1 for classifications.*

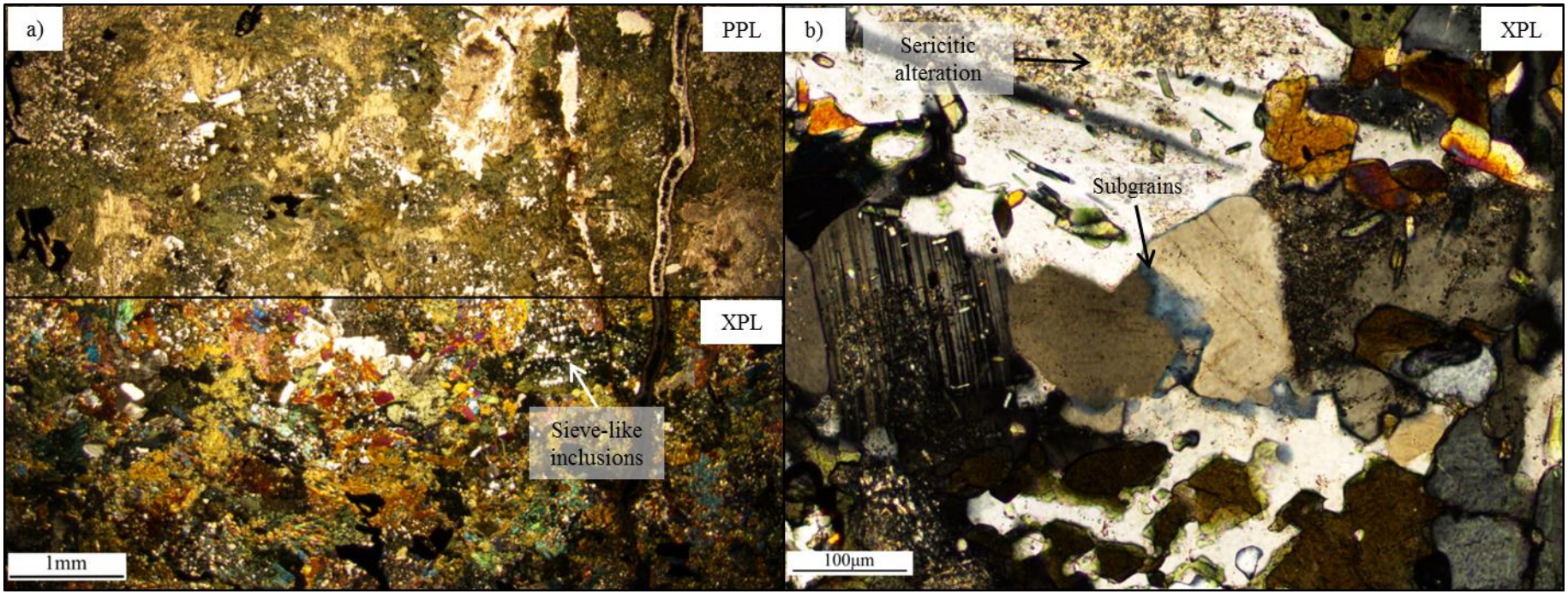

Fig 5.3. *Centre of the undeformed Scourie dyke at Lochinver, a) PPL (upper) and XPL (lower) views b) Subgrains and sericitic alteration within the dyke.*

10% quartz (≤500μm), 5% K feldspar (mostly sanidine, ≤1mm), and <1% microcline (500μm). Most of the quartz is present as rounded, sieve-like inclusions (25-50μm) within the hornblende crystals (Fig. 5.3a), with the quartz displaying regular extinction. Quartz grains not present as inclusions display patchy undulose extinction, and in some cases, subgrains (100-300μm) have started to form (Fig. 5.3b). Plagioclase feldspar shows moderate amounts of sericitic alteration.

Hornblende occurring in a sieve texture with quartz has also been found within undeformed dykes in studies by Pearce and Wheeler (2014) and MacDonald et al (2017). The former suggests the nature of the amphibole within the undeformed Scourie dyke near Scourie represents early (silicic) amphibole replacing igneous pyroxenes following dyke intrusion at depth (O'Hara, 1961; Tarney, 1973), with further hornblende growth during later metamorphism. These sieve textures are likely to represent static retrogression during the Laxfordian tectonometamorphic event (MacDonald et al., 2017). Quartz sieve textures are only present within the undeformed dyke at Lochinver, and undeformed dykes within the literature (Pearce and Wheeler, 2014; MacDonald et al., 2017), but are not widespread within the Assynt terrane. The textures are, however, frequent within the Gairloch region (Shelley, 1967). The differences in the abundance of sieve textures between the Assynt and Gairloch terranes may be due to the differences in structural depth during the Laxfordian (Park, 2005; Mason 2012, 2016). The mineralogy within these samples is indicative of amphibolite facies metamorphism of the (originally doleritic) dykes during and shortly after their emplacement (Tarney, 1963).

5.5. Dyke margins: undeformed

Figure 5.4 shows the undeformed dyke margin at Lochinver with original igneous textures preserved, including a chilled margin. The dyke here consists of 70% hornblende, 20% quartz, 5% K feldspar (sanidine), and 5% plagioclase feldspar, most of which is sericitically altered. A gradational increase in grain size is observable from the margin of

Fig 5.4. *Undeformed dyke margin at Lochinver showing a chilled margin at the contact with the gneiss and spinifex-like texture indicating a large degree of undercooling at the time of emplacement. Sharp upper margin of spinifex-like texture, followed by small decrease in grain size. General increase in grain size up the section. Thin section taken in a horizontal plane.*

the dyke to the centre (Figs. 5.3, 5.4). Quartz and hornblende crystals within the dyke at the dyke margin are ~50μm, with hornblende crystals increasing to 100 μm ~1cm from the dyke margin. This couples an increase in the abundance of alkali feldspars (sanidine), which occasionally reach 1.4mm in length; these are overgrown by the hornblende. The chilled margin is direct evidence of fast cooling at the dyke margins during the emplacement of the dyke, indicating that the country rock was somewhat cooler than the magma.

The orthogonal texture present in the field (see section 4.2) is also preserved in thin section, characterised by elongate hornblende crystals (Fig. 5.4). Mafic and felsic compositional bands are also present; these display sweeping extinction across the whole band length (5mm), away from the dyke margin, but this is only present within this layer. The orthogonal texture has a sharp upper boundary (indicated in Fig. 5.4), with a small decrease (10%) in the grain sizes of all minerals just above this. To the northeast of the sharp boundary, grain sizes steadily increase (up to 3cm from the dyke margin) to a millimetre scale, reaching equal sizes to those seen in the centre of the dyke (see section 5.4). The orthogonal texture is similar to spinifex textures (Fig. 5.1e); the term was first formally introduced by Nesbitt (1971) to describe skeletal or dendritic crystal morphologies normally of olivine and pyroxene crystals within komatiite lavas that have experienced rapid cooling and supercooling (Viljoen and Viljoen, 1969a, 1969b). The presence of the texture within an undeformed Scourie dyke suggests that secondary hornblende replaced primary (platy) pyroxene during amphibolite facies metamorphism. This replacement has been shown to occur quite widely in some Archean rocks (Lowrey et al., 2017). The sharp upper boundary of the spinifex-like texture indicates another intrusion event re-melted the existing chilled margin. The preservation of these igneous textures is consistent with a lack of deformation post-dyke emplacement.

5.6. Ductile dextral deformation

Field analysis of dyke margins at Achmelvich North and the southern margin of Achmelvich South indicate that lower amphibolite/upper greenschist facies ductile fabrics are dominant at these margins. These are localised shear zones of dextral schistose mylonites developed either side of the original dyke margin: biotite muscovite schist (derived from quartzo-feldspathic gneiss protolith) and hornblende schist (derived from doleritic dyke protolith). These are described below in relation to their protoliths, generalising textures across the two localities unless there are significant differences.

5.6.1. Achmelvich: Schistose mylonites

Biotite muscovite schist: Biotite muscovite schists contain the assemblage: 50% plagioclase feldspar (albite, 100-200µm), 15% quartz (150µm), 10% K feldspar (100-200µm), 10% hornblende (200-500µm at Achmelvich North, 50-1750µm at Achmelvich South), 5% biotite (~300µm) and 5% muscovite (50µm). A penetrative schistose fabric is observed within the thin sections cut normal to foliations and parallel to the lineations along the dyke margins, with the schistose foliations reaching up to 2mm in width. Deformation of both quartz and feldspar grains are characterised by cuspate-lobate grain boundaries within quartzo-feldspathic grain aggregates, with equigranular quartz crystals (~50µm). Some of the quartz and feldspar grains show 'pinning' microstructures (Fig. 5.1d) typical of GBM recrystallisation (Fig. 5.5a). ~70% of grains in the sample show a reduction in grain size compared to the adjacent protoliths.

Compositional layering in rocks, along with preferred orientation of micas, may be transected by subparallel minor shear zones (known as shear bands, or shear band cleavage), developing by extension along older foliation within the rock. Figure 5.1f outlines the terminology for these shear bands, with two main types of shear band cleavage distinguished: C and C'. C fabrics represents inhomogenous simple shear, with the shear sense synthetic with that of the main shear zone, contrary to C' fabrics, oblique to shear zone boundaries (Passchier and Trouw, 2005). Widespread Type I S-C-C' fabrics (shear

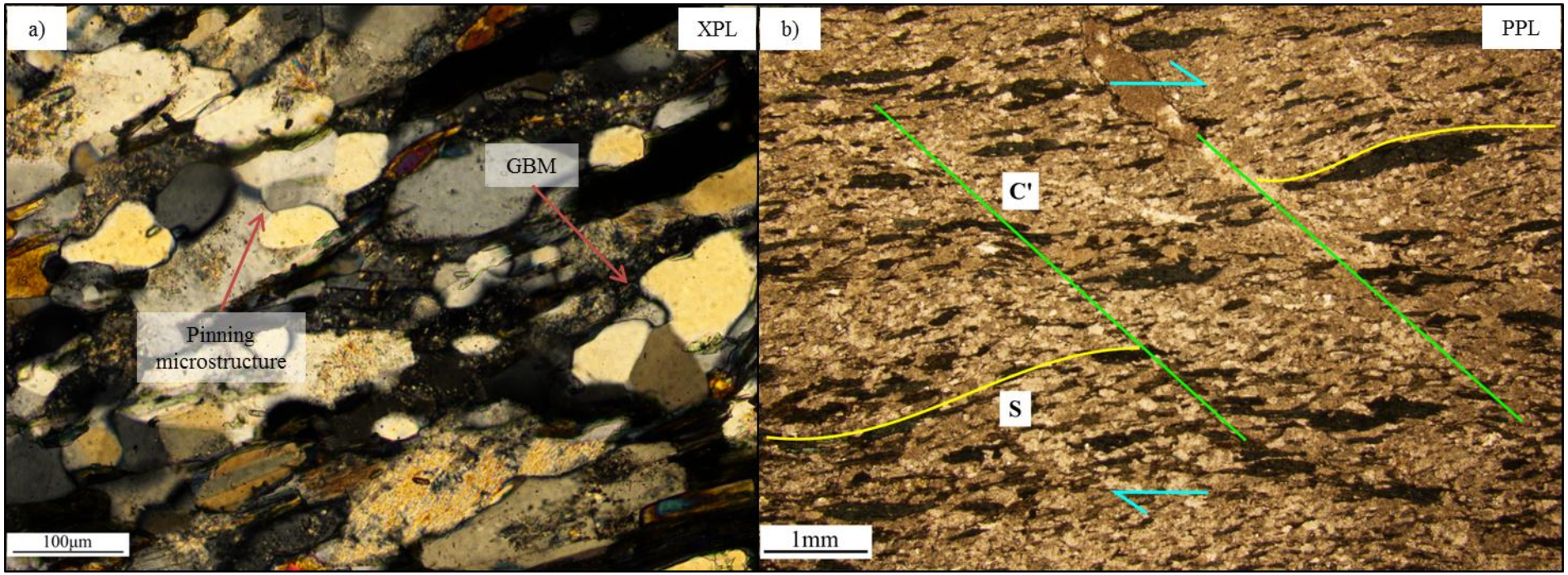

Fig 5.5. *Biotite muscovite schist, Achmelvich a) Deformation microstructures, see Figure 5.2 for definitions b) S-C' banding within the biotite muscovite schist at Achmelvich North, indicating dextral shearing (blue arrows) within the schistose viscous mylonite. Thin section taken in a dipping plane (to the NE), lineation parallel.*

bands) affect the schistose fabric within the fault rocks at Achmelvich, with C planes inclined to the right indicative of dextral shearing. Sample 8, collected from the southern dyke margin at Achmelvich North (Appendix 2) displays a strong C' fabric; hornblende and/or biotite lines the S bands, and the C' bands (trending top left to bottom right) are primarily accented by quartz (Fig. 5.5b). A 1mm wide quartz vein follows one of the shear bands within the sample from Achmelvich North for 1.5cm (Fig. 5.6). Quartz crystals within the vein are ~500µm, and most show patchy undulose extinction and the development of subgrains (200µm). The pure quartz vein would have prevented pinning of the grain boundaries, resulting in coarser grains here as a secondary grain growth texture. Vein margins follow dextral S-C mylonitic fabrics within the schist (Fig. 5.6), indicative of a syn-tectonic time of vein emplacement.

The contact: The contact between the biotite muscovite schist and hornblende schist is observed within sample 3, collected from the southern dyke margin at Achmelvich South (Appendix 2) (Fig. 5.7a). This is defined along most of its length by a layer ~30µm wide of dark brown material (Figs. 5.7b-c). This does not show any evidence for a melt phase and/or characteristic features of pseudotachylyte e.g. flow textures; vesicles; microlitic/spherulitic texture (Maddock, 1983; Maddock et al., 1987; Magloughlin and Spray, 1992; Sibson et al., 2006) under examination with an optical microscope. It is therefore more likely that this is a resultant brittle deformation of the biotite from very localised shearing along the contact. An alternative explanation is later iron oxide mineralisation; iron-oxide staining is typically associated with 'Late Laxfordian' faulting (Beacom, 1999).

Hornblende schist: Sample 3 contains hornblende schists comprised of: 65% hornblende (200-600µm), 15% plagioclase feldspar (100µm), 15% quartz (100µm) and 5% biotite (300µm), and accessory chlorite (500µm). Plagioclase feldspar shows heavy sericitic alteration. In the 1.5mm nearest to the contact, biotite starts to replace the hornblende

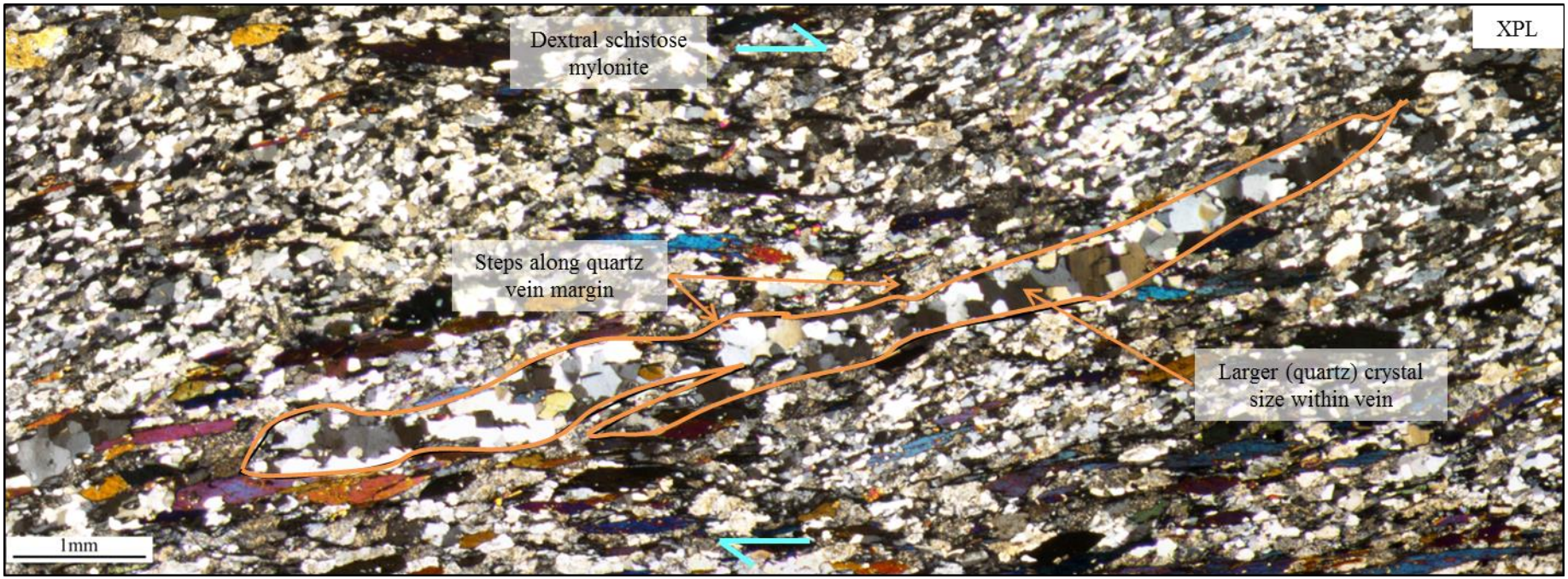

Fig 5.6. *Biotite muscovite schist from Achmelvich North. Quartz vein highlighted, sheared in with the schistose foliations, some subgrains present within. Thin section taken in a dipping plane (to the NE), lineation parallel.*

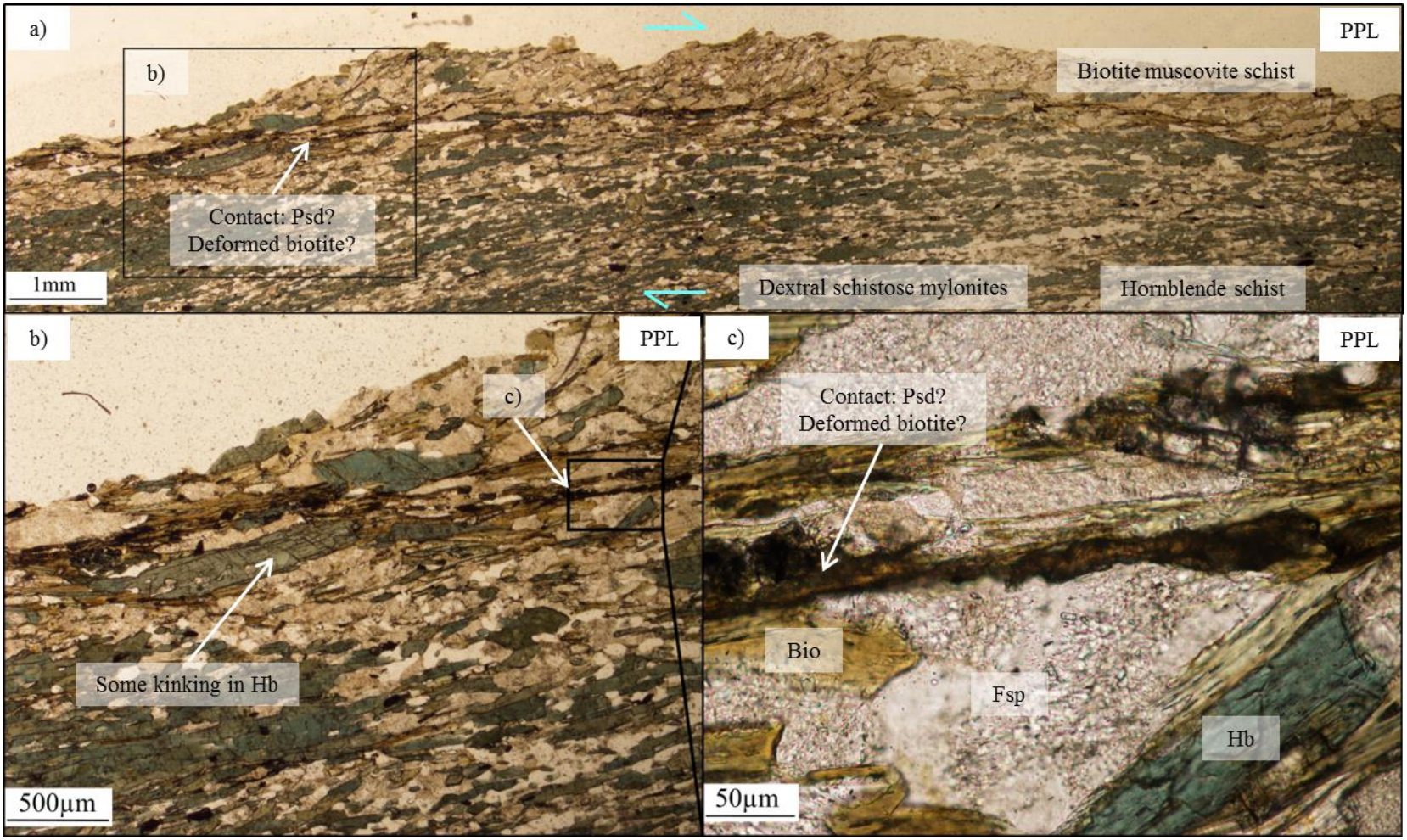

Fig 5.7. *a-c) Contact between the biotite-muscovite schist (above) and hornblende schist (below) at Achmelvich South (southern margin) showing possible pseudotachylytes (psd)/deformed biotite at different magnifications in PPL. Thin section taken in a horizontal plane, lineation parallel.*

(40% hornblende + 25% biotite). A finer (~1mm foliation spacing) schistose fabric is observable parallel to the dyke margins within the hornblende schist compared to the biotite muscovite schist, with centimetre scale mylonitic S-C banding (Fig. 5.7a). C planes inclined to the right are indicative of dextral shearing. Deformation within the quartz is defined by 50µm subgrains, with the majority of these having undergone SGR recrystallisation. In total, 15% of the schist shows grain size reduction within the sample.

5.6.2. Summary

Kinematic and mineralogical similarities of these dextral schistose mylonites with those in the central part of the Canisp shear zone are thought indicate the presence of Laxfordian deformation at Achmelvich (Park and Cresswell, 1973). There is a much higher degree of strain within the millimetres surrounding the contact, which facilitates the alteration from hornblende to biotite (Beach, 1976) within the hornblende schist. C' banding (Achmelvich North) normally develops during retrograde metamorphism (McCaig, 1987; Norrell et al., 1989), with this type of cleavage normally developing during late shear zone activity, after the development of a strong shape preferred orientation (SPO) within the minerals (Passchier and Trouw, 2005). This implies that the S-C-C' fabrics developed due to strain during progressive cooling. Mineral assemblages and deformation textures suggest lower amphibolite to upper greenschist deformation within the Laxfordian (e.g. Coward and Park, 1987; Park et al., 1987), summarised in Table 5.3.

5.7. Sinistral deformation

Field observations suggest that two distinct phases of sinistral deformation are recognised from Loch Assynt: narrow bands of sinistral ultramylonites indicative of high strain are overprinted by discrete brittle sinistral faults. Most sinistral deformation is localised along the dyke margins, with additional brittle fracturing within the gneiss and the dyke. This deformation phase shows complex, cyclic overprinting relationships, and association with fluid influx (giving rise to retrograde assemblages of epidote ± quartz ±chlorite) associated with 'Late Laxfordian' deformation (Beacom et al., 2001; Vernon et al., 2014). Brittle

Table 5.3. *Summary table of indicators for metamorphic facies from thin section analysis and the literature, including mineral assemblages, fabric and deformation microstructures.*

Indicator		**Temperature estimates (ºC)**	**Facies**
Fabric developed in the Laxfordian	Schistose mylonites		Amphibolite
Mineral assemblage developed in the Laxfordian	Biotite, muscovite, chlorite		Amphibolite/ Greenschist
	Garnets (Sutton and Watson, 1950; Droop et al., 1999)	>470 (Droop et al., 1999)	Amphibolite
Deformation microstructures	GBM recrystallisation (quartz)	500-600	Amphibolite
	SGR recrystallisation (quartz)	400-500	Greenschist

deformation is also evident at Achmelvich South (northern margin), with microstructural evidence for pseudotachylytes generated during sinistral shearing. These are cross-cut by calcite + zeolite veins. Sinistral deformation is described below with respect to the two localities (see Loch Assynt and Achmelvich South field maps, section 4), with a regional synthesis for each.

5.7.1. Loch Assynt: Ductile sinistral

Ultramylonites at the Loch Assynt dyke margins contain: 40% amphibole (+ other aphanitic mafic minerals, <10µm), 35% plagioclase feldspar (10µm), and 25% quartz (30-50µm); these compositions refer to the matrix of the ultramylonite. Plagioclase feldspar also shows sericitic alteration at this locality. Sample 11 was collected at the southern margin of the larger dyke at Loch Assynt (Appendix 2), and preserves distinct quartzo-feldspathic and mafic (likely amphibole rich) compositional bands 100-200µm in width (Fig. 5.8). The compositional bands are likely to represent pre-existing compositional bands existing within a quartzo-feldspathic gneiss protolith. Within the compositional bands, quartz is characterised by pervasive SGR recrystallisation, with typical homogeneously flattened grains with a strong crystal preferred orientation (CPO, see

a)

PPL


NE
Folds
Shear
Ultramylonite
S-C fabric
Breccia
Cataclasite
Quartz-epidote
veins
1mm
SW

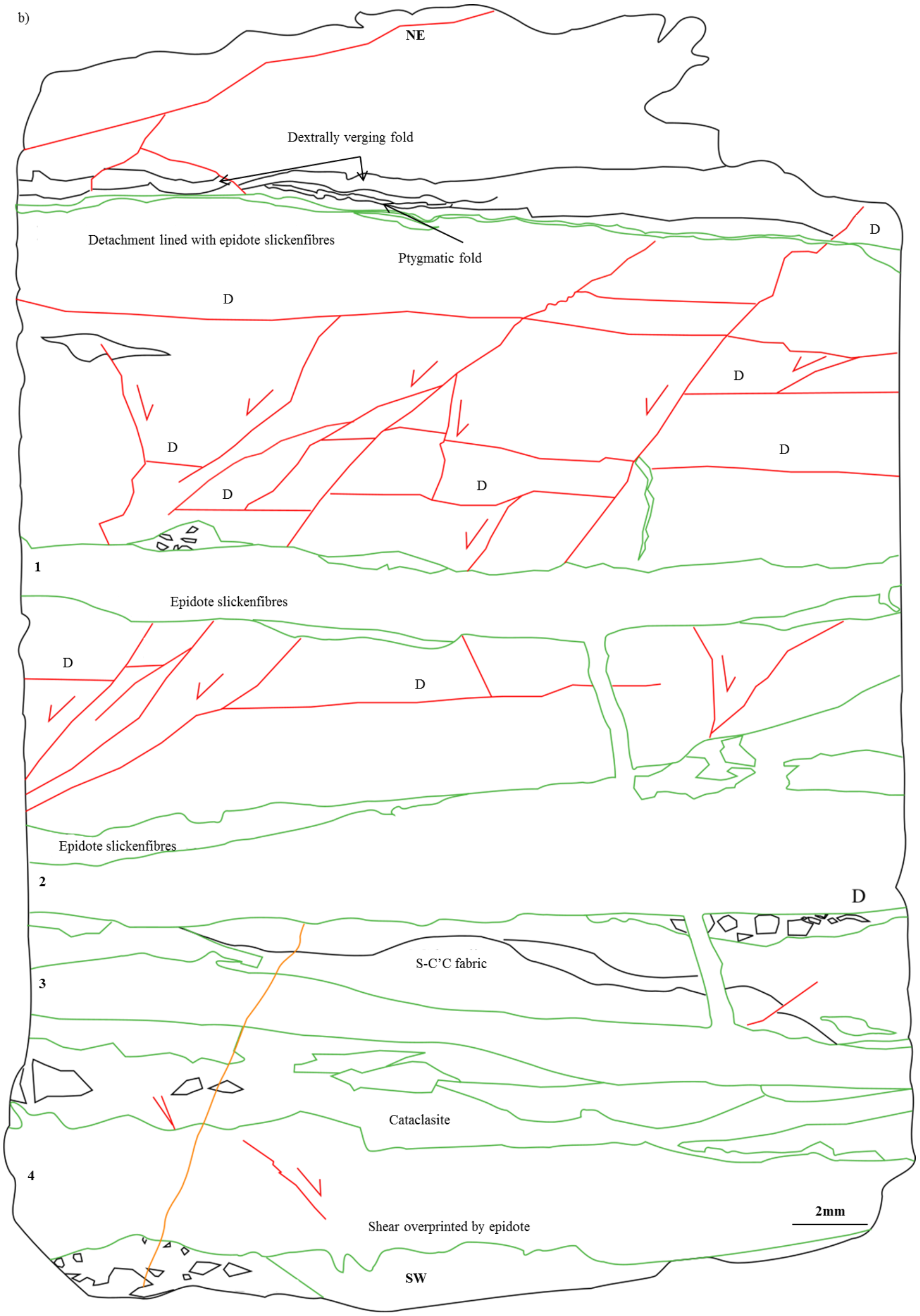

Fig 5.8. *Whole section view of Loch Assynt sample showing overprinting relationships between ductile ultramylonites and folds, brittle structures; shears, breccias, cataclasites, and quartz epidote veins from the dyke margin. Thin section taken in a dipping plane (to the NW), lineation parallel. a) PPL (for XPL, see Appendix Fig. 3.2) b) Labelled line drawing, D; Detachment.*

section 5.1), and widespread subgrain development (30µm) (Fig. 5.9a). Feldspar, however, is almost completely recrystallised during bulging recrystallisation (BLG) (10µm). There are occasionally larger feldspar crystals present (100µm) with lobate grain boundaries as a core to the BLG recrystallisation (Fig. 5.9b). Grains of mafic minerals are too small to determine their deformation textures using an optical microscope; further SEM study is needed for this and to therefore determine deformation mechanisms. In total, 95% of the grains within the sample show grain size reduction.

Type I S-C-C' fabrics are present, especially in the southwestern half of the sample, and are commonly lined by fine grained, fibrous epidote (Fig. 5.8). Curved S planes are inclined to the right, with C planes slightly inclined to the left, indicating sinistral shearing. Asymmetric feldspar and epidote sigmoidal porphyroclasts (1mm in width, 1-2mm in length) are sporadically distributed throughout the ultramylonite. The porphyroclast tails stair step to the left, indicating a sinistral sense of shear (Fig. 5.9c). In the upper part of this sample, folded felsic layers are visible (Fig. 5.10); the fold axial surface within the feldspathic layers shows a clockwise rotation from the top (NE) of the photomicrograph (dextral vergence, a remnant of Laxfordian shearing?). Comparatively, the quartz rich layers beneath this appear ptygmatic (Fig. 5.10a), with the main fold limb showing sinistral vergence (Fig. 5.10b-c).

Sample 21 was collected at the exposed northern margin of the larger dyke by the Loch shore (Appendix 2), and incorporates a contact between the quartzo-feldspathic and mafic fault rocks (quartzo-feldspathic gneiss and doleritic dyke protoliths respectively, Fig. 5.11). ≥90% of the felsic fault rock has undergone grain size reduction, with similar deformation mechanisms to those described above: BLG recrystallisation of the feldspar (10µm) and SGR recrystallisation of the quartz (50µm). The mineralogy of the mafic fault rock is estimated at 60% hornblende (<10µm), 10% plagioclase feldspar (<10µm), 5% quartz containing subgrains (50µm), and the remaining 25% an aphanitic, dark brown, iron

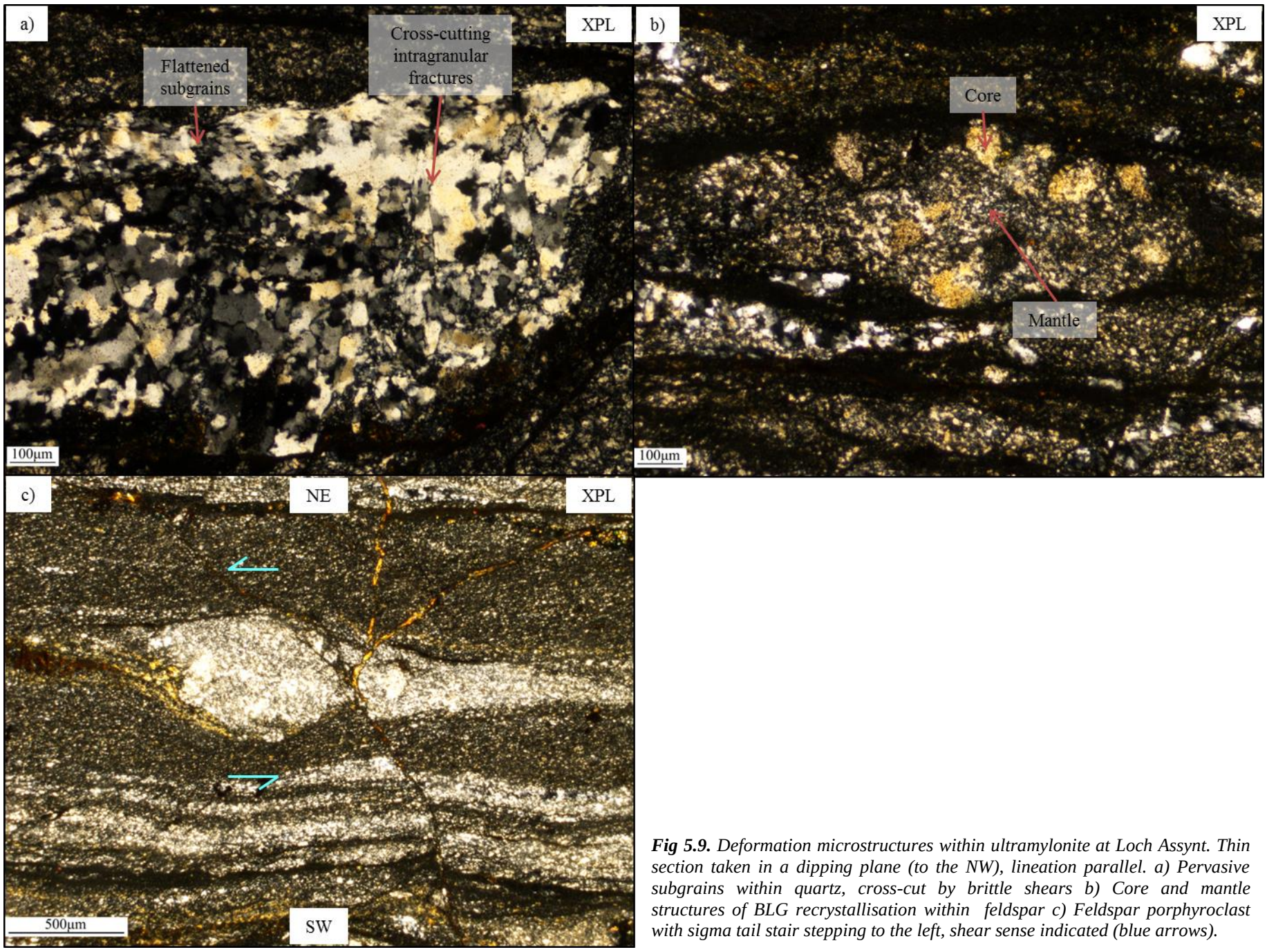

Fig 5.9. *Deformation microstructures within ultramylonite at Loch Assynt. Thin section taken in a dipping plane (to the NW), lineation parallel. a) Pervasive subgrains within quartz, cross-cut by brittle shears b) Core and mantle structures of BLG recrystallisation within feldspar c) Feldspar porphyroclast with sigma tail stair stepping to the left, shear sense indicated (blue arrows).*

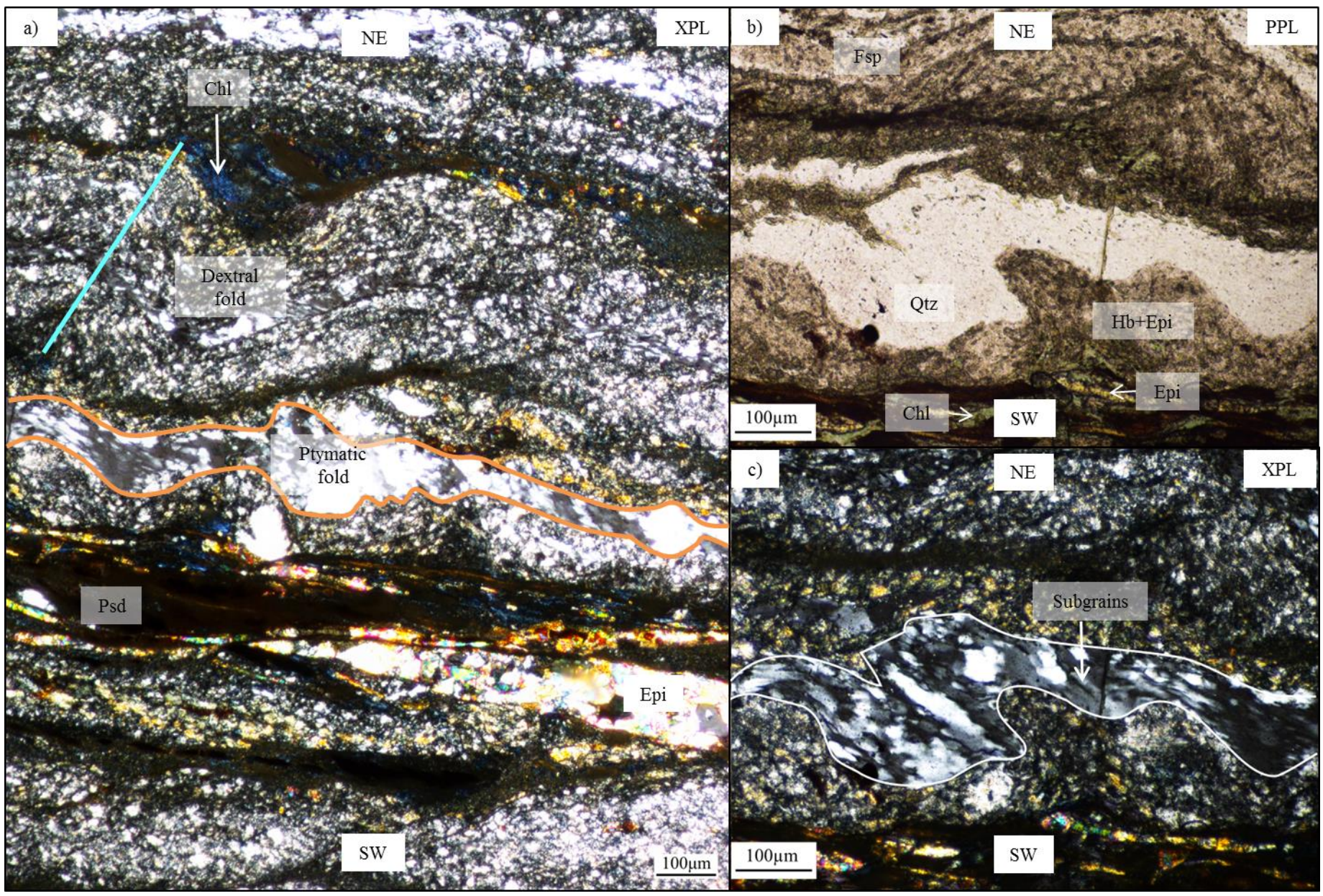

Fig 5.10. *Deformation within the ultramylonite from Loch Assynt: ductile folding and later overprinting pseudotachylytes. Thin section taken in a dipping plane (to the NW), lineation parallel. a) XPL view of overprinting relationships; top to bottom of section – pseudotachylytes overprinting chlorite (anomalous blue), dextrally verging feldspathic rich fold, fold axis indicated by blue line, quartz rich fold outlined in orange, pseudotachylytes overprinting epidote and chlorite b) Quartz rich fold in PPL, sinistrally verging feldspathic b) Quartz rich fold in XPL.*

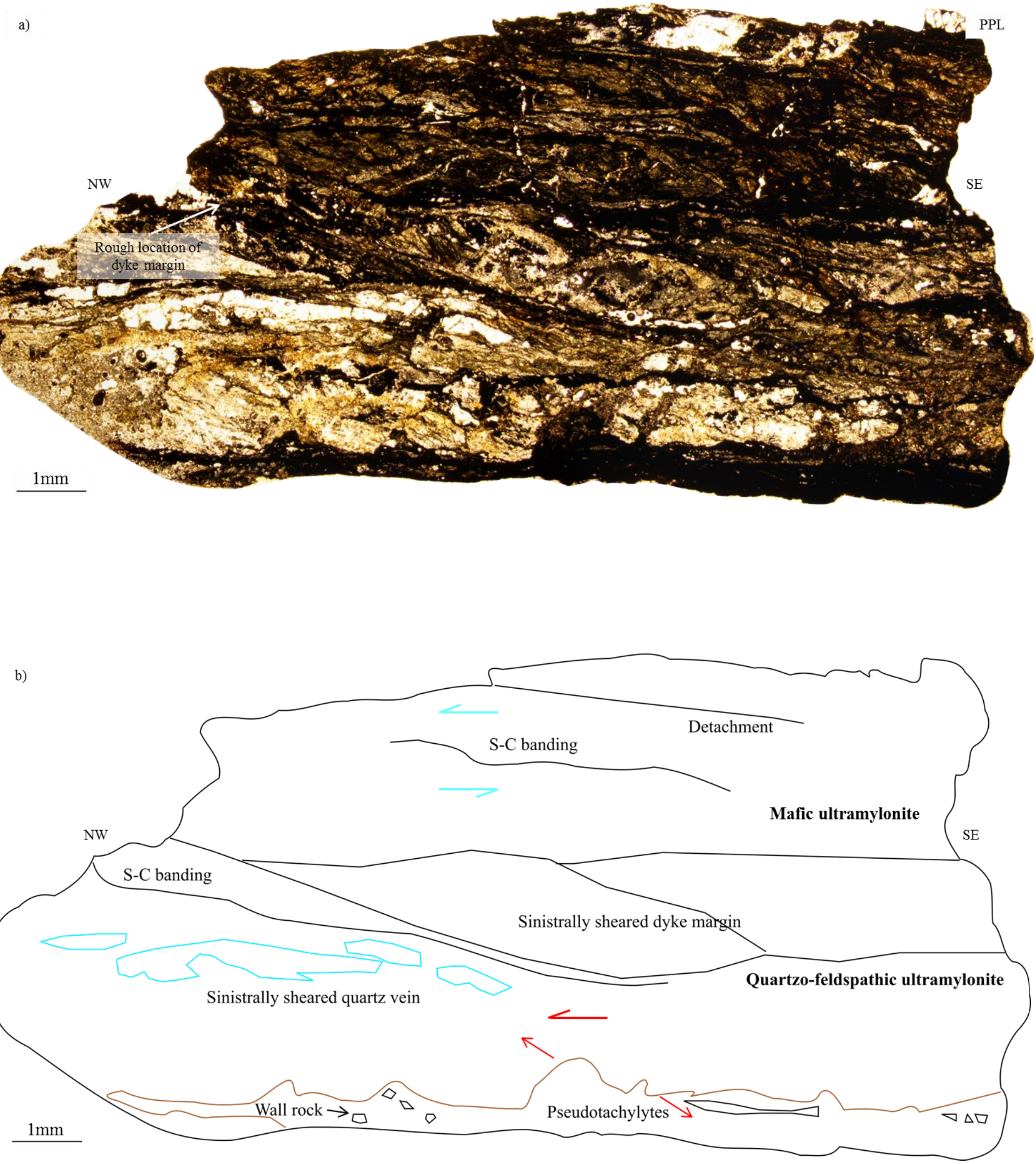

Fig 5.11. *Whole section view of fault rocks at the dyke margin, Loch Assynt, with ductile S-C bands and shearing of the dyke margin, and brittle pseudotachylytes at the base. Thin section taken in a dipping plane (to the ESE), lineation parallel. a) XPL view b) Labelled line drawing.*

stained fault material. The mafic part of the sample shows a higher percentage of grain size reduction (>95%), with an unidentifiable deformation mechanism due to the size of the grains (<10μm). Mylonitic S-C-C' banding is pervasive throughout the sample in both halves, along with a sheared quartz vein in the quartzo-feldspathic ultramylonite following the sinistral S-C fabric (Fig. 5.11).

5.7.2. Loch Assynt: Brittle sinistral

Brittle deformation: Brittle deformation is more prominent within the northeastern half of sample 11, offsetting the foliation within the ultramylonite (Fig. 5.8). The orientation of the thin section is such that the NE, brittle, end is closer to the dyke margin than the SW end. This indicates that within the brittle deformation phase, stresses were more concentrated at the dyke margin compared to the ductile mylonitic phase.

Discrete microscale faults offset marker layers by ≤1mm sinistrally, with associated dextral faults with similar offsets of an opposite dip to the former. These are interpreted to be antithetic to the main sinistral faults. Brittle detachments trend sub-parallel to the foliation across the sample (Fig. 5.8). Faults terminate at, or directly offset, and are themselves offset by these foliation-parallel detachments. Figure 5.12 highlights three detachments; between the two lower detachments, curved, apparently listric faults (in this view) are seen to offset marker layers by ~50μm sinistrally. The upper two detachments are lined by a dark brown/opaque fault rock, with offshoots of the same fault rock into the surrounding ultramylonite sub-parallel to the listric faulting. These fault rocks are interpreted to host pseudotachylytes, which have developed in a 'paired generation zone' (Grocott, 1981). These pseudotachylytes are associated with small (50μm wide, ≤1mm long) en-echelon veins showing an anticlockwise rotation from the main plane of pseudotachylyte generation; these features are interpreted to be injection veins, indicating sinistral shear (e.g. Fig. 5.12a). Most of the brittle faults and detachments within the sample are associated with two main features; a pseudotachylyte-like material, or; fine grained,

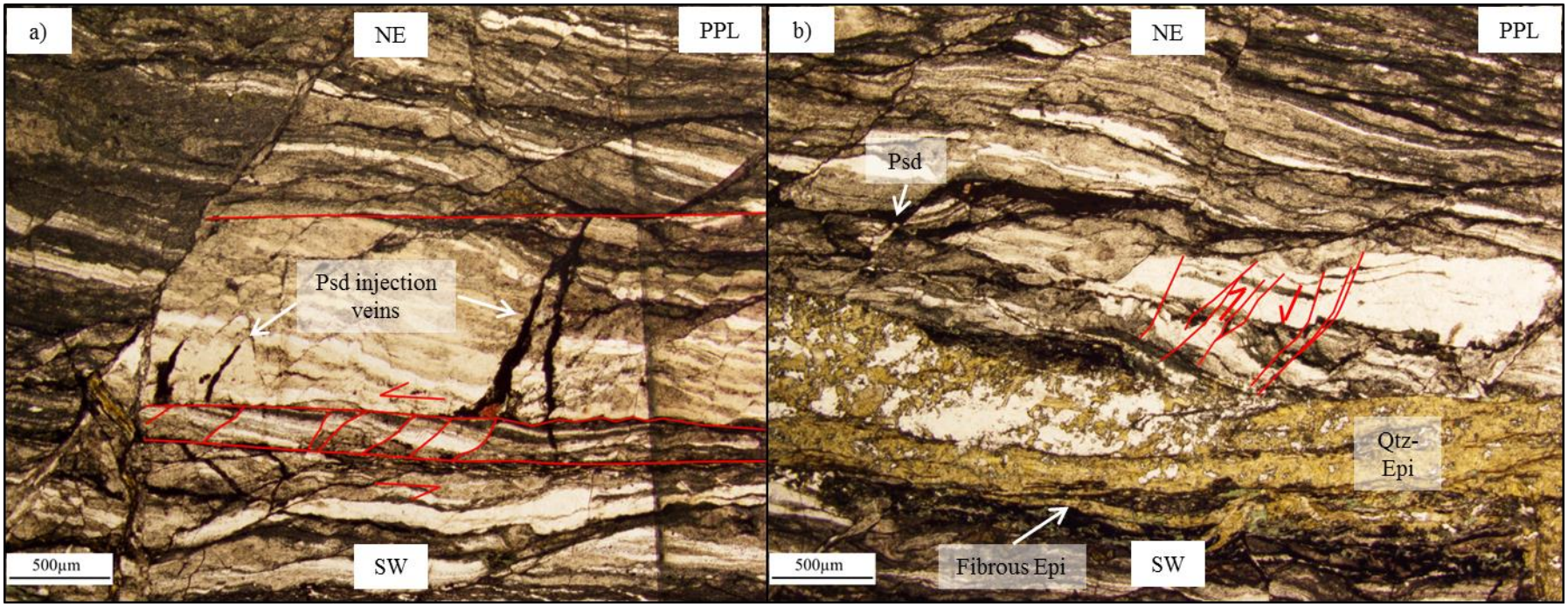

Fig 5.12. *Brittle features overprinting the ultramylonite at Loch Assynt. Thin section taken in a dipping plane (to the NW), lineation parallel. a) Two lower detachments with strain accommodated by apparently listric faulting (in this view), lower detachment lined by epidote. Paired pseudotachylyte generation zone between upper and middle detachments b) Shears overprinted by quartz-epidote vein. Possible syn-tectonic pseudotachylyte can be seen to the centre left of the image.*

fibrous epidote mineralisation of a similar style to that lining the S-C fabric of the ultramylonite. At the southwestern edge of sample 21 within the quartzo-feldspathic ultramylonite, a band of dark brown, opaque rock is observable, occasionally containing clasts of ultramylonite 50-800μm in length and 50μm in width. There are small (~150μm) offshoots of this material into the ultramylonite, trending top right to bottom left (Fig 5.11). This once again shows the characteristics of a pseudotachylyte, with sinistral shear sense indicators.

Figure 5.12b outlines other small-scale faulting patterns within the ultramylonite in sample 11; most of these show sinistral offsets of ~50μm. Some branching faults show one splay offsetting marker layers dextrally, and one limb offsetting marker layers sinistrally. Small-scale breccias (2mm in length, 1mm in width) overprint the ultramylonites, and are themselves overprinted by larger epidote crystals and veins (Fig. 5.8). The breccias are matrix supported, containing 200-500μm clasts of ultramylonite set within a fine-grained matrix of epidote and a dark brown, aphanitic fault material. Cataclastic deformation affects epidote at the SW end of the sample, with fractured grains~10μm in areas up to 12mm in length, 3mm in width. This brittle deformation is therefore likely to be associated with early epidote mineralisation.

The patterns shown by the brittle deformation features in Figure 5.8 are highly comparable with those inferred from the aerial photo of the coastal outcrop of the Canisp shear zone (Fig. 5.13), despite the difference in scale. The fracture patterns are geometrically similar in both cases, however despite sinistral shearing and associated features being found within the Canisp shear zone (Beacom, 1999; Beacom et al., 2001), further field examination of this outcrop is needed to ascertain the kinematics of particular fractures. This similarity lends support to the hypothesis that 'Late Laxfordian' brittle sinistral reactivation of dyke margins also affected main stage Laxfordian shear zones within the Assynt terrane (Beacom, 1999; Beacom et al., 2001).

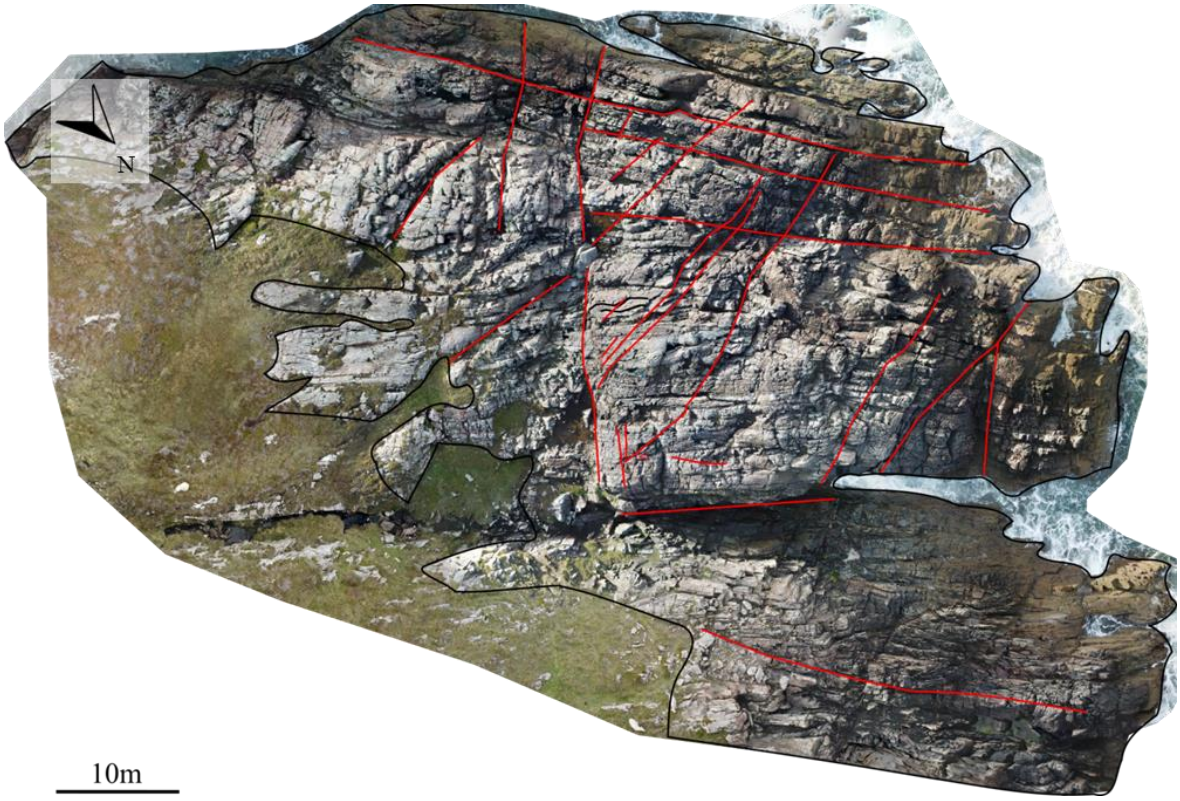

Fig 5.13. *Line drawing over aerial photo of outcrops within the Canisp shear zone at the coast showing similar patterns to those in Fig. 5.8.*

Sample AS4 was collected by R.E. Holdsworth from the southern margin of the larger dyke (similar location to sample 11; Appendix 2). It is an ultramylonite, preserving evidence of larger quartz crystals (up to 2mm) and associated subgrains (100µm), forming core-mantle structures. The subgrains show a strong CPO (see section 5.1), especially along shears sub-parallel to the dyke margin (Appendix Fig. 3.1). This sample also contains a brown, fine grained (<10µm), heavily deformed fault rock containing 5-10% fractured clasts of quartz and feldspar (~200µm), within an aphanitic, mafic matrix; it is interpreted as an ultracataclasite. This is locally weakly foliated, with debatable S-C bands giving a sinistral shear sense (Appendix Fig. 3.1b). One part of this fault rock contains 35% fractured clasts of plagioclase, epidote and quartz (~500µm), and 65% fine grained, epidote-rich matrix, and is closer to being a cataclasite (Appendix Fig. 3.1c). Clasts of plagioclase here show tapered deformation twinning on a 50µm scale.

Fluid influx: Large quartz-epidote±chlorite veins up to 5mm wide (numbered for reference, Fig. 5.8b) cut across the foliation and S-C-C' fabric of the ultramylonite; these typically run parallel to the dyke margin, and the brittle detachments within sample 11. Quartz-epidote veins (and partially infilled fractures) within sample AS4 cross-cut the ultracataclasite, and are up to 1cm wide at the dyke margin (Appendix Fig. 3.1). Clasts of wall rock are occasionally incorporated into the veins (e.g. sample 11, vein 2, clast of ultramylonite 1mm in length and 0.5mm in width).

Epidote shows a variation in crystal size, ranging from 20-600μm in sample 11, and up to 5mm in sample AS4. The smaller crystals are generally found at the edges of veins (e.g. sample 11, veins 3-4), are sometimes fibrous in nature (e.g. sample 11 veins 1-2), generally associated with chlorite (Fig. 5.10a). There is no systematic orientation of the larger epidote crystals within the veins, and they appear to lack any internal deformation. The larger crystals overgrow earlier (smaller) crystals of epidote, and the brittle shear within vein 4, as well as the small-scale breccias and cataclasites. These larger crystals appear to be somewhat younger than the smaller crystals and their associated brittle deformation. A fifth quartz-epidote vein lies sub-perpendicular to the main veins, and connects veins 1-3 (Fig. 5.8), terminating at the bottom of vein 1, and top of vein 3. This is sub-parallel to the antithetic dextral shears within the section. Where this vein crosses vein 2, its general orientation is offset 0.5cm sinistrally, with no vein margin apparent within vein 2; the mineral fills appear synchronous. This vein could represent syn-tectonic fluid influx, with the accommodation of the sinistral shearing along the parallel detachments that are the vein margins.

The average crystal size within the vein quartz is ~500μm, with larger crystals reaching 2250μm. Brittle deformation affects quartz within vein 4 (Figs. 5.8b, 5.14, Appendix Fig. 3.2), with shears running sub-parallel to the antithetic dextral shears within the section, leading to prominent areas of irregular undulose extinction within the quartz. To the

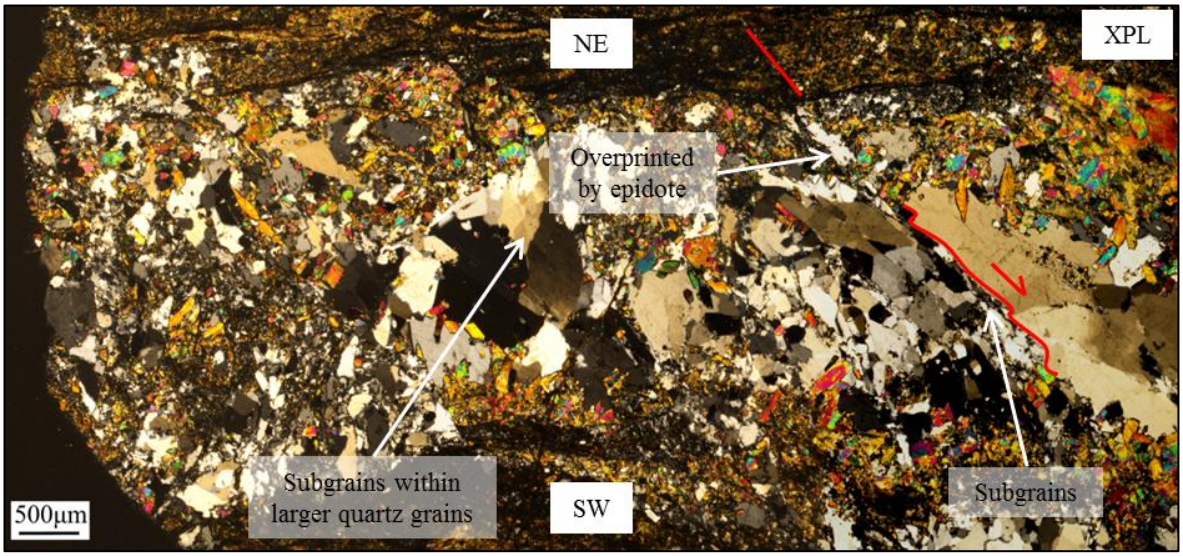

Fig 5.14. *XPL view of lower quartz-epidote vein from Fig. 5.8; subgrains line the left of the dextral shear (red), overprinted by later epidote mineralisation. Thin section taken in a dipping plane (to the NW), lineation parallel.*

northwest of this main shear within the vein, there are subgrains 50µm in length and 30µm in width, with their long axes parallel to the shear and a strong CPO. The stepped nature of the shear plane is similar to a slickenline arrangement, with this stair stepping arrangement indicating dextral shearing (Fig. 5.14). Comparatively, the quartz crystals within vein 3 are mostly equigranular (~500µm) and lack undulose extinction. The discrete shears within the section only affect vein 4, whereas veins 1-3 overprint the shears that cut across the foliations within the ultramylonite. This suggests vein 4 may have been emplaced priorto shearing, with the other veins emplaced post-shear. Quartz mineralisation appears to decrease up-section (towards the dyke margin to the NE); there may be a compositional control here, or if the veins decrease in relative age SW-NE, this may suggest a decrease in silicic fluids over time.

5.7.3. Loch Assynt: Synthesis

Complex overprinting relationships are seen on a microscale at Loch Assynt. Table 5.4 presents the observable microscale events and evidence for temperature and/or depth estimates for each. Deformation and associated mineralisation appears to be cyclic in nature, with initial sinistral ultramylonites and/or ultracataclasites (associated with early epidote) indicating high strains at the dyke margins. Grain scale deformation processes

Table 5.4. *Summary table of events recognized in thin section for the 'Late Laxfordian', their microstructures and affected minerals, and how these relate to estimates of temperature, depth and metamorphic facies.*

Event	Deformation microstructures	Minerals involved	Temperature estimates	Depth estimates	Facies
Ultramylonite formation + epidote association	BLG	Feldspar	400-600	~15km	Greenschist
	SGR	Quartz, mafic minerals?	400-500		
Epidote-chlorite mineralisation	Associated brecciation	Epidote, chlorite	<350 (Bird and Spieler, 2004)	-	Lower greenschist
Faulting	Discrete faults, pseudotachylytes	-		10-15km	
Quartz-epidote mineralisation	-	Epidote, quartz	<350	-	Lower greenschist

within the samples (pervasive BLG and SGR recrystallisation) indicate relatively low temperatures (400-500^{o}C) during deformation (Table 5.4); this is consistent with the close association of viscous mylonites and brittle fault rocks (ultracataclasite, pseudotachylyte). Viscous behaviour was locally followed by the emplacement of early, fibrous epidote-chlorite veins, characterised by the small epidote crystals. Whilst being kinematically compatible with the ultramylonite, the lack of dynamic recrystallisation of the material suggests they are not coeval features. This later fluid influx was associated with brecciation and cataclasis, mainly around the periphery of the epidote-chlorite veins, shown by the presence of early epidote within the matrix of the brittle fault rocks. The onset of more brittle, strike slip deformation ensued, with discrete, microscale sinistral faults (mainly seen within the northeastern half of sample 11; Fig. 5.8), some of which cross-cut the ultramylonite and lowest quartz-epidote vein. Foliation parallel detachments within the sample acted as pseudotachylyte generation zones. Subsequent mainly foliation and detachment-parallel quartz-epidote mineralisation post-dated earlier ductile and brittle features, along with the pre-existing epidote-chlorite vein fills. The veining is mostly accommodated along the pre-existing detachments, vein 2 for example has a particularly straight lower boundary (Fig. 5.8). The texturally close association between quartz,

epidote and chlorite within these samples is very similar to the mineralisation styles observed on 'Copper Island' where these minerals are associated and contemporaneous with local developments of copper-iron sulphides (see section 4.5). This similarity and the general abundance of fault- and fracture-hosted quartz-epidote veins in the Lewisian gneisses around Loch Assynt suggests that widespread mineralisation occurs across this locality. The sulphides have been dated at 1.55 Ga (using Re-Os geochronometry, as yet unpublished data; R.E. Holdsworth, personal communication), and are thought to be related to the sinistral 'Late Laxfordian' Loch Assynt fault (see section 4.5).

5.7.4. Achmelvich: Brittle sinistral deformation

Grain scale deformation: Gneisses at the deformed northern margin of the dyke exposed at Achmelvich South contain the average assemblage: 60% plagioclase feldspar (albite, 300μm), 25% hornblende (200-500μm), 15% quartz (up to 1.5mm), and <1% microcline (250μm). As at other localities, feldspar shows widespread sericitic alteration. Some quartz crystals are polygonal, with triple junctions and little intracrystalline deformation, indicative of GBAR recrystallisation (Fig. 5.15a). Other quartz crystals have lobate grain boundaries indicative of GBM recrystallisation, however many also contain typical flattened subgrain arrangements (100μm in length, 50μm in width) and sweeping undulose extinction, with core and mantle structures defining new grains formed by SGR recrystallisation (Fig. 5.15b). Some quartz crystals also contain fluid inclusions running ~parallel to the dyke margin within the sample. These are overprinted by perpendicular intragranular fractures up to 1.5mm in length (Fig. 5.15c). This evidence shows a retrogressive deformation history at Achmelvich which is consistent with deformation during progressive exhumation of the gneisses.

The dyke carries a remnant of schistose mylonites (1-1.5cm wide), originally developed at the dyke margin with a dextral shear sense. Dykes here have average mineralogical compositions of 50% hornblende (200μm), 30% plagioclase feldspar (100μm), 13% quartz

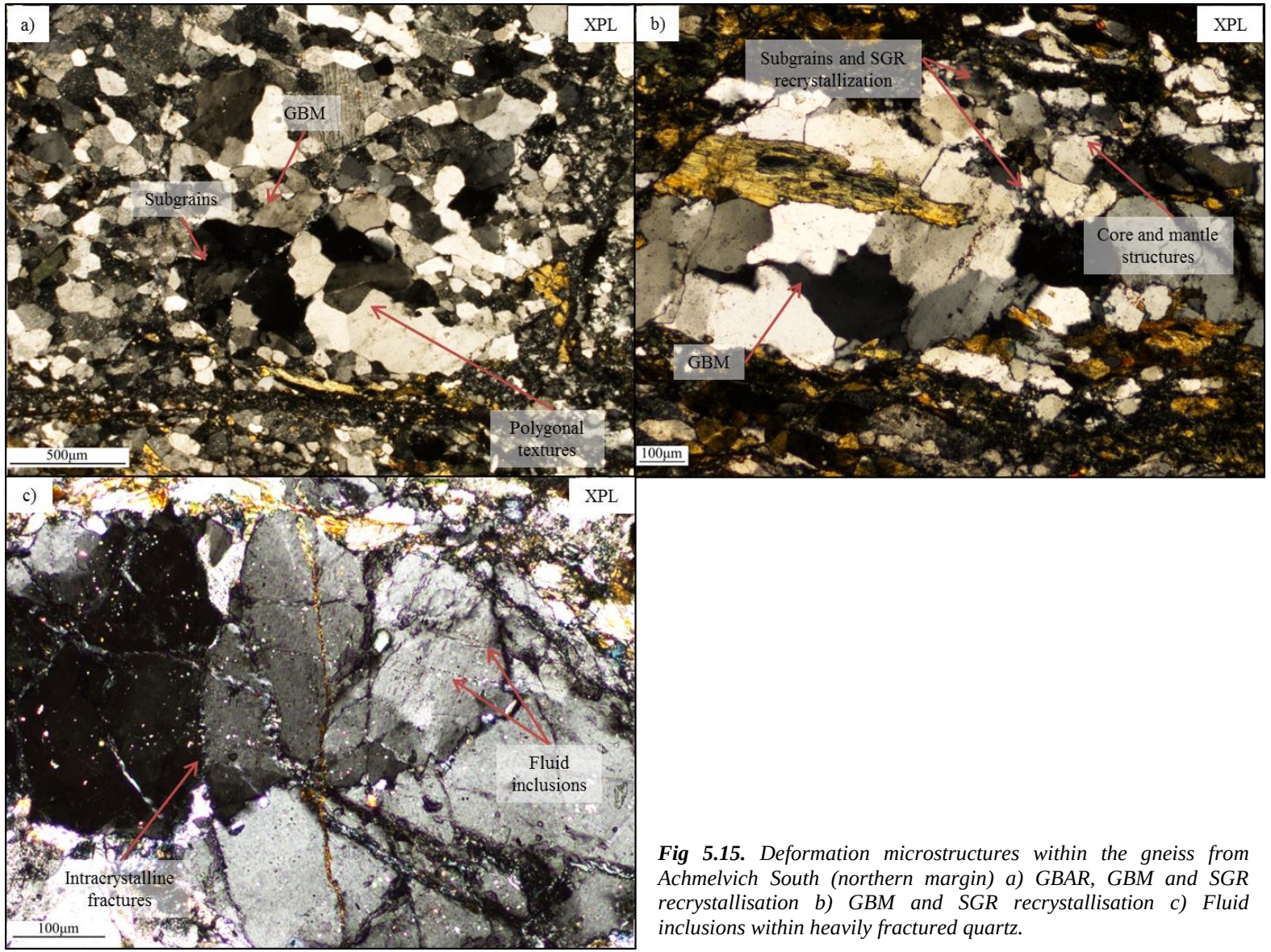

Fig 5.15. *Deformation microstructures within the gneiss from Achmelvich South (northern margin) a) GBAR, GBM and SGR recrystallisation b) GBM and SGR recrystallisation c) Fluid inclusions within heavily fractured quartz.*

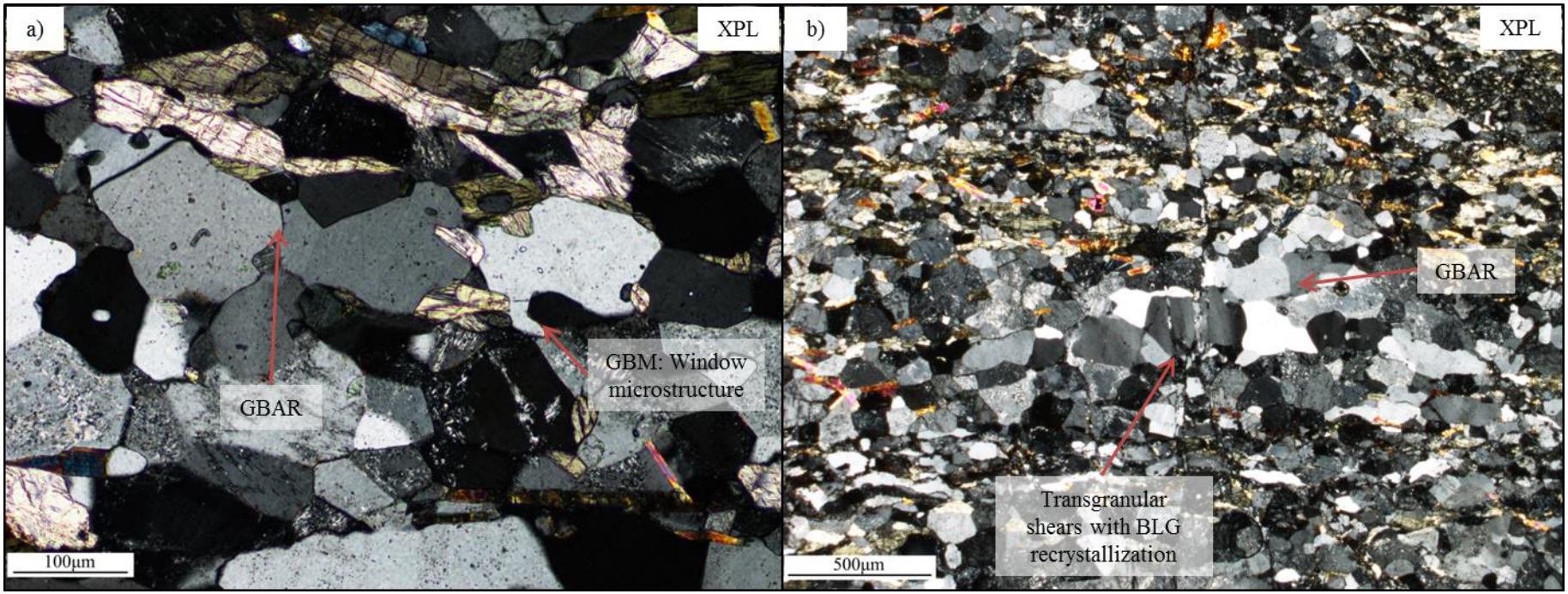

Fig 5.16. *Deformation microstructures within the Scourie dyke from Achmelvich South (northern margin) a) GBAR and GBM recrystallisation b) GBAR, GBM recrystallisation and fracturing.*

(300μm), 2% cleaved chlorite (≤750μm) and <1% monazite crystals (25μm). These latter crystals tend to contain zircons and show a fuzzy outer grain boundary. Hornblende shows some (5%) intracrystalline alteration to biotite (Appendix Fig. 3.3), showing a bimodal distribution of crystals sizes; ~50μm and ~300μm. 75% of the quartz and feldspar crystals within a quartz-rich band within the dyke typically show polygonal textures, with 120^{o} triple junctions (Fig. 5.16a), lacking a clearly defined CPO. Some quartz crystals are further deformed, with 'pinning' and 'window' microstructures (~50μm, Figs. 5.1d, 5.16a) typical of grain boundary migration recrystallisation (GBM) (Jessell, 1987). Figure 5.16b shows transgranular fractures that are accentuated by new grains from BLG recrystallisation. Nevertheless, the GBAR textures are mainly preserved.

Dyke margin brittle deformation: The dyke margins within the samples are heavily deformed by brittle deformation; representative cataclasites are composed of 15% chlorite (50μm), 10% quartz (25μm), 5-15% hornblende (30μm) and 20-60% fine grained quartzo-feldspathic matrix (<10μm). These clearly cross-cut the schistose mylonitic textures. Within the gneiss, bands of cataclasite are arranged in a Riedel shear arrangement, suggesting sinistral senses of shear (e.g. Fig. 5.17a-b); the microscale kinematics are consistent with sinistral slickenlines on faulted dyke margins at Achmelvich South (section 4.5). Cataclastic bands are, on average, at an angle of 70^{o} anticlockwise to the dyke margins. Cataclastic bands are also seen cutting the hornblende schist from the southern dyke margin (Achmelvich South), 100μm in width and up to 7mm in length (Fig. 5.18), appearing to terminate at the biotite rich layer at the top of this sample. The biotite muscovite schist contains discrete shears at a high angle to the schistose mylonitic foliation with dextral offsets of crystals of 100μm and anticlockwise block rotations of quartz clasts (Appendix Fig. 3.4). These shears are sub-parallel to the aforementioned cataclastic bands within the hornblende schist.

Fig 5.17. *Achmelvich South (northern margin); sinistral injection veins of pseudotachylyte overprinting cataclastic banding and some relict dextral mylonitic fabric within the gneiss. Thin section taken in a dipping plane (to the SE), lineation parallel. a) XPL whole section view b) Labelled line drawing – same scale as photomicrograph c) PPL view of flow textures within the pseudotachylyte injection vein, arrow represents direction of flow.*

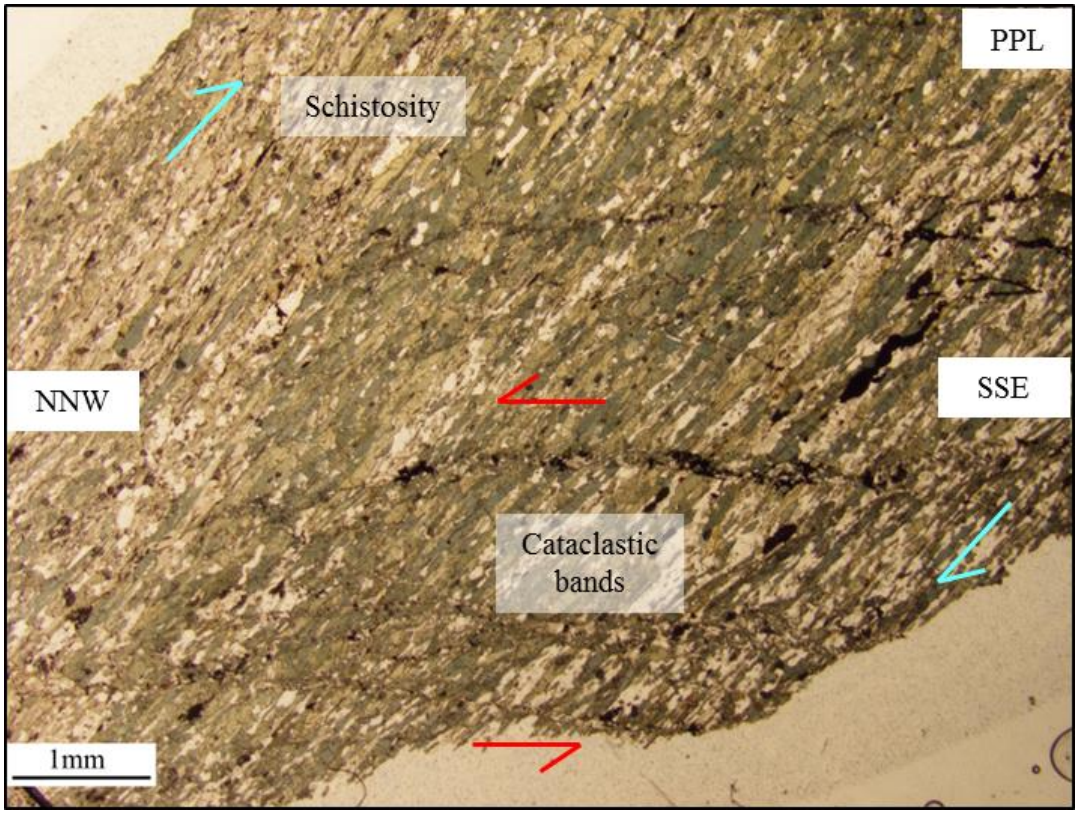

Fig 5.18. *Cataclastic bands within the hornblende schist at the dyke margin of Achmelvich South (southern margin), focussed in the hornblende rich part of the sample. Blue; ductile behaviour, red; brittle behaviour. Thin section taken in a horizontal plane, lineation parallel.*

Hornblende crystals within the dyke show zones of deformation ~5 µm in width perpendicular to the long axes of the crystal in samples from both the northern and southern dyke margins at Achmelvich South (Fig. 5.19). These do not show even spacing, with intervals of 20-100µm. These are kink bands (Fig. 5.1g), with a left-lateral offset of the cleavage across them; these are indicative of sinistral shear (Fig. 5.5, Vernon, 2004), with slip parallel to the main cleavage shown in Figure 5.19.

All samples of the dyke margin from this locality contain a dark brown fault rock that cross-cuts the cataclasite at the dyke margins and is also intermixed with the cataclastic bands (Figs. 5.17, 5.20). This is a pseudotachylyte which locally contains clasts of the cataclasite and gneiss ~500µm in diameter (Fig. 5.20). Zones of cataclasite border the pseudotachylyte veins irregularly (Fig. 5.20), which indicates cataclasite formation predates the subsequent assimilation and melting during pseudotachylyte generation.

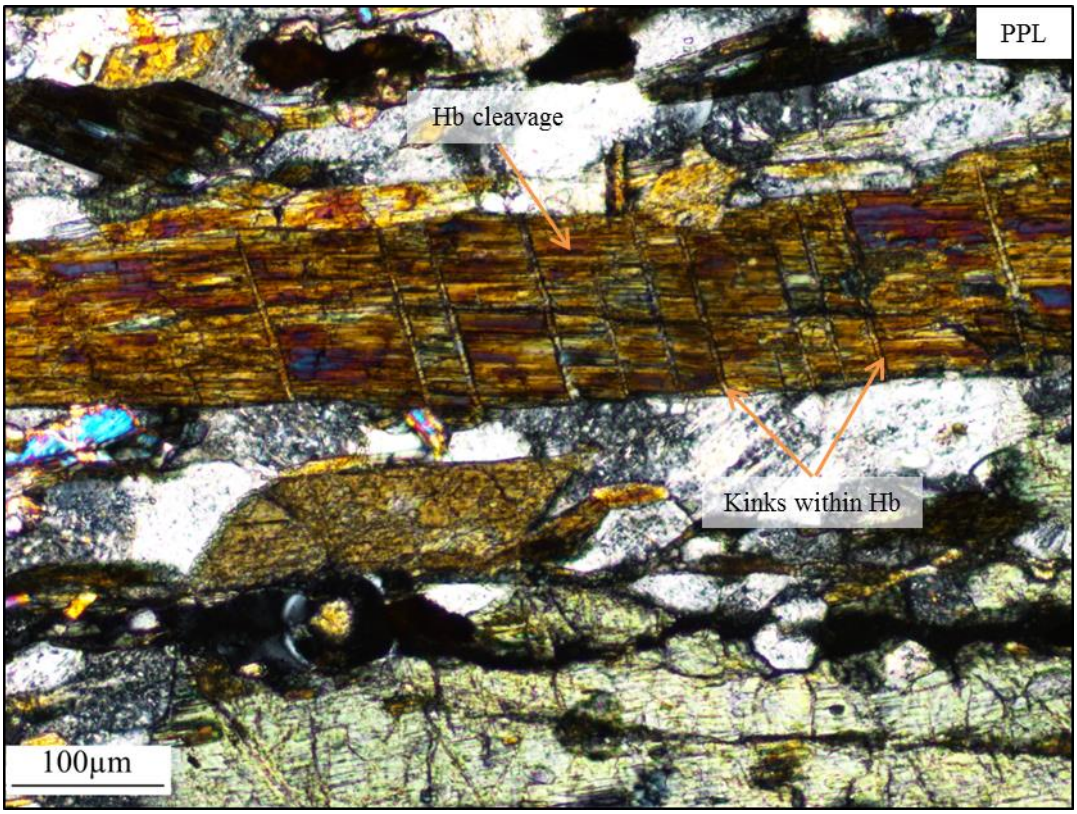

Fig 5.19. *Kinking within a hornblende crystal within the biotite muscovite schist from Achmelvich South.*

All Clasts of wall rock are common as nucleation sites for microlitic textures in the friction melts. Offshoots of the pseudotachylyte into the gneiss sub-parallel to cataclastic bands are very common, reaching up to 2cm in length (e.g. Fig. 5.17c). Compositional layering is preserved within the pseudotachylyte, with bands of darker brown and green-brown visible (Fig. 5.17c). Within the offshoot in Figure 5.17c, greenish-brown layers at the end furthest from the dyke margin contain rounded clasts of the darker brown layers below this, from the end closest to the dyke margin. The evidence stated above indicates that several generations of melt phases are present, with evidence for this including; microlitic/spherulitic texture; glass and; flow textures (Maddock, 1983; Maddock et al., 1987; Magloughlin and Spray, 1992; Sibson et al., 2006). This fault rock can therefore confidently be defined as a pseudotachylyte, generated under repeated episodes of sinistral shear. Some brecciation of the pseudotachylyte at the dyke margin is observable within samples ACH1 and AM, collected by R.E. Holdsworth from the northern dyke margin at Achmelvich South (Appendix 2), with pseudotachylyte clasts preserved in a (lighter

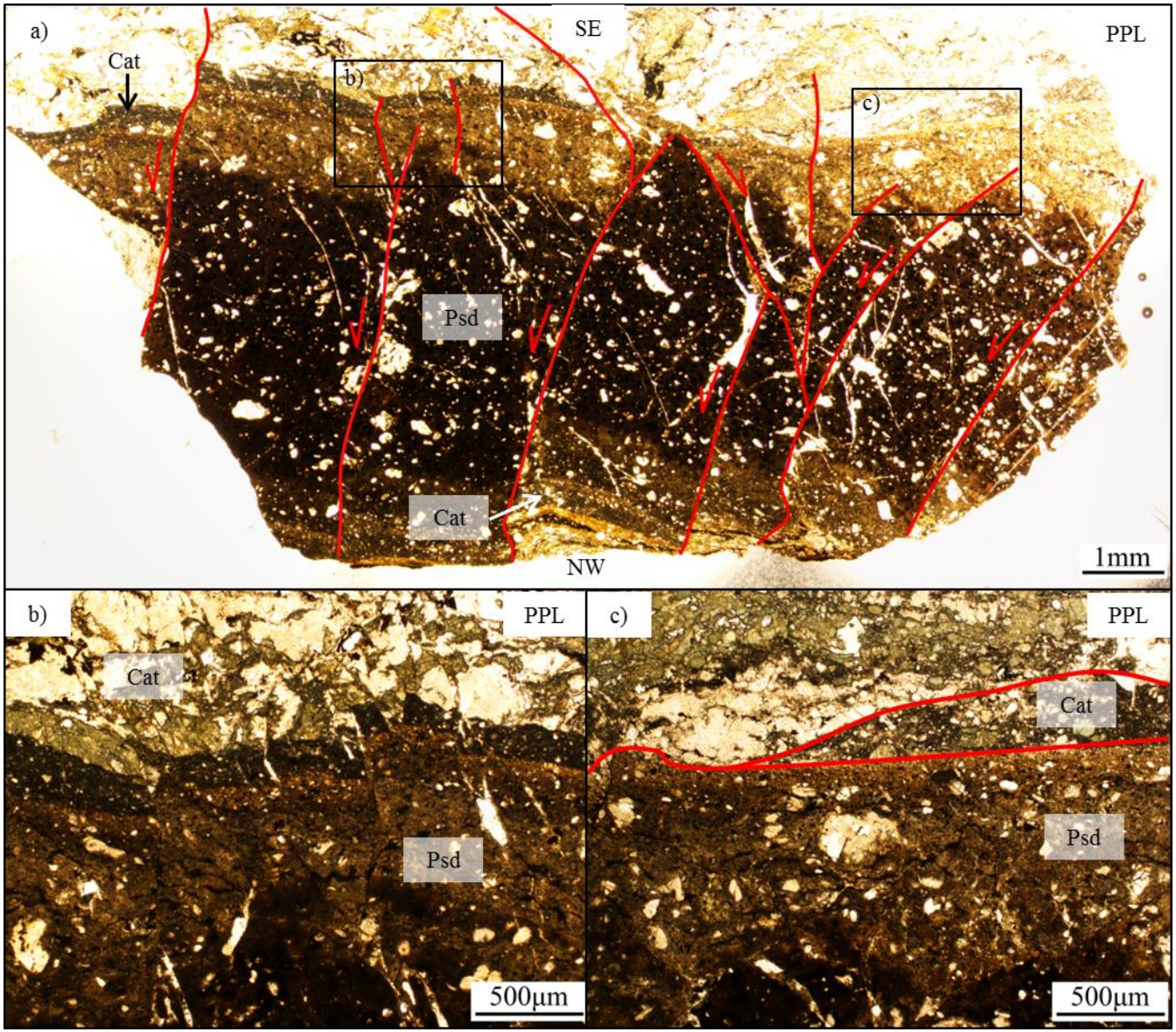

Fig 5.20. *a) PPL view of relationships between pseudotachylytes (psd) and cataclasites (cat), cross cut by later sinistral and antithetic dextral shears b-c) Zoomed in sections of cataclasis. Thin section taken in a dipping plane (to the ESE), lineation parallel.*

brown) pseudotachylyte matrix within the dyke (Fig. 5.21). Discrete sinistral shears cutting across and offsetting clasts by 100µm trend top right to bottom left. These shears connect the dyke margin to the edge of the brecciation zone, with the overall structure somewhat similar to sidewall rip-out (Swanson, 1989) occurring during cyclic sinistral pseudotachylyte generation along the dyke margin.

Calcite (≤5mm) and zeolite (50-300µm) mineralisation occurs in close proximity to the dyke margins at both localities at Achmelvich (Fig. 5.22a, Appendix Figs. 3.5-3.7). Mineralisation parallel to the dyke margins at Achmelvich South is up to 1.5mm in width, with offshoot veins extending into the pseudotachylyte associated with brecciation (Fig.5.22). The mineralisation is therefore younger than the main episode of sinistral shearing that is associated with pseudotachylyte generation. In thin section, calcite + zeolite injection veins show both top to the left and top to the right opening directions (e.g. Fig. 5.22a), making it difficult to interpret a shear sense from microstructural evidence

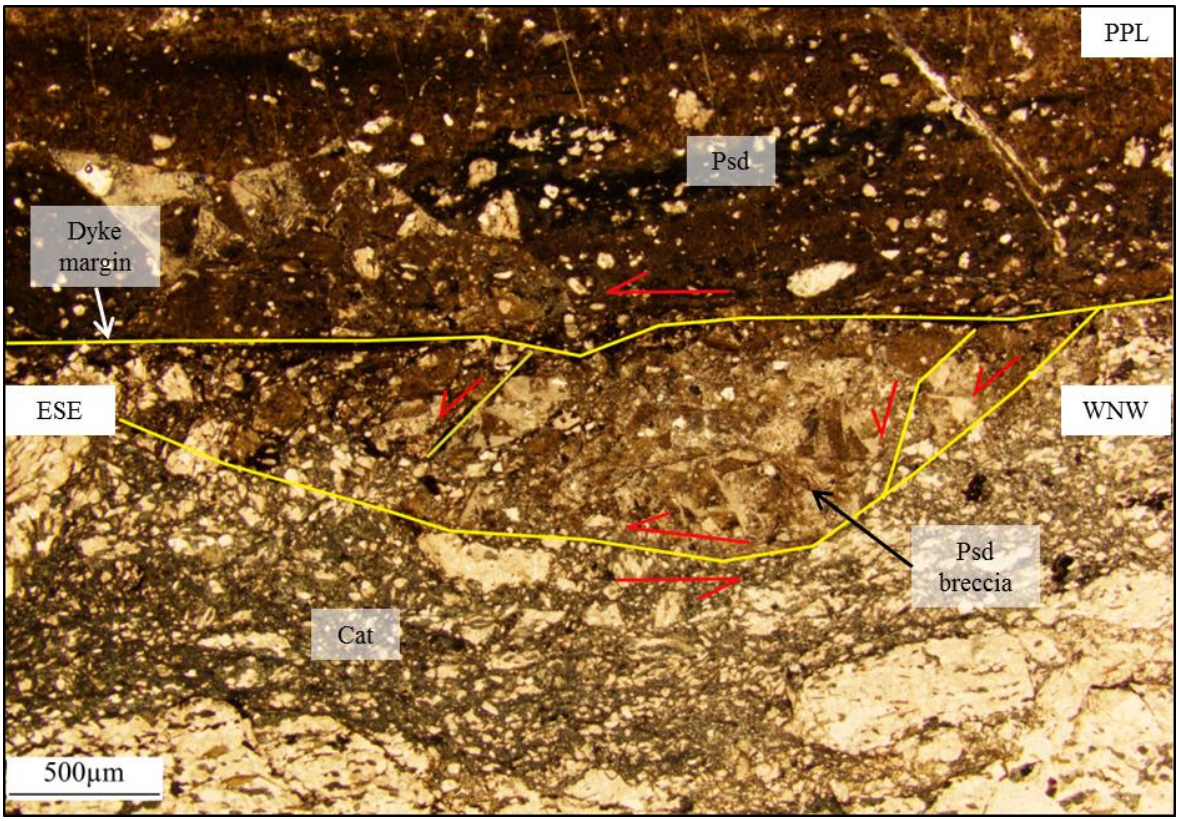

Fig 5.21. *Achmelvich South (northern margin): Sidewall ripout at the dyke margin, sinistral shear sense indicated (Swanson, 1989). Contains clasts of brecciated pseudotachylyte within a pseudotachylyte matrix, new pseudotachylyte generated at the dyke margin. Cataclasite seen below.*

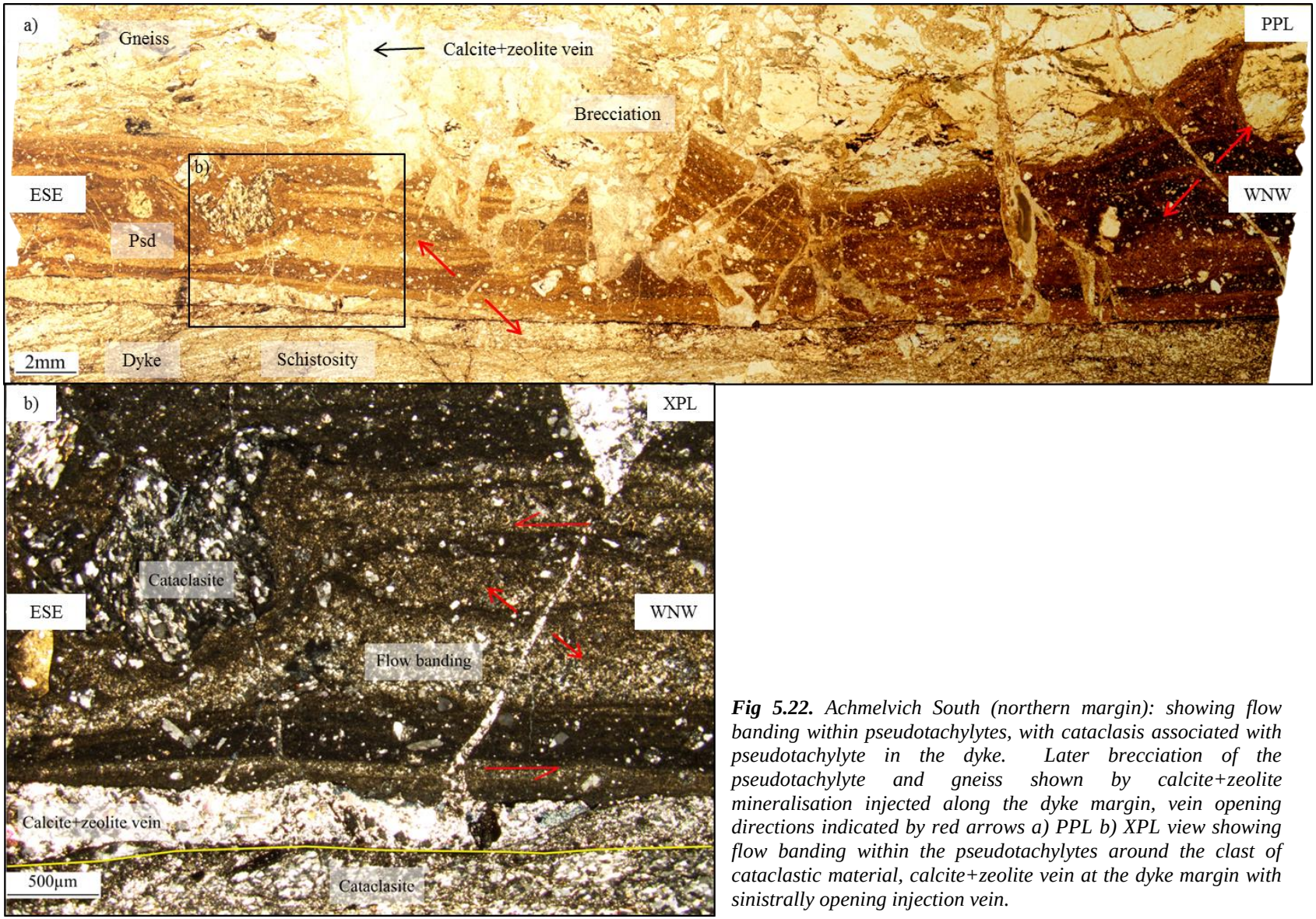

Fig 5.22. *Achmelvich South (northern margin): showing flow banding within pseudotachylytes, with cataclasis associated with pseudotachylyte in the dyke. Later brecciation of the pseudotachylyte and gneiss shown by calcite+zeolite mineralisation injected along the dyke margin, vein opening directions indicated by red arrows a) PPL b) XPL view showing flow banding within the pseudotachylytes around the clast of cataclastic material, calcite+zeolite vein at the dyke margin with sinistrally opening injection vein.*

alone. Brecciation has produced angular clasts ≤5mm of pseudotachylyte, which show clockwise rotations where their original position can be identified (Fig. 5.22a).

Pseudotachylyte and gneiss are cross cut by small-scale shears (Figs. 5.20, 5.23) offsetting markers such as cataclasite-pseudotachylyte contacts and a 500µm wide zeolite vein by up to 1.5mm sinistrally. These shears are more prominent within the pseudotachylyte and cataclasite; some of the shears do not extend into the gneiss, perhaps having taken advantage of structures already present within the pseudotachylyte, e.g. natural variations in the structure of the darker brown layers (Fig. 5.20). Some of these shears dip in the opposite direction, and show right lateral offsets of marker layers. All shears within this sample have a Riedel shear arrangement, with a sinistral shear sense indicated (Fig. 5.23)

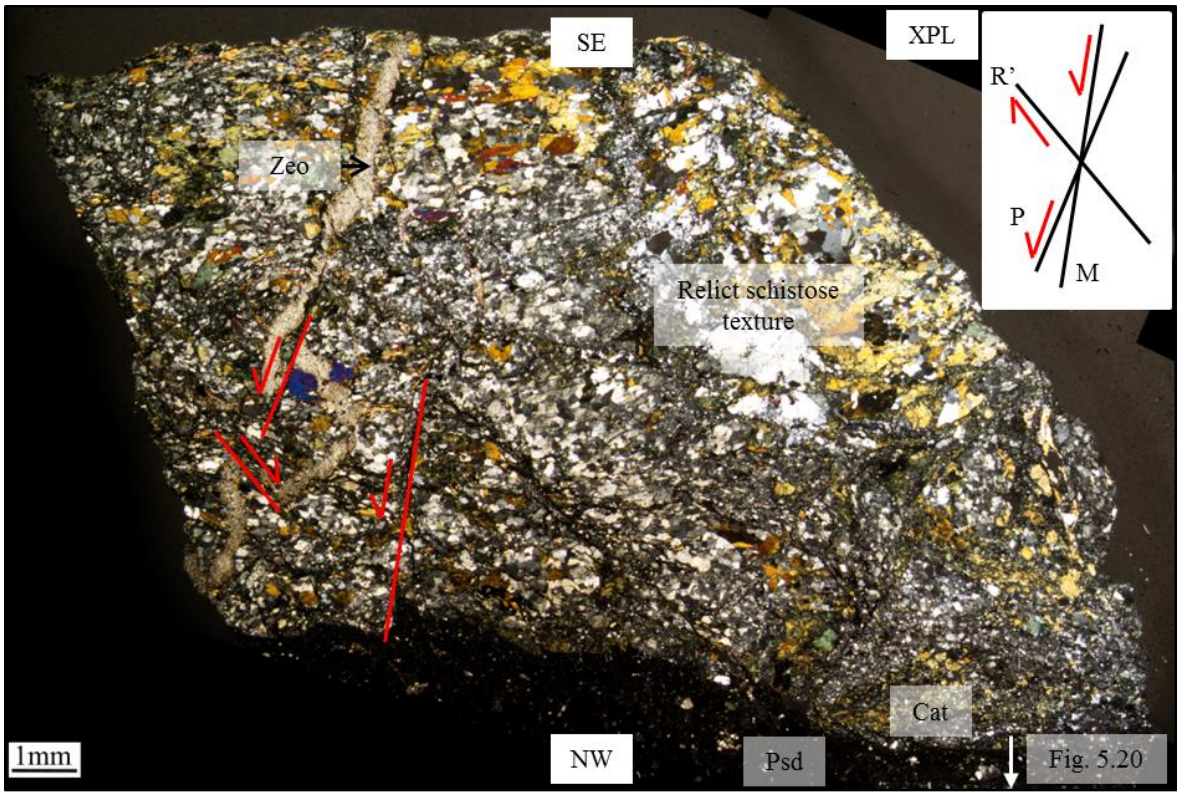

Fig 5.23. *Achmelvich South (northern margin): XPL view of upper part of section from Fig. 5.18, relict dextral schistose texture overprinted by cataclastic bands and a large zeolite vein, later cross cut by brittle shearing. Sinistral shear arrangement indicated. Thin section taken in a dipping plane (to the ESE), lineation parallel.*

5.7.5. Achmelvich South: Calcite twinning

Calcite twinning in naturally deformed samples can be used as a piezometer; twins are easily measured and can therefore be used to estimate stress conditions in rocks (e.g. Turner, 1953; Tullis, 1980; De Bresser and Spiers, 1997). Rowe and Rutter (1990) and Rybacki et al (2013) have shown experimentally that twin density in calcite (per mm^2) is related to the differential stress applied to the crystals. The main purpose of using a calcite piezometer in this study is to determine approximate stress estimates for events relating to the 'Late Laxfordian'. Samples from this study can therefore be used to determine the stress condition within the veins during their deformation, with comparative analysis of different crystals within the same vein used to determine how the stresses changed with distance from the dyke margin.

Samples ACH1 and AM, collected from the northern dyke margin at Achmelvich South, contain large calcite crystals, commonly with Type II deformation twinning at angles of $120/60^o$ (e.g. Fig. 5.24). In sample ACH1, the twinning ranges from up to three sets at the dyke margin (base of the vein), down to just one set furthest from the dyke margin. Twins are especially clear in XPL, but show different orientations in different crystals, with one twin set always parallel to the vein margin (Fig. 5.24). Visual observations suggest a decrease in twinning moving away from the dyke margin, with thicker twins at the dyke margin and one set of twins always forming at a closer spacing than other sets within each crystal. Kinked twins are present within one of the calcite crystals close to the dyke margin.

Twin density was calculated by eye; counting the number of twins in a representative area of $1mm^2$ using the drawing package Inkscape (Appendix Fig. 4.1a). It is likely there would have been some human error with this method, especially where the twins were particularly thick or where there was a high twin density (>1 twin/5μm). It is also worth noting that these calculations are only for one sample; further analysis is required to

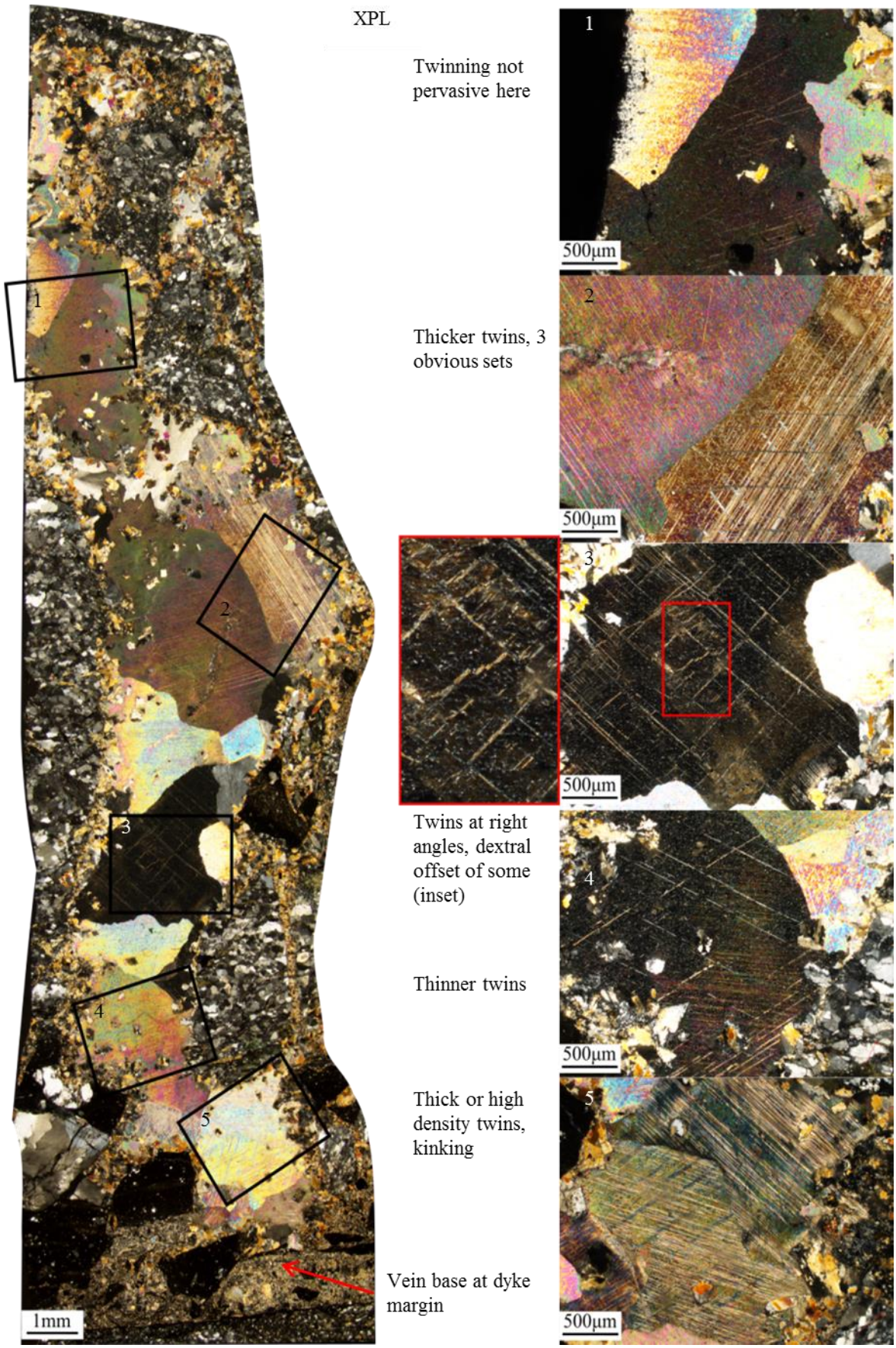

Fig 5.24. *Calcite vein from Achmelvich South (northern margin): XPL view of the whole vein, vein base taken to be the base of the larger calcite crystals at the dyke margin, zoomed sections of individual crystals in the orientations that best show twinning.*

provide a more reliable stress estimate. Using the calculations from Rybacki et al (2013) (see Appendix Table 4.1, Fig. 4.1b) for the calcite + zeolite vein in sample ACH1 (Fig. 5.24), values for the differential stress (σ) vary from 335 MPa closest to the dyke margin, to 194 MPa furthest away from the margin. When plotting the (exponential) distance from the dyke margin and σ against twin density, they show very similar patterns (Appendix Fig. 4.1c); σ decreases with decreasing twin density (R^2=0.99), with lower twin densities occurring further from the dyke margin/base of the vein (R^2=0.95). This indicates the highest differential stresses occurred at the dyke margin, which is to be expected.

5.7.6. Achmelvich: Synthesis

Brittle sinistral features overprint and postdate relict schistose mylonites (likely relating to the main phase of Laxfordian shearing along the CSZ, see section 4.5). Cataclasis at least locally occurred as a pre-cursor to the development of the pseudotachylytes, which show evidence for generation during sinistral shear along the dyke margins. These are therefore likely to be similar to the sinistrally generated 'Late Laxfordian' pseudotachylytes from Loch Assynt, perhaps of a similar age. Brittle deformation and calcite + zeolite mineralisation at Achmelvich South, however, will have occurred closer to the zeolite facies regime; vein zeolites are common retrogressive assemblages within orogenic belts, precipitating from the dissolution of feldspars within gneisses (or granites) within the 'zeolite window' (<250^{o}C), commonly growing on a substrate (e.g. calcite) (Weisenberger, 2009). Zeolites have been identified as being important components of fault rocks in the late stages of exhumation of fault zones (Dempsey et al., 2014; Crider, 2015; Forand et al, 2018; Axen et al, 2018).

Zeolite mineralisation is present within the central pull apart within the dyke, which shows the same strike as tensile fractures and pseudotachylyte injection veins within the gneiss (see Achmelvich South field map and section 4.5). Both the pseudotachylytes along the dyke margin and the calcite + zeolite mineralisation were generated in sinistral oblique

shear regimes. It is therefore assumed that the calcite + zeolite mineralisation occurred after, but within the same event as, pseudotachylyte generation (the 'Late Laxfordian'). The differential stresses obtained from the calcite twinning data furthest from the dyke margin (σ=194 MPa) are most indicative of whole-rock stresses at this time. When using the corresponding shear stress value of 138 MPa (Appendix Table 4.1), these values can be compared to Figure 7.14a from (Fossen, 2010, p. 129) (Appendix Fig. 4.2). This appears to lie close to the line for Coulomb fracture criteria (μ=0.6) where it intersects the second largest Mohr circle. However, it must be noted that the diagram in Fossen (2010) is schematic, and at these stress values, the Coulomb fracture criterion line would be starting to flatten out.

Figure 3A from Lacombe (2007) (Appendix Fig. 4.3) can be used to estimate depth estimates from σ=194 MPa. A hydrostatic regime was assumed due to the syn-tectonic fluid influx (λ=0.38). Pressure estimates are not available for the 'Late Laxfordian', therefore both μ=0.9 (normally used for <200MPa) and μ=0.6 (>200MPa) values were used to calculate depth estimates. These give depth estimates of 10 and 14km respectively; this range lies within the brittle-ductile transition (see Fig. 1.2). When coupling depth estimates with earlier temperature estimates of <250^{o}C, this would place the pseudotachylyte generation event (likely related to the 'Late Laxfordian' at Loch Assynt due to identical kinematics) within the zeolite facies at Achmelvich South. Further work such as clumped isotope analysis (Bergman et al., 2013), in addition to analysing the Ca/Mg ratios through LA-ICPMS could refine these estimates.

5.8 Microstructures summary

Badcallian & Inverian: Evidence of Badcallian metamorphism and deformation can be found at Lochinver and Achmelvich South, represented by GBAR of quartz, GBM recrystsallisation of feldspar, and BLG recrystallisation of hornblende within the gneiss

(Table 5.5). GBM recrystallisation of the quartz, also at these localities, is indicative of lower temperatures, perhaps associated with the Inverian.

Scourie dyke emplacement: The chilled margins seen in the field at Lochinver are present in thin section, with crystal sizes increasing from ~50μm at the dyke margin to 2mm in the centre of the dyke. The spinifex-like texture is obvious within the thin section, indicative of a large degree of undercooling during the emplacement of the dykes (Lowrey et al., 2017).

Laxfordian: Schistose viscous mylonites at the dyke margins at Achmelvich North and the southern margin at Achmelvich South preserve S-C and S-C-C' fabric, with kinematics indicative of dextral shearing. Quartz mineralisation is seen to be syn-tectonic, with little deformed, coarser quartz grains preventing pinning, with the vein margins following the S-C banding within the mylonite. SGR recrystallisation of quartz is common (Table 5.5).

'Late Laxfordian': Loch Assynt is the type-locality within this study of 'Late Laxfordian' deformation. Sinistral ultramylonites prevalent at the dyke margins also preserve evidence of BLG recrystallisation of feldspar and SGR recrystallisation of quartz (Table 5.5). These ultramylonites are cross-cut by discrete brittle sinistral shears associated with pseudotachylytes, and later quartz-epidote mineralisation. This has also been seen on 'Copper Island' with accompanying Cu mineralisation, dated using Re-Os geochronology at 1.55 Ga. The northern dyke margin at Achmelvich South also preserves brittle sinistral deformation: cataclasis and 1-2cm thick pseudotachylytes at the dyke margin, preserving characteristic flow structures (Maddock, 1983; Maddock et al., 1987; Magloughlin and Spray, 1992; Sibson et al., 2006), and sinistral injection veins. Sinistral zeolite+calcite mineralisation and brecciation cross-cuts the pseudotachylytes. Twinning within the calcite was used as a piezometer to tentatively estimate whole-rock differential stresses of 194 MPa, and therefore depths of 10-14km. Coupled with temperature estimates of <250^{o}C, this places the 'Late Laxfordian' within the brittle-viscous transition.

Table 5.5. *Summary of deformation mechanisms found in each locality in the gneiss and the dyke. Minerals affected are indicated: Qtz, Quartz; Hb, Hornblende; Fsp, Feldspar.*

Deformation mechanism	**Locality**							
	Lochinver		Achmelvich North		Achmelvich South		Loch Assynt	
	Gneiss	Dyke	Gneiss	Dyke	Gneiss	Dyke	Gneiss	Dyke
Brittle deformation					✓	✓	✓	✓
Kinking					✓ Hb	✓ Hb		
BLG recrystallisation	✓ Qtz, Hb						✓ Fsp	
SGR recrystallisation	✓ Qtz	✓ Qtz	✓ Qtz		✓ Qtz		✓ Qtz	
GBM recrystallisation	✓ Qtz, Fsp				✓ Qtz, Fsp			
GBAR recrystallisation	✓ Qtz				✓ Qtz			

6. Summary and Discussion

The new field and microstructural observations of structures and associated fabrics spatially associated with the Scourie dykes seem to be broadly consistent with the current understanding of tectonometamorphic episodes affecting the Lewisian Complex. In particular, the Scourie dykes have been observed to cross cut both Badcallian (ca. 2.75 Ga) and Inverian (ca. 2.5 Ga) fabrics and structures. In turn, the dykes are themselves deformed and cross-cut by dextral Laxfordian (ca. 1.75 Ga) and sinistral 'Late Laxfordian' (ca. 1.55 Ga) fabrics and structures. The two post-dyke events are associated with localised syn-tectonic fluid influx, using the dyke margins as conduits, and this has directly influenced the resulting deformation style along the dyke margins. Figure 6.1 summarizes the deformation history of the Assynt terrane, including the field relationships of dyke margin reactivation, with Figure 2.3 providing a timeline of events. Table 6.1 presents the localities where each event can be found.

6.1 Summary

6.1.1. Lewisian Gneisses: Badcallian and Inverian deformation

Lewisian gneisses at all field localities show evidence for pre-dyke folding, and this is especially prominent at Achmelvich South (section 4.1). The shallowly dipping axial planes are likely to be representative of Badcallian structures (Davies, 1976). However, it is difficult to distinguish between Badcallian and Inverian folding on geometry alone; Badcallian folds are cross cut by pegmatites, and these pegmatites are deformed by later Inverian deformation (Evans and Lambert, 1974). Steeply NE dipping foliations at Achmelvich North are indicative of deformation and foliation tilting associated with the Inverian Lochinver monocline on the southern side of the Canisp Shear Zone (CSZ) (Evans and Lambert, 1974), whereas Badcallian foliations striking NE-SW at the other field localities are prevalent, indicating the monocline had a lesser effect at these localities (section 4.1).

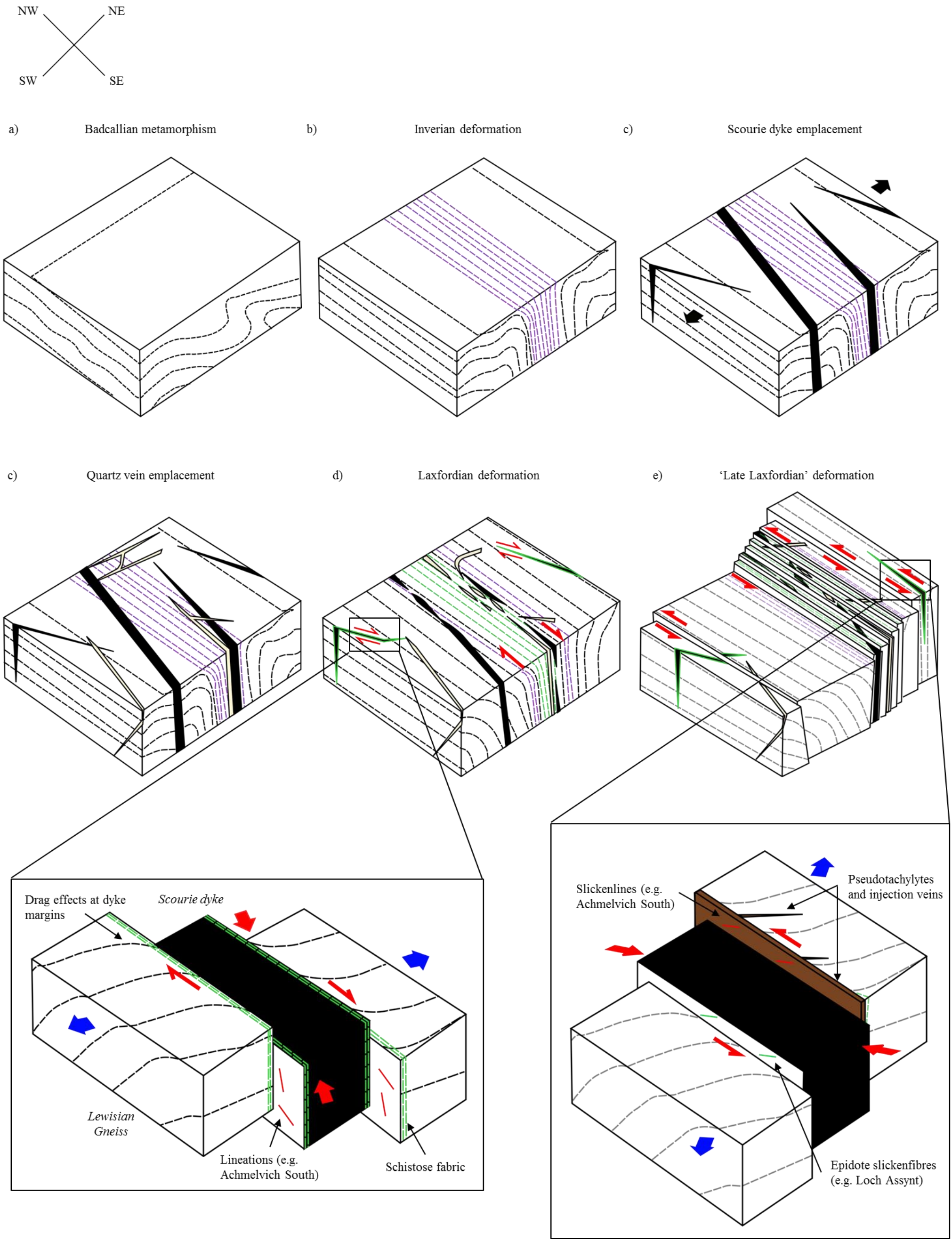

Fig 6.1. *Schematic block diagrams illustrating the tectonometamorphic history of the mainland Lewisian from the Late Archaean (Badcallian) to the Mesoproterozoic ('Late Laxfordian'). Diagrams are not drawn to scale. Insets to parts d and e show the affect of these deformation events on the Scourie dyke margins, as observed in the field, schematic compression (red) and extension (blue) shown (adapted from Pless, 2012). See Table 6.1 for localities where these events are preserved.*

Table 6.1. *Preservation of different events at the four main field localities, one tick: present; two ticks: extensive.*

Locality	**Event**				
	Badcallian	Inverian	Ductile dextral	L. Laxfordian ductile	L. Laxfordian brittle
Lochinver	✓	✓			
Achmelvich North	✓	✓	✓✓		✓
Achmelvich South	✓	✓	✓		✓✓
Loch Assynt	✓	✓		✓✓	✓✓

Table 6.2 summarizes the different deformation microstructures found within the Lewisian gneisses from the main localities that may be used to estimate associated syn-tectonic temperatures. These microstructural observations (see section 5) suggest that temperatures decrease over time, indicating a progressive exhumation of the region with deformation over time (Fig. 6.2, section 6.2.1), however pressures are difficult to estimate; estimates from the literature are detailed in section 6.2.1. Microstructural textures and inferred deformation mechanisms associated with the Badcallian (Table 6.2) are preserved within quartzo-feldspathic gneisses at Lochinver and Achmelvich South (GBAR, GBM recrystallisation). These are locally overprinted by textures associated with lower temperature deformation mechanisms and in places this later deformation obliterates Badcallian textures. For example, the ultramylonites at Loch Assynt (section 5.7.1) display lower temperature (400-600^{o}C) deformation mechanisms (SGR, BLG recrystallisation) than Badcallian deformation mechanisms (800^{o}C) (Table 6.2).

6.1.2. Undeformed Scourie dykes and early quartz veins

Within the Scourie dykes, relict igneous textures and features associated with igneous intrusions are preserved on outcrop and microstructural scales. These include chilled margins, baked gneiss, cooling joints and xenoliths. The former are observable at

***Table 6.2**. Deformation microstructures and their inferred temperatures from microstructural observations, with associated possible events postulated. Abbreviations defined within section 5.1. For more details on Laxfordian and 'Late Laxfordian', see Tables 5.3 and 5.4 respectively.*

Main area(s) present	**Deformation mechanisms**	**Mineral affected**	**Indicated temperatures (ºC)**	**Likely event**
Lochinver, Achmelvich South	GBAR	Quartz	~800	Badcallian
Lochinver, Achmelvich South	GBM recrystallisation	Feldspar	~800	Badcallian
Lochinver	BLG recrystallisation	Hornblende	>700	Badcallian
Lochinver, Achmelvich South	GBM recrystallisation	Quartz	500-600	Inverian/Laxfordian
Loch Assynt, Achmelvich South	SGR recrystallisation	Quartz	400-500	Laxfordian/'Late Laxfordian'
Loch Assynt	BLG recrystallisation	Feldspar	400-600	Laxfordian/'Late Laxfordian'
Loch Assynt	Epidote + chlorite/epidote + quartz mineralisation	-	<350	'Late Laxfordian'
Achmelvich South	BLG recrystallisation	Quartz	~300	'Late Laxfordian'
Loch Assynt, Achmelvich South	Fracturing/faults, cataclasis/breccia	All	<300	'Late Laxfordian'
Achmelvich South	Zeolite mineralisation	-	<250	'Late Laxfordian

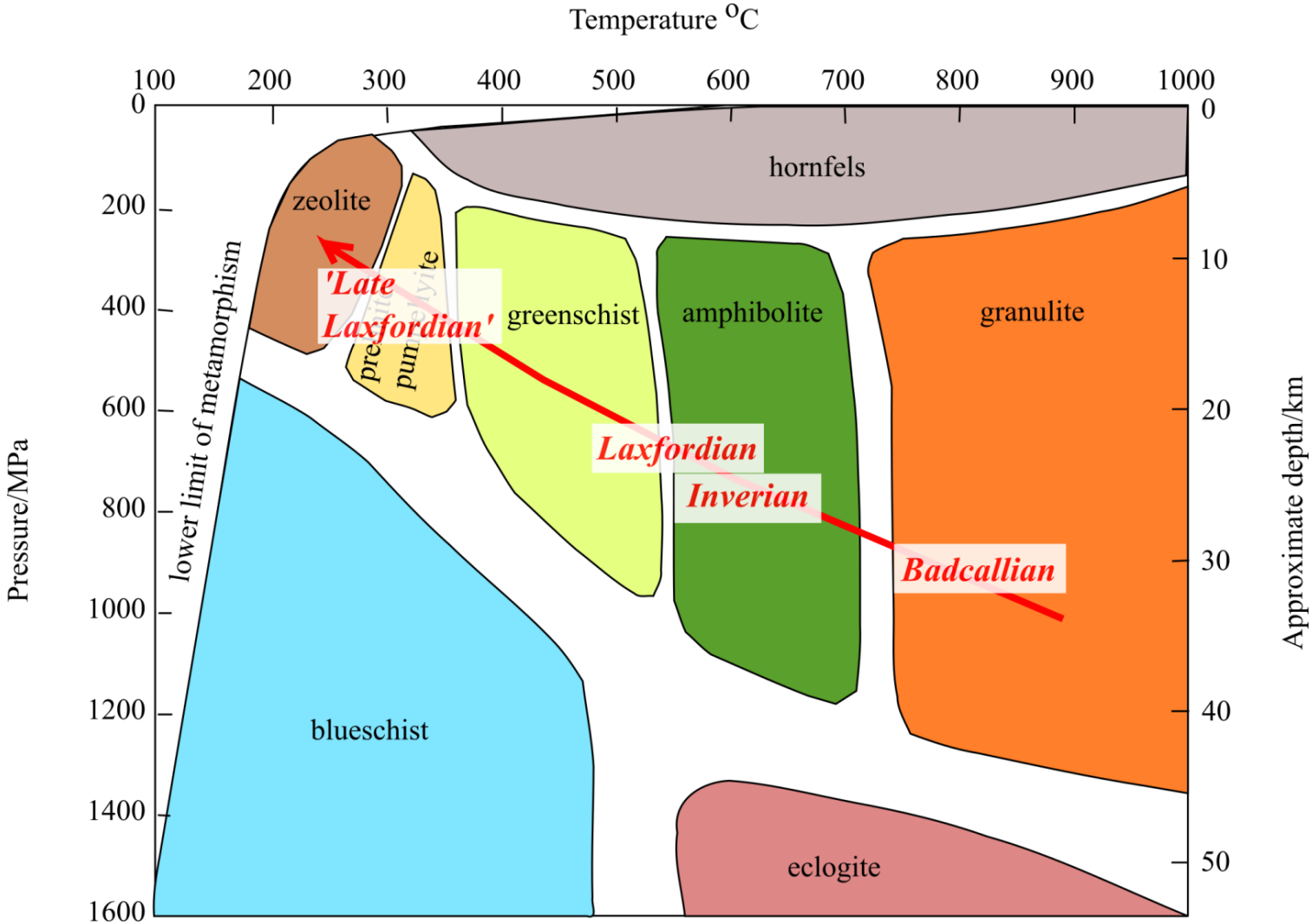

Fig 6.2 *Estimated temperatures and pressures of Archaean and Proterozoic events affecting the Lewisian gneiss, with the Laxfordian and 'Late Laxfordian' also affecting the Scourie dykes.*

Lochinver, which Tarney (1973) suggests to be indicative of dyke-emplacement into somewhat cooler country rock. The orthogonal, spinifex-like textures observed in the field and in thin section indicate undercooling of the magma during emplacement (Lowrey et al., 2017). The upper boundary of the chilled margin in the field corresponds to the sharp upper margin of the spinifex-like texture. This is followed by the small grain size decrease and resumption of the chilled margin, suggesting later intrusion events after the dyke had been emplaced. This is fairly likely, as the igneous province was seemingly long lived (~40 Ma) (Davies and Heaman, 2014), with two main doleritic intrusion events hypothesized (Evans and Tarney, 1964). Xenoliths (Achmelvich North) may preserve pre-Scourie dyke metamorphic assemblages due to the localisation of strain at the dyke margins and other preexisting anisotropies (MacDonald et al., 2017). Earlier Scourie dykes show a higher degree of metamorphism compared to those intruded later, which indicates their emplacement during, and towards the close of a metamorphic episode. Early dykes also preserve coarse grained margins and a complex crystallisation history; viscosity contrasts, rather than temperature contrasts are suggested to play a part in the formation of the chilled margins within the basic dykes (Tarney, 1963). These observations are consistent with the dykes being emplaced at mid-crustal depths (Tarney, 1973; Wheeler et al., 2010). Timing and placement of these dykes indicates they may have formed during post-collisional (NE-SW) extension (Goodenough et al., 2010). It is likely that the Scourie dyke swarm represents the deep crustal plumbing of a large igneous province, potentially spanning across several cratons (Davies and Heaman, 2014), showing extension and igneous activity were prevalent during this period.

Widespread NE-SW trending quartz veins cross cutting the Scourie dykes at Loch Assynt have been studied by Vernon et al (2014). The quartz-pyrite veins were dated, using Re-Os of pyrites, at ca. 2.2 Ga. This event is contemporaneous in the Assynt and Gruinard terranes, but notably absent within the Rhiconich terrane (Vernon et al., 2014), consistent

with terrane models suggesting amalgamation of the Assynt and Gruinard terranes prior to the Inverian, and final amalgamation of the Rhiconich terrane during the Laxfordian (summarized in Friend and Kinny, 2001).

6.1.3. Laxfordian deformation

When outlining Lewisian chronology, early work split the Laxfordian into phases of deformation based on deformation style and shear sense (Giletti et al., 1961; Evans, 1965; Moorbath and Park, 1971; Lyon et al., 1973; Chapman, 1979; Park et al., 1987; Park and Tarney, 1987). The so-called D1 and D2 deformations (ca. 1.8 Ga) are associated with normal dip slip and dextral strike slip mineral lineations (Park et al., 1987); this seems to be consistent with in situ kinematic indicators measured directly from sheared dyke margins (slickenlines) in this study (section 4.3).

Localities at Achmelvich Bay preserve evidence of dextral shearing consistent with Laxfordian shearing within the nearby CSZ (Attfield, 1987). This shearing is commonly associated with the localised development of hornblende and mica schists (Sutton and Watson, 1950), observed in the field as schistose mylonites (mainly <1m in width) along the dyke margins. The development of schistose fabrics associated with the Scourie dykes was first noted by Teall (1885), who focused in particular on the distribution, mineralogy and fabrics associated with the hornblende schist; this was discussed further by Peach et al (1907). These are important because they allow Laxfordian deformation to be placed within the viscous regime (Fig. 1.2). Laxfordian shearing along the dyke margins is also associated locally with syn-tectonic quartz mineralisation, concentrated along the dyke margins (e.g. Figs. 4.7, 5.6).

6.1.4. 'Late Laxfordian' deformation

'Late Laxfordian'/D4 shearing is recognized within the literature, commonly associated with brittle structures and NW-SE trending crush belts with pseudotachylytes and cataclasites, with low temperature mineral assemblages (including chlorite) common (Park, 1964; Moorbath and Park, 1971; Park et al., 1987; Shihe and Park, 1993; Beacom et al.,

2001). Initial K-Ar dating of gneisses and basic intrusive bodies place this ca. 1.4 Ga, however hornblendes within the gneiss, and some whole rock analyses gave ages ca. 1.52 Ga. Some ultrabasic lenses within the gneiss gave older (Laxfordian) ages of ca. 1.719 Ga (Evans and Park, 1965; Moorbath and Park, 1971).

Both outcrop and microscale structures provide evidence for a 'Late-Laxfordian' phase of sinistral shearing. Loch Assynt preserves early ductile features (ultramylonites) overprinted by discrete brittle shears and associated pseudotachylytes on a microscale, and widespread sharp, brittle shears on an outcrop-scale. Fluid influx accompanies both brittle and ductile deformation, defined by epidote lining the S-C-C' bands within the ultramylonite on a microscale, and epidote slickenfibres with clear sinistral shear sense indicators. Associated grain scale deformation processes include pervasive BLG recrystallisation of feldspar and SGR recrystallisation of quartz (section 5.7.1), indicating low temperatures and high strain during this deformation event (Tables 5.4, 6.2). Dyke margin-parallel pseudotachylytes from Achmelvich South (northern margin) and their sinistral injection veins (sections 4.5, 5.7.4) are likely to be synchronous with the phase of brittle shearing at Loch Assynt associated with pseudotachylytes (section 5.7.2). The pseudotachylytes at Achmelvich South are similar in style to the pseudotachylytes found within the CSZ; however the latter are enclosed by NW-SE foliation parallel faults (Beacom, 1999; Beacom et al., 2001), with the former associated with the NW-SE trending dyke margins. Long term structural inheritance is displayed by the NW-SE trending Inverian/Laxfordian shear zones, as well as the Scourie dyke margins, which act as a control for the later 'Late Laxfordian' faults and associated features (Beacom, 1999). 'Late Laxfordian' faults within the CSZ are commonly foliation parallel (i.e. trending NW-SE), occurring where there is little to no pre-existing folding of the gneissose foliations, for example at Alltan na Bradhan (Pless, 2012). Microstructural analysis shows that cataclasis is a commonly a precursor to frictional melting and pseudotachylyte generation at

Achmelvich South (northern margin). Pseudotachylytes within the CSZ zone show similar relationships to those within this study; the concentration of hydrous minerals within the cataclasite could lead to preferential melting of the cataclasites compared to the gneiss, coupled with the increased surface area within cataclasites due to pervasive grain scale fracturing (Beacom, 1999). Frictional sliding is most commonly accommodated within crystalline quartzo-feldspathic rocks possessing a high shear strength and significant water content locked in hydrous minerals (Allen, 1979), explaining the preferential melting of the quartzo-feldspathic gneisses compared to the ultramafic Scourie dykes (with higher melting temperature minerals) during pseudotachylyte generation. This provides some evidence of pseudotachylyte generation associated with hydrous conditions. However this is heavily debated within the literature, with some studies interpreting two 'windows' of pseudotachylyte generation. These include 'dry' pseudotachylytes forming in a single rupture event, and 'wet' pseudotachylyte, forming after the formation of a leaky damage zone (Fig. 6.3) (Bjørnerud, 2010).

Epidote mineralisation is prevalent across the locality at Loch Assynt, in particular around the dyke margins and associated with certain Late Laxfordian fault zones; microstructural analysis presents evidence of several cycles of epidote mineralisation (see section 5.7). Field evidence from 'Copper Island' shows the association of epidote, quartz and chlorite (similar to that found at dyke margins) with copper mineralisation (section 4.5). An as yet unpublished Re-Os date of the sulphides (based on methods from Selby and Creaser, [2003]) from this field locality provide an age of ca. 1.55 Ga (Holdsworth, 2018 personal communication). These dates match one outlying sample within the study by Vernon et al (2014), which gives an age of ca. 1.5 Ga, compared to ages of mostly ca. 2.2 Ga relating to the NE-SW quartz-pyrite veins. This younger age possibly represents a later pyrite mineralisation contemporaneous with the copper mineralisation on 'Copper Island'

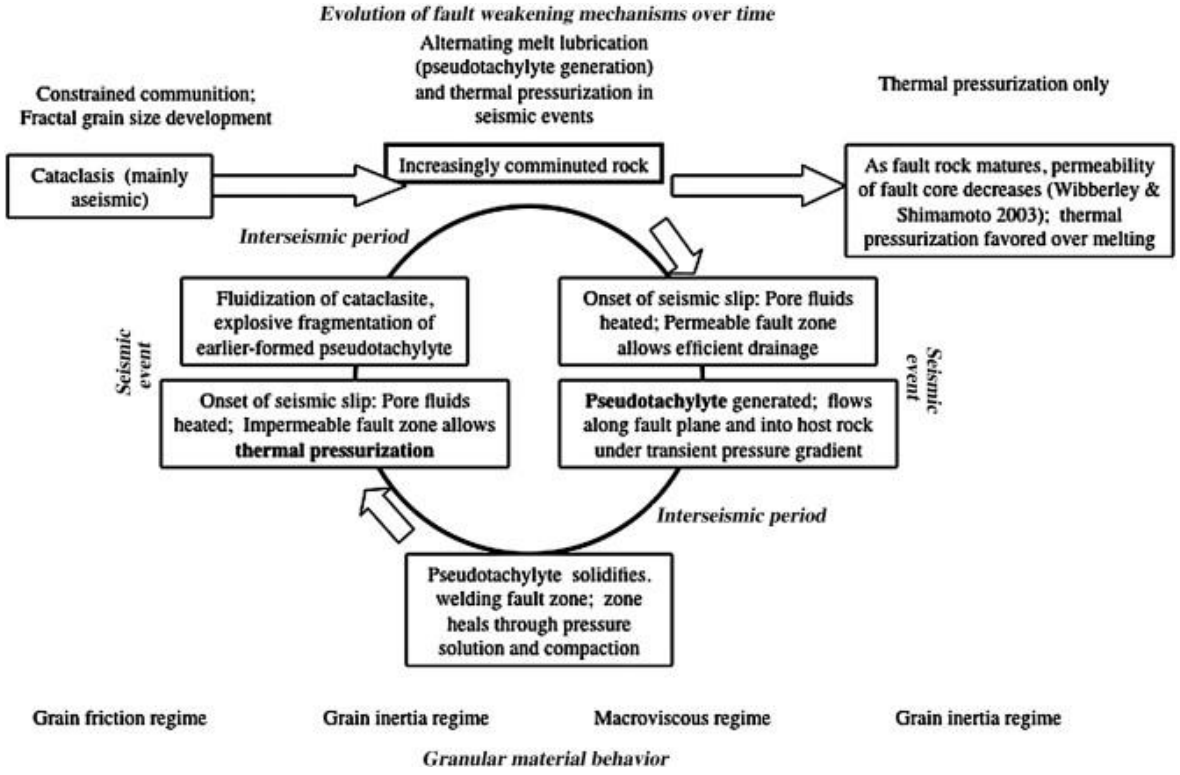

Fig 6.3. *Conceptual model of seismogenic fault zone evolution within hydrated rocks (Bjørnerud, 2010).*

(Vernon et al., 2014), and pre-Caledonian ('Late Laxfordian') movement along the Loch Assynt Fault; this pre-Caledonian movement was determined by point analysis of the fault by Krabbendam and Leslie (2010).

Brecciation and syn-tectonic calcite + zeolite mineralisation at Achmelvich cross-cuts the schistose fabric and pseudotachylytes, therefore post-dating these features, however the exact age of the mineralisation is not known. 2-5mm equant calcite crystals overgrow the gneiss within samples from Clashnessie, with these samples also containing branching cataclasite bands (Pless, 2012). Observations by Pless (2012) are concurrent with the microstructural observations from Achmelvich South within this study, indicating these localities were at similar structural levels during 'Late Laxfordian' shearing event. As the calcite crystals are found along the sinistral Loch Assynt Fault, with active within the 'Late Laxfordian', it is likely that calcite (+zeolite) mineralisation at Achmelvich South (also giving sinistral kinematics) occurred during the later stages of the 'Late Laxfordian' event, as assumed in section 5.7.6.

6.2 Discussion

6.2.1 Regional implications

The inferred temperature estimates from microstructural analysis within this study are shown in Table 6.2. GBAR and GBM recrystallisation of feldspar within samples from Achmelvich South and Lochinver are interpreted to be representative of Badcallian metamorphism, indicating temperatures ~800^{o}C. This is consistent with estimates within the literature of 710-834^{o}C (Ti-in-zircon thermometry [MacDonald et al., 2015]). Badcallian pressure estimates lie between 850-1150 MPa (mineral equilibria modelling in TTG gneisses [Johnson and White, 2011]). Temperatures within the Inverian are estimated at 520-550^{o}C (mineral equilibria modelling of metasedimentary rocks [Zirkler et al., 2012], ion-exchange thermometers on TTG gneisses [Sills, 1983]), which matches temperature estimates from the GBM recrystallisation of quartz (500-600^{o}C) within samples at Lochinver and Achmelvich South. Inverian pressures are difficult to estimate, as there are few reliable geobarometers; some estimates place pressures ~500 MPa using a gt-sill-plag-qz geobarometer (Sills and Rollinson, 1987), however it is noted within their study that garnet has a low Grossular content, and the authors are not certain that the garnet and sillimanite are in equilibrium. Comparing this to recent estimates for Laxfordian pressures of 650 MPa/24 km (ion exchange thermometry on Loch Maree Group [Droop et al., 1999]), the estimates for Inverian pressures are not likely to be correct considering the retrogressive deformation path of the complex over the period of study. It has therefore been assumed in Figure 6.2 that the Inverian lies at similar P-T conditions to the Laxfordian. Laxfordian temperatures lie at 530-630^{o}C (ion exchange thermometry on Loch Maree Group [Droop et al., 1999]), consistent with temperature estimates form the SGR recrystallisation of quartz at Achmelvich South (400-600^{o}C). Similar pressure and temperature estimates for the Inverian and Laxfordian tectonometamorphic event also take into account the similar styles of viscous deformation during both events.

Temperature estimates of the deformation at Loch Assynt during the 'Late Laxfordian' place early ultramylonite formation at 400-600ºC, with later epidote + chlorite mineralisation associated with brecciation and cataclasis at <350ºC (Table 5.4). These temperatures fall within the greenschist facies (Fig. 6.2). Deformation at Loch Assynt is assumed to be synchronous with pseudotachylyte generation at Achmelvich South due to the identical kinematics. Lower temperatures were observed during later zeolite mineralisation at Achmelvich South (<250ºC). The analysis of calcite twinning within the calcite + zeolite vein at the (northern) dyke margin of Achmelvich South provided a tentative range of depth estimates of 10-14km, and therefore pressures 300-400 MPa (Fig. 6.2). Stress was concentrated along the dyke margins; using the calcite twinning piezometer, it was determined that increasing the distance from the dyke margin produced an exponential decrease in stress. Both depth and temperature estimates place the 'Late Laxfordian' within the region of the frictional-viscous transition (see Fig. 1.2).

$^{40}Ar/^{39}Ar$ studies by Sherlock et al (2008) have dated pseudotachylytes within the Lewisian basement from the Gairloch region. Localised along NW-SE trending faults, crush breccias are associated with pseudotachylytes in narrow strands, or discrete pods. These breccias comprise randomly oriented Lewisian gneiss clasts set in a pseudotachylyte matrix. Crush belts documented by Sherlock (2008) produce similar kinematics and orientations to those documented within the CSZ (Beacom et al., 2001). The pseudotachylytes have been dated ca. 1.019 – 0.91 Ga, which would place them within the Grenvillian orogeny. Successful $^{40}Ar/^{39}Ar$ dating of pseudotachylyte relies on two main assumptions: 1) all radiogenic Ar (^{40}Ar) within the sample has accumulated since the pseudotachylyte cooled; and 2) the pseudotachylyte has not experienced heating and argon loss after formation. If the pseudotachylyte sampled has experienced multiple melting events over multiple deformation cycles, the age of the youngest event will be preserved. Within their study, Sherlock et al (2008) found clusters of older ages of pseudotachylytes

in the centre of pseudotachylyte veins. As the vein margins will be the most likely to be reactivated/re-melted during later events, this suggests that both assumptions for successful dating were not met; the ages determined may not be reliable.

Dating minerals within the host rock can provide corroborative evidence as to whether the pseudotachylyte has been reset. Within the study by Sherlock et al (2008), hornblendes give ages of 1.69-1.56 Ga (concordant with Moorbath and Park, 1971), and biotites give ages of 1.3-1.1 Ga, suggestive of a later tectonic event that did not exceed the closure temperature of Ar within the amphiboles (~550^{o}C). These later dates are consistent with the Grenville orogeny (e.g. Moorbath and Park, 1972; Cliff and Rex, 1989), and the deposition of the sedimentary Stoer Group (Turnbull et al., 1996), with some sediment (Stoer Group) filled fractures within the basement gneisses (Beacom et al., 1999). Sherlock et al (2008) interpret the hornblende ages to be related to Laxfordian cooling. Lower age limits (ca. 1.56 Ga) of the hornblende resetting event, and data suggesting amphiboles are typically reset at 500-550^{o}C, overlap with the upper limits of deformation conditions from the Re-Os dating of sulphides, which are associated with epidote mineralisation, and therefore deformation, at Loch Assynt (section 6.1.4), as well as temperature estimates from analysis of deformation mechanisms (see Table 6.2). Microstructural analysis of hornblende within samples associated with both Laxfordian and 'Late Laxfordian' deformation show microscale kinking of the hornblende, indicative of later deformation. The kinking suggests whole rock reworking; it is therefore entirely possible that the initial pseudotachylyte generation occurred at a similar time and temperature to the event resetting the hornblendes within samples in the Sherlock et al (2008) study. Subsequent events could then have locally reworked the pseudotachylytes and reset biotites to give the younger (Grenvillian) ages.

Field and microstructural analysis suggests the 'Late Laxfordian' was a regional sinistral strike slip event that predominantly localised along pre-existing anisotropies such as dyke

margins and shear zones (e.g. CSZ). The abundance of pseudotachylyte observed within these structures shows the 'Late Laxfordian' was clearly associated with seismogenesis, especially at Achmelvich South. The fault rock assemblage (pseudotachylytes, cataclasites, breccias, and ultramylonites) suggests that the majority of the deformation occurred as the rocks were exhumed through the brittle-viscous transition. The kinematics and fault rocks of the earlier ca. 1.75 Laxfordian event are very different to those associated with the ca. 1.55 Ga 'Late Laxfordian', with the latter occurring at a shallower structural level.

The 'Late Laxfordian' is referred to in the literature on outcrop, and regional scales (Beacom, 1999; Beacom et al., 2001; Pless, 2012; Vernon et al., 2014); however its significance in relation to continental scale events is little described. A continental break-up event of the Columbia supercontinent (Senshu et al., 2009; Meert, 2012) has been inferred around 1.5 Ga by Condie (2012). However other studies have postulated that amalgamation was still ongoing at this time (Cutts et al., 2013). A long lived orogenic event within Laurentia (1.8-1.0 Ga) has been suggested by Karlstrom et al (2001), which also spread to Baltica and Australia. Contemporaneous to the 'Late Laxfordian' within Baltica was the Gothian orogeny, associated with widespread crustal accretion and calc-alkaline volcanics (summarised in Gaál and Gorbatschev). Whilst these events are of similar ages to the 'Late Laxfordian', it cannot be said if, and how, they affected NW Scotland at 1.55 Ga.

6.2.2. Implications for fluid assisted weakening

Widespread microstructural evidence of fluid influx is preserved within the samples, including the undeformed dyke. This is present as the alteration of feldspar to sericite aggregates within all samples. Laxfordian shearing is shown to be associated with fluid influx (see section 5.4), including the syn-tectonic quartz mineralisation and the development of mica schists. Within these schists, the growth of micas would have led to

reaction softening of the rock (Steffen et al., 2001; Gueydan et al., 2003; Passchier and Trouw, 2005; Oliot et al., 2010). The development of a CPO (see section 5.1) during the formation of the schistose fabric also aligns the mineral grains in orientations of easy slip. This is referred to as geometric softening, and therefore also weakens the rock (Rutter et al., 2001; Ji et al., 2004; Passchier and Trouw, 2005).

Ductile 'Late Laxfordian' shearing is associated with epidote mineralisation, as well as the fluid influx initiating the early brecciation and cataclasis of the ultramylonite at Loch Assynt. Fluid influx associated with shearing at the frictional viscous transition is fundamental in switching the grainsize controlled deformation mechanisms to diffusional creep, normally within high strain parts of the fault zone (e.g. localised high strain along the dyke margins) (Stewart et al., 2000). Grainsize controlled dislocation creep mechanisms are common within samples within this study (section 5), however no obvious microstructures associated with diffusional creep are present. Diffusion-accommodated grain boundary sliding (GBS) within ultramylonites has been noted within some high temperature quartzo-feldspathic rocks, accommodated by fine, internally strain-free grains (Behrmann and Mainprice, 1987), however as ultramylonites within this study show grain sizes <10μm, SEM analysis is required to determine whether these mechanisms were active during deformation. Long term weakening of fault zones can be initiated by the onset of diffusion dominated creep (e.g. Schmid et al., 1977; Schmid, 1982; Handy, 1989), with a potential shallowing of the frictional viscous transition from normal depths (10-15km) due to this (Stewart et al., 2000). However, processes such as the generation of frictional melts can, in fact, lead to the long term strengthening of a fault zone due to the formation of the glass (e.g. Fialko and Khazan, 2005). It should, however, also be considered that over time, the devitrification of the glass would form a fine-grained aggregate that is potentially highly susceptible to grain-size sensitive deformation processes. As there do not appear to be any shearing events post-'Late Laxfordian' that

have affected and/or reactivated the dyke margins, this was not observed within the current study.

It is important to consider that the dykes, and large scale shear zones, can transect the whole crust, and at times the entire lithosphere (Vauchez et al., 2012; Tikoff et al., 2013); we therefore only examine a thin slice of the deformation history when conducting field and microstructural analyses of the exhumed portions of the dykes and/or shear zones. They may therefore show the full range of microstructural textures associated with different deformation mechanisms and metamorphic facies at different depths (Fig. 1.2) (Fossen and Cavalcante, 2017). Thus, deformation and weakening mechanisms need to be placed into a wider context. 'Late Laxfordian' textures from Loch Assynt and Achmelvich South can be compared to gain an insight into the wider context during this period of sinistral deformation. Ultramylonites and micrometre-scale pseudotachylytes dominate the dyke margin contacts at Loch Assynt, whereas centimetre-scale pseudotachylytes, calcite + zeolite mineralisation and brecciation are predominant at Achmelvich South. Large scale brecciation is also dominant at the northwestern end of the Loch Assynt Fault where it outcrops at Clashnessie. It therefore appears that for the 'Late Laxfordian' event at least, a shallower structural level is attained to the west, with more brittle deformation dominant. The tilting that led to this could have been related to the normal faulting associated with the Stoer Group deposition, resulting in block rotation and uplift (Fig. 6.4). Using simple trigonometric calculations, the amount of uplift can be estimated. Loch Assynt lies 15.05km to the SE of Clashnessie, and Stoer Group sediments at the present day dip ~20^{o} to the NW (British Geological Survey, 2002). These values would give a value of ~5.5km of uplift; however they are gross simplifications, as other factors may affect the uplift values. For example, further tilting associated with the Caledonian reactivation of the Loch Assynt Fault, with this event dying out moving further from the Moine Thrust Zone to the NW, perhaps due to differential loading by the Moine Nappe.

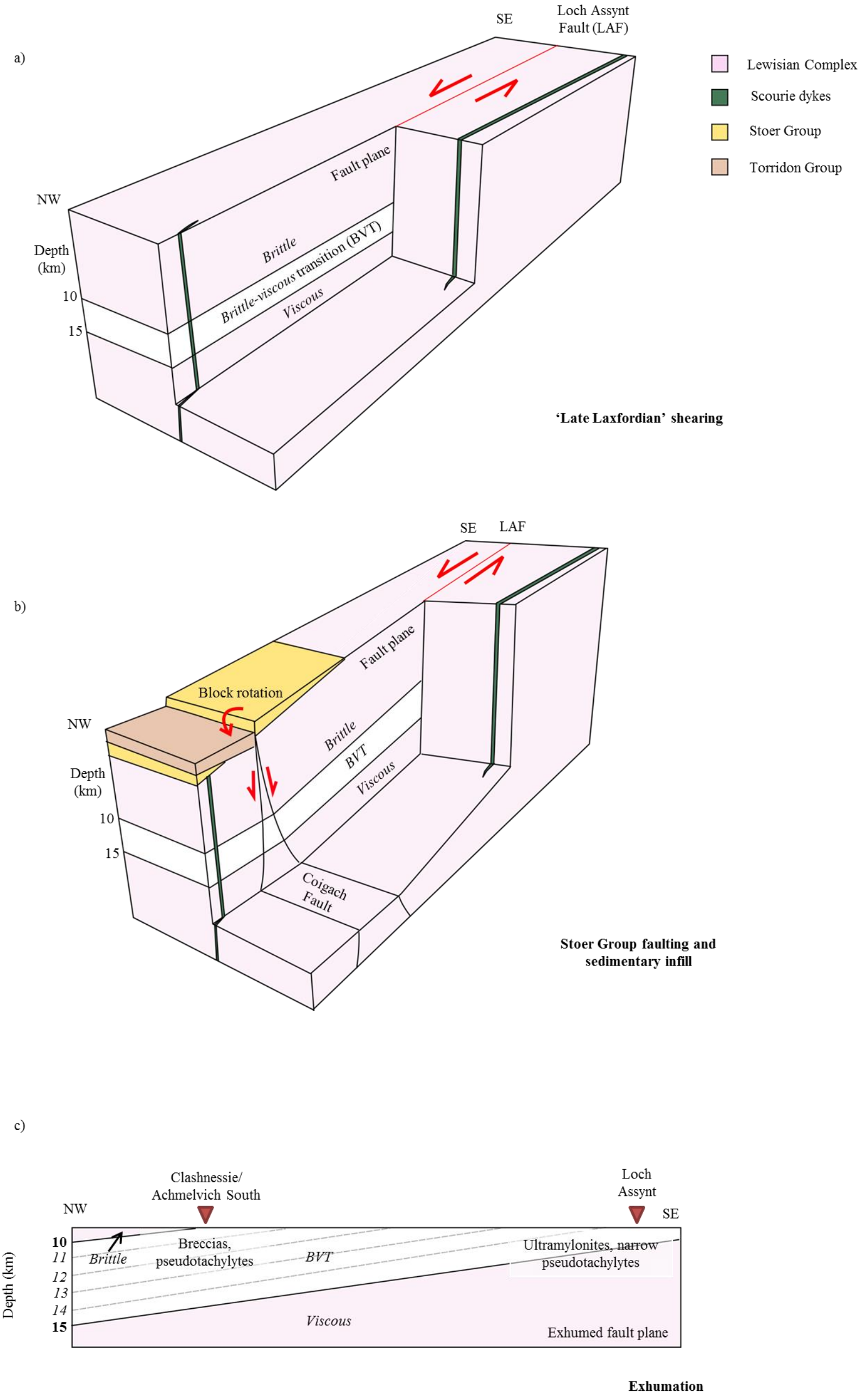

Fig 6.4. *Schematic block diagrams illustrating the deformation and block rotation along the Loch Assynt Fault (LAF) with respect to the brittle-viscous transition (BVT), diagrams are not to scale a) 'Late Laxfordian' shearing along the LAF b) Block rotation due to normal faulting during the deposition of the Stoer Group c) Schematic cross sectional view post LAF exhumation.*

6.2.3. Implications for reactivation and basin inheritance

In many continental deformation terrains, strain is localised along pre-existing anisotropies, including shear zones and dyke margins, during reactivation events (Fossen and Cavalcante, 2017). Dyke swarms provide powerful natural mechanical heterogeneities within a basement complex (e.g. different Young's modulus, Poisson's ratio to the country rock), which is likely to result in the localisation of deformation within the system. This is dependent on the orientation of the tectonic stresses during the reactivation event; predominantly strike-slip reactivation during the Laxfordian (e.g. Attfield, 1987) and 'Late Laxfordian'/D4 (e.g. Park et al., 1987) and therefore a horizontal σ_1 would have been better able to reactivate (for example) sub-vertical dyke margins, compared to an entirely compressional or extensional regime (Anderson, 1951). Direct field evidence for this is observable; undeformed dyke margins seem to dip more shallowly than those preserving clear evidence for reactivation (Table 6.3); for example, the dyke margins displaying 'Late Laxfordian' reactivation display dips of >80°. The kinematics of later events therefore play an important role in structural inheritance and the reactivation of earlier structures, as it is more energetically favourable to reactivate pre-existing mechanical anisotropies than to form new faults and/or fractures. The vertical dykes have small surface areas, and

Table 6.3. *Deformation features preserved compared to dip of the dyke margin at each of the main field localities.*

Location	**Average dyke margin dip**	**Original intrusive features?**	**Deformation preserved**
Lochinver	124/68 NE	Y - undeformed	None, undeformed
Achmelvich North	120/77 SW	Y - xenoliths	Laxfordian – dextral schistose mylonites
Achmelvich South	111/85 NNE	N	Laxfordian – dextral schistose mylonites 'Late Laxfordian' – (sinistral) pseudotachylytes
Loch Assynt	115/83 NNE	Y – sporadic baked margins, sharp undeformed margin	'Late Laxfordian – narrow band of sinistral ultramylonites, brittle sinistral faults + fractures

traverse across many kilometres vertically, as a direct route to the mantle. Storti et al (2003) argue that steeper faults do not have to be as large to cut through a horizontal, load bearing layer of thickness 't' (Fig. 1b, Storti et al., 2003). The CSZ represents an exhumed deep root of a strike slip fault zone, and also shows evidence for reactivation during both the Laxfordian and 'Late Laxfordian' events. Therefore, pre-existing mechanical anisotropies such as sub-vertical Scourie dykes, and strike-slip shear zones, are particularly prone to reactivation in continental settings.

Reactivation of pre-existing mechanical anisotropies in this way could therefore influence the locations of later sedimentary basins, and therefore play a part in hydrocarbon development within basement terranes. Within the East African rift system, the Eyasi-Wembre Rift (a seismically active splay in Tanzania) shows evidence of parallelism between NE-SW trending Archean dykes within the basement and the Eyasi-Wembre Rift (Halls et al., 1987; Fig 9, Ebinger et al., 1997). Within the Archean, there is a strong correlation between orientations of rift faults, and metamorphic fabrics and dykes of the Archean basement (Ebinger et al., 1997). This finding is key, as the main rift system trends roughly N-S; if reactivation of pre-existing metamorphic structures and dykes has occurred here, these may have influenced the orientation of the Eyasi-Wembre splay of the East African Rift. Changes in tectonic stresses in NW Scotland after the 'Late Laxfordian' meant this tectonic inheritance was not observed during the deposition of the Stoer Group sediments, indicated by NE-SW trending sediment filled fractures. The NE-SW trending normal faults associated with Stoer Group deposition dip steeply to the NW, with slickenfibres on fault surfaces indicating sinistral movement. Palaeostress inversions give a NW-SE extension direction (Beacom et al., 1999).

6.3. Further work

Further work based on this study would include looking for evidence for the 'Late Laxfordian' event within other terranes in NW Scotland, and perhaps even Greenland (and the timing compared to the Nagssugtoqidian orogeny?). On a smaller scale, dating of the calcite (e.g. Roberts and Walker, 2016; Nuriel et al., 2017) from Achmelvich South would provide evidence further supporting, or disproving, its association with the 'Late Laxfordian' event, which is assumed within this study. Clumped isotope analysis could also provide a further understanding of the calcite + zeolite mineralisation, for example measuring the growth temperatures (e.g. Bergman et al., 2013). SEM analysis of epidote mineralisation, and potential ultramylonites within the sample containing the dyke margin at Loch Assynt, would provide further insight into the deformation mechanisms, and also the relationship of the epidote with the different cycles of deformation at this locality.

7. Conclusions

1. Consistent patterns of overprinting and reactivation are recognized across the Assynt terrane, especially along pre-existing anisotropies such as dyke margins and shear zones. Furthermore, the 'Late Laxfordian' event is seen to form a kinematically coherent and distinct event, which has been dated.
2. This study gives some important insights into the nature of deformation processes around the frictional viscous transition, and indicates that syn-shearing fluid influx plays an important role in the resulting style of deformation.
3. Pre-existing anisotropies are very important during reactivation, provided the tectonic stresses are favourably oriented for subsequent shearing; long term structural inheritance is very often more likely that new structures forming, but not always.
4. As dyke margins are common within basement terranes worldwide (see Fig. 1.1), and provide natural heterogeneity, they form an integral part of providing planes of weakness prone to reactivation.
5. Fluid association at the frictional viscous transition may lead to weakening processes within the rocks, and control the deformation style.

Bibliography

Allen, A. (1979) 'Mechanism of frictional fusion in fault zones', *Jounral of Structural Geology*, 1(3), pp. 231–243. doi: 10.1016/0191-8141(79)90042-7.

Anderson, E.M. (1951) *The Dynamics of Faulting and Dyke Formation: With Applications to Britain.* 2nd Edition, London: Oliver and Boyd.

Arndt, N., Fowler, A. (2004) 'Textures in komatiites and variolitic basalts' in Eriksson, P. et al., *The Precambrian Earth: tempos and events*. Elsevier, pp. 298–311. <hal-00101711>

Attfield, P. (1987) 'The structural history of the Canisp Shear Zone', *Geological Society, London, Special Publications*, 27(1), pp. 165–173. doi: 10.1144/gsl.sp.1987.027.01.14.

Axen, G.J., Selverstone, J., Luther, A. (2018) 'A rock record of paleoseismic cycling: Unique layered cataclasites below the West Salton detachment fault, southern California', *Geosphere*, 14(1), pp.187-214.

Beach, A. (1976) 'The interrelations of fluid transport, deformation, geochemistry and heat flow in early Proterozoic shear zones in the Lewisian complex', *Philosophical Transactions of the Royal Society A: Mathematical, Physical and Engineering* Sciences, 280(1298), pp. 569-604. doi: 10.1098/rsta.1976.0014.

Beacom, L.E. (1999). *The Kinematic Evolution of Reactivated and Non-Reactivated Faults in Basement Rocks, NW Scotland*. Ph.D. The Queen's University of Belfast.

Beacom, L., Anderson, T., Holdsworth, R. (1999). 'Using basement-hosted clastic dykes as syn-rifting palaeostress indicators: an example from the basal Stoer Group, northwest Scotland', *Geological Magazine*, 136(3), pp. 301–310. doi: 10.1017/s0016756899002605.

Beacom, L.E., Holdsworth, R.E., McCaffrey, K.J.W., Anderson, T.B. (2001) 'A quantitative study of the influence of pre-existing compositional and fabric heterogeneities upon fracture-zone development during basement reactivation', *Geological Society, London, Special Publications*, 186(1), pp. 195-211. doi: 10.1144/gsl.sp.2001.186.01.12.

Behr, W.M., Platt, J.P. (2014) 'Brittle faults are weak, yet the ductile middle crust is strong: Implications for lithospheric mechanics', *Geophysical Research Letters*, 41(22), pp. 8067–8075. doi: 10.1002/2014gl061349.

Behrmann, J., Mainprice, D. (1987) 'Deformation mechanisms in a high-temperature quartz-feldspar mylonite: evidence for superplastic flow in the lower continental crust', *Tectonophysics*, 140(2-4), pp. 297–305. doi: 10.1016/0040-1951(87)90236-8

Bergman, S.C., Huntington, K.W., Crider, J.G. (2013) 'Tracing paleofluid sources using clumped isotope thermometry of diagenetic cements along the Moab Fault, Utah', *American Journal of Science*, 313(5), pp. 490–515. doi: 10.2475/05.2013.03.

Billings, M.P. (1942) 'Description and Classification of Faults', *Structural Geology*, pp. 130–155.

Bird, D.K., Spieler, A.R. (2004) ‘Epidote in geothermal systems’, *Reviews in Mineralogy and Geochemistry*, 56(1), pp. 235–300. doi: 10.2138/gsrmg.56.1.235.

Bjørnerud, M. (2010) ‘Rethinking conditions necessary for pseudotachylyte formation: Observations from the Otago schists, South Island, New Zealand’, *Tectonophysics*, 490(1-2), pp. 69–80. doi: 10.1016/j.tecto.2010.04.028.

Bowes, D., Bhattacharjee, C. (1967), ‘The metamorphic and migmatitic history of the Lewisian rocks north-west of Loch Tollie, Ross-shire, Scotland’, *Krystalinikum*, 5, pp. 7-60.

British Geological Survey (2002) *Point of Stoer,* Sheet 107W, 1:50 000. Keyworth: British Geological Survey (Geological Survey of Scotland, 1:63,360/1:50,000 geological map series).

Chapman, H. (1979) ‘2,390 Myr Rb–Sr whole-rock for the Scourie dykes of north-west Scotland’, *Nature*, 277(5698), pp. 642–643. doi: 10.1038/277642a0.

Chen, W., Molnar, P. (1983) ‘Focal depths of intracontinental and intraplate earthquakes and their implications for the thermal and mechanical properties of the lithosphere’, *Journal of Geophysical Research: Solid Earth,* 88(B5), pp. 4183–4214. doi: 10.1029/jb088ib05p04183.

Cliff, R., Rex, D. (1989) ‘Short Paper: Evidence for a “Grenville”event in the Lewisian of the northern Outer Hebrides’, *Journal of the Geological Society,* 146(6), pp. 921–924.

Corfu, F., Heaman, L., Rogers, G. (1994) ‘Polymetamorphic evolution of the Lewisian Complex, NW Scotland, as recorded by U-Pb isotopic compositions of zircon, titanite and rutile’, *Contributions to Mineralogy and Petrology,* 117(3), pp. 215–228. doi: 10.1007/bf00310864.

Condie, K.C. (2002) ‘Breakup of a Paleoproterozoic supercontinent’, *Gondwana Research,* 5(1), pp. 41–43. doi: 10.1016/s1342-937x(05)70886-8.

Coward, M.P., Park, R.G. (1987) ‘The role of mid-crustal shear zones in the Early Proterozoic evolution of the Lewisian’ in Park, R.G., Tarney, J. (eds) *Evolution of the Lewisian and Comparable Precambrian High Grade Terrains*. Oxford: Blackwell Scientific Publications, pp. 127–138.

Coward, M. (1990) ‘Shear zones at the Laxford front, NW Scotland and their significance in the interpretation of lower crustal structure’ *Journal of the Geological Society*, 147(2), pp. 279–286. doi: 10.1144/gsjgs.147.2.0279.

Crider, J.G. (2015) ‘The initiation of brittle faults in crystalline rock’, *Journal of Structural Geology*, 77, pp.159-174. doi: 10.1016/j.jsg.2015.05.001.

Cutts, K., Kelsey, D., Hand, M. (2013) ‘Evidence for late Paleoproterozoic (ca 1690–1665 Ma) high-to ultrahigh-temperature metamorphism in southern Australia: implications for Proterozoic supercontinent models’, *Gondwana Research,* 23(2), pp. 617–640. doi: 10.1016/j.gr.2012.04.009.

Davies, F.B. (1976) ‘Early Scourian structures in the Scourie-Laxford region and their bearing on the evolution of the Laxford Front’, *Journal of the Geological Society,* 132(5), pp. 543–554. doi: 10.1144/gsjgs.132.5.0543.

Davies, J., Heaman, L. (2014) 'New U–Pb baddeleyite and zircon ages for the Scourie dyke swarm: A long-lived large igneous province with implications for the Paleoproterozoic evolution of NW Scotland' *Precambrian Research,* 249, pp. 180–198. doi: 10.1016/j.precamres.2014.05.007.

De Bresser, J., Spiers, C. (1997) 'Strength characteristics of the r, f and c slip systems in calcite', *Tectonophysics,* 272(1), pp. 1–23. doi: 10.1016/s0040-1951(96)00273-9.

Dempsey, E.D., Holdsworth, R.E., Imber, J., Bistacchi, A. and Di Toro, G. (2014) 'A geological explanation for intraplate earthquake clustering complexity: The zeolite-bearing fault/fracture networks in the Adamello Massif (Southern Italian Alps)', *Journal of Structural Geology*, 66, pp.58-74. doi: 10.1016/j.jsg.2014.04.009.

Doblas, M. (1998) 'Slickenside kinematic indicators', *Tectonophysics*, 295(1-2), pp. 187–197. doi: 10.1016/s0040-1951(98)00120-6.

Droop, G.T.R, Fernandes, L.A.D, Shaw, S. (1999) 'Laxfordian metamorphic conditions of the Palaeoproterozoic Loch Maree Group, Lewisian Complex, NW Scotland', *Scottish Journal of Geology,* 35(1), pp. 31–50. doi: 10.1144/sjg35010031.

Ebinger, C., Djomani, Y.P., Mbede, E., Foster, A., Dawson, J. (1997) 'Rifting archaean lithosphere: the Eyasi-Manyara-Natron rifts, East Africa', *Journal of the Geological Society,* 154(6), pp. 947–960. doi: 10.1144/gsjgs.154.6.0947.

Evans, C.R., Tarney, J. (1964) 'Isotopic Ages of Assynt Dykes' *Nature*, 204(4959), pp. 638–641. doi: 10.1038/204638a0.

Evans, C.R. (1965) 'Geochronology of the Lewisian Basement near Lochinver, Sutherland', *Nature,* 207(4992), pp.54-56. doi: 10.1038/207054a0.

Evans, C., Park, R. (1965) 'Potassium–argon age determinations from the Lewisian of Gairloch, Ross-shire, Scotland', *Nature,* 205(4969), pp. 350-352. doi: 10.1038/205350a0.

Evans, C.R., Lambert, R.S.J. (1974) 'The Lewisian of Lochinver, Sutherland; the type area for the Inverian metamorphism', *Journal of the Geological Society,* 130(2), pp. 125-150. doi: 10.1144/gsjgs.130.2.0125.

Fialko, Y., Khazan, Y. (2005) 'Fusion by earthquake fault friction: Stick or slip?', *Journal of Geophysical Research: Solid Earth,* 110(B12). doi: 10.1029/2005jb003869.

Forand, D., Evans, J.P., Janecke, S.U., Jacobs, J. (2018) 'Insights into fault processes and the geometry of the San Andreas fault system: Analysis of core from the deep drill hole at Cajon Pass, California', *GSA Bulletin*, 130(1-2), pp.64-92. doi: 10.1130/b31681.1.

Fossen, H. (2010) *Structural Geology.* 1st edn. Cambridge: Cambridge University Press. pp. 463.

Fossen, H., 2016. *Structural geology*. 2nd edn. Cambridge: Cambridge University Press.

Fossen, H., Cavalcante, G.C.G. (2017) 'Shear zones–A review' *Earth Science Reviews,* 171, pp. 434–455. doi: 10.1016/j.earscirev.2017.05.002.

Friend, C., Kinny, P. (1995) ‘New evidence for protolith ages of Lewisian granulites, northwest Scotland’, *Geology*, 23(11), pp. 1027–1030. doi: 10.1130/0091-7613(1995)023<1027:nefpao>2.3.co;2.

Friend, C., Kinny, P. (2001) ‘A reappraisal of the Lewisian Gneiss Complex: geochronological evidence for its tectonic assembly from disparate terranes in the Proterozoic’, *Contributions to Mineralogy and Petrology*, 142(2), pp. 198–218. doi: 10.1007/s004100100283.

Gaál, G., Gorbatschev, R. (1987) ‘An outline of the Precambrian evolution of the Baltic Shield’, *Precambrian Research*, 35, pp. 15–52. doi: 10.1016/0301-9268(87)90044-1.

Geological Survey of Great Britain, (1972) *Sutherlandshire, Caithness (West), and Ross and Cromartyshire (N.W. Part)*, sheet 5, 1: 253 440, 2nd edn, Southampton: Ordnance Survey of Scotland (Quarter-inch geological map of Scotland series).

Giletti, B.J., Moorbath, S., Lambert, R.S.J. (1961) ‘A Geochronological Study of the Metamorphic Complexes of the Scottish Highlands’, *Quarterly Journal of the Geological Society*, 117(1-4), pp. 233-264. doi: 10.1144/gsjgs.117.1.0233.

Goodenough, K.M., Park, R.G., Krabbendam, M., Myers, J.S., Wheeler, J., Loughlin, S.C., Crowley, Q.G., Friend, C.R.L., Beach, A., Kinny, P.D., Graham, R.H. (2010) ‘The Laxford Shear Zone: an end-Archaean terrane boundary?’ *Geological Society, London, Special Publications*, 335(1), pp. 103-120. doi: 10.1144/SP335.6.

Goodenough, K., Crowley, Q., Krabbendam, M., Parry, S. (2013) ‘New U-Pb age constraints for the Laxford Shear Zone, NW Scotland: Evidence for tectono-magmatic processes associated with the formation of a Paleoproterozoic supercontinent’, *Precambrian Research*, 233, pp. 1–19. doi: 10.1016/j.precamres.2013.04.010.

Grocott, J, (1981) ‘Fracture geometry of pseudotachylyte generation zones: a study of shear fractures formed during seismic events’, *Journal of Structural Geology*, 3(2), pp. 169–178. doi: 10.1016/0191-8141(81)90012-2.

Gueydan, F., Leroy, Y.M., Jolivet, L., Agard, P. (2003) ‘Analysis of continental midcrustal strain localization induced by microfracturing and reaction softening’, *Journal of Geophysical Research: Solid Earth*, 108(B2). doi: 10.1029/2001jb000611.

Halfpenny, A., Prior, D.J. and Wheeler, J. (2006) ‘Analysis of dynamic recrystallization and nucleation in a quartzite mylonite’, *Tectonophysics*, 427(1-4), pp.3-14. doi: 10.1016/j.tecto.2006.05.016.

Hamilton, P., Evensen, N., O’nions, R., Tarney, J. (1979) ‘Sm—Nd systematics of Lewisian gneisses: implications for the origin of granulites’, *Nature*, 277(5691), pp. 25-28. doi: 10.1038/277025a0.

Handy, M.R. (1989) ‘Deformation regimes and the rheological evolution of fault zones in the lithosphere: the effects of pressure, temperature, grainsize and time’, *Tectonophysics*, 163(1-2), pp. 119–152. doi: 10.1016/0040-1951(89)90122-4.

Heaman, L.M., Tarney, J. (1989) ‘U-Pb baddeleyite ages for the Scourie dyke swarn, Scotland: evidence for two distinct intrusion events’, *Nature*, 340(6236), pp. 705-708. doi: 10.1038/340705a0.

Hirth, G., Tullis, J. (1992) 'Dislocation creep regimes in quartz aggregates', *Journal of Structural Geology,* 14(2), pp. 145–159. doi: 10.1016/0191-8141(92)90053-y.

Holdsworth, R., Stewart, M., Imber, J., Strachan, R. (2001) 'The structure and rheological evolution of reactivated continental fault zones: a review and case study', *Geological Society, London, Special Publications,* 184(1), pp. 115–137. doi: 10.1144/gsl.sp.2001.184.01.07

Hou, G., Kusky, T.M., Wang, C. and Wang, Y. (2010) 'Mechanics of the giant radiating Mackenzie dyke swarm: a paleostress field modeling', *Journal of Geophysical Research: Solid Earth*, 115(B2). doi: 10.1029/2007jb005475.

Jensen, L.N. (1984) 'Quartz microfabric of the Laxfordian Canisp Shear Zone, NW Scotland', *Journal of Structural Geology,* 6(3), pp. 293–302. doi: 10.1016/0191-8141(84)90053-1.

Jessell, M. (1987) 'Grain-boundary migration microstructures in a naturally deformed quartzite', *Journal of Structural Geology,* 9(8), 1007–1014. doi: 10.1016/0191-8141(87)90008-3.

Ji, S., Jiang, Z., Rybacki, E., Wirth, R., Prior, D., Xia, B. (2004) 'Strain softening and microstructural evolution of anorthite aggregates and quartz–anorthite layered composites deformed in torsion', *Earth and Planetary Science Letters,* 222(2), pp. 377-390. doi: 10.1016/s0012-821x(04)00204-3.

Johnson, T., White, R. (2011) 'Phase equilibrium constraints on conditions of granulite-facies metamorphism at Scourie, NW Scotland', *Journal of Structural Geology,* 168(1), pp. 147–158. doi: 10.1144/0016-76492010-069.

Karlstrom, K.E., Åhäll, K.-I., Harlan, S.S., Williams, M.L., McLelland, J., Geissman, J.W. (2001) 'Long-lived (1.8–1.0 Ga) convergent orogen in southern Laurentia, its extensions to Australia and Baltica, and implications for refining Rodinia', *Precambrian Research,* 111(1-4), pp. 5–30. doi: 10.1016/s0301-9268(01)00154-1.

Kelly, N., Hinton, R., Harley, S., Appleby, S. (2008) 'New SIMS U–Pb zircon ages from the Langavat Belt, South Harris, NW Scotland: implications for the Lewisian terrane model', *Journal of Structural Geology,* 165(5), pp. 967–981. doi: 10.1144/0016-76492007-116.

Kinny, P.D., Friend, C.R.L., Love, G.J. (2005) 'Proposal for a terrane-based nomenclature for the Lewisian Gneiss Complex of NW Scotland', *Journal of the Geological Society,* 162(1), pp. 175-186. doi: 10.1144/0016-764903-149.

Krabbendam, M., Leslie, A. (2010) 'Lateral variations and linkages in thrust geometry: the Traligill transverse zone, Assynt Culmination, Moine thrust belt, NW Scotland', *Geological Society, London, Special Publications,* 335(1), pp. 335–357. doi: 10.1144/sp335.16.

Lacombe, O. (2007) 'Comparison of paleostress magnitudes from calcite twins with contemporary stress magnitudes and frictional sliding criteria in the continental crust: Mechanical implications', *Journal of Structural Geology,* 29(1), pp.86-99. doi: 10.1016/j.jsg.2006.08.009.

Love, G.J., Kinny, P.D., Friend, C.R.L. (2004) 'Timing of magmatism and metamorphism in the Gruinard Bay area of the Lewisian Gneiss Complex: comparisons with the Assynt Terrane and implications for terrane accretion', *Contributions to Mineralogy and Petrology,* 146(5), pp. 620–636. doi: 10.1007/s00410-003-0519-1.

Lowrey, J.R., Ivanic, T.J., Wyman, D.A., Roberts, M.P. (2017) 'Platy pyroxene: new insights into spinifex texture', *Journal of Petrology,* 58(9), pp. 1671–1700. doi: 10.1093/petrology/egx069.

Lyon, T.D., Pidgeon, R.T., Bowes, D.R., Hopgood, A.M. (1973) 'Geochronological investigation of the quartzofeldspathic rocks of the Lewisian of Rona, Inner Hebrides', *Journal of the Geological Society,* 129(4), pp. 389–402. doi: 10.1144/gsjgs.129.4.0389.

MacDonald, J.M., Goodenough, K.M., Wheeler, J., Crowley, Q., Harley, S.L., Mariani, E., Tatham, D. (2015) 'Temperature–time evolution of the Assynt Terrane of the Lewisian Gneiss Complex of Northwest Scotland from zircon U-Pb dating and Ti thermometry'. *Precambrian Research,* 260, 55–75. doi: 10.1016/j.precamres.2015.01.009.

MacDonald, J.M., Magee, C., Goodenough, K.M. (2017) 'Dykes as physical buffers to metamorphic overprinting: an example from the Archaean–Palaeoproterozoic Lewisian Gneiss Complex of NW Scotland', *Scottish Journal of Geology*, 53(2), pp. 41-52. doi: 10.1144/sjg2017-004.

Maddock, R. (1983) 'Melt origin of fault-generated pseudotachylytes demonstrated by textures', *Geology*, 11(2), pp. 105–108. doi: 10.1130/0091-7613(1983)11<105:moofpd>2.0.co;2.

Maddock, R.H, Grocott, J., Van Nes, M. (1987) 'Vesicles, amygdales and similar structures in fault-generated pseudotachylytes', *Lithos*, 30(5), pp. 419–432. doi: 10.1016/0024-4937(87)90019-3.

Magloughlin, J.F., Spray, J.G. (1992) 'Frictional melting processes and products in geological materials: introduction and discussion', *Tectonophysics*, 204(3-4), pp. 197–204. doi: 10.1016/0040-1951(92)90307-r.

Mason, A., Parrish, R., Brewer, T. (2004) 'U–Pb geochronology of Lewisian orthogneisses in the Outer Hebrides, Scotland: implications for the tectonic setting and correlation of the South Harris Complex', *Journal of the Geological Society*, 161(1), 45–54. doi: 10.1144/0016-764902-140.

Mason, A.J. (2012) 'Major early thrusting as a control on the Palaeoproterozoic evolution of the Lewisian Complex: evidence from the Outer Hebrides, NW Scotland', *Journal of the Geological Society,* 169(2), pp. 201–212. doi: 10.1144/0016-76492011-099.

Mason, A.J. (2016) 'The Palaeoproterozoic anatomy of the Lewisian Complex, NW Scotland: evidence for two 'Laxfordian' tectonothermal cycles', *Journal of the Geological Society*, 173(1), pp. 153-169. doi: 10.1144/jgs2015-026.

McCaig, A. (1987) 'Deformation and fluid-rock interaction in metasomatic dilatant shear bands', *Tectonophysics*, 135(1-3), pp. 121–132. doi: 10.1016/0040-1951(87)90156-9.

Meert, J.G. (2012) ‘What’s in a name? The Columbia (Paleopangaea/Nuna) supercontinent’, *Gondwana Research,* 21(4), pp. 987–993. doi: 10.1016/j.gr.2011.12.002.

Moorbath, S., Park, R. (1971). ‘The Lewisian chronology of the southern region of the Scottish mainland’, *Scottish Journal of Geology,* 8(1), pp. 51–74. doi: 10.1144/sjg08010051.

Nesbitt, R. (1971) ‘The case for liquid immiscibility as a mechanism for nickel sulphide mineralization in the Eastern Goldfields, Western Australia’ in Glover, J.E. (ed), The Archaean Rocks, Geological Society of Australia Special Publication, Adelaide: Geological Society of Australia, p.253.

Norrell, G.T., Teixell, A., Harper, G.D. (1989) ‘Microstructure of serpentinite mylonites from the Josephine ophiolite and serpentinization in retrogressive shear zones, California’, *Geological Society of America Bulliten,* 101(5), 673–682. doi: 10.1130/0016-7606(1989)101<0673:mosmft>2.3.co;2.

Nuriel, P., Weinberger, R., Kylander-Clark, A., Hacker, B., Craddock, J. (2017) ‘The onset of the Dead Sea transform based on calcite age-strain analyses’, *Geology,* 45(7), pp. 587–590. doi: 10.1130/g38903.1

O’Hara, M.J. (1961) ‘Petrology of the Scourie dyke, Sutherland (Plate XVIII)’ *Mineralogical Magazine and Journal of the Mineralogical Society,* 32(254), pp. 848-865. doi: 10.1180/minmag.1961.032.254.02.

Obst, K., Katzung, G. (2006) ‘Spatial distribution and emplacement features of Permo-Carboniferous dykes at the southwestern margin of the Fennoscandian Shield’ in Hanski, E., Mertanen, S., Rämö, T., Vuollo, J. (eds.), *Dyke Swarms - Time Markers of Crustal Evolution.* Boca Raton: Taylor & Francis, pp. 257–271.

Oliot, E., Goncalves, P., Marquer, D. (2010) ‘Role of plagioclase and reaction softening in a metagranite shear zone at mid-crustal conditions (Gotthard Massif, Swiss Central Alps)’, *Journal of Metamorphic Geology,* 28(8), pp. 849–871. doi: 10.1111/j.1525-1314.2010.00897.x.

Park, R.G. (1964) ‘The structural history of the Lewisian rocks of Gairloch, Wester Ross, Scotland’, *Quarterly Journal of the Geological Society*, 120(1-4), pp. 397–426. doi: 10.1144/gsjgs.120.1.0397.

Park, R.G. (1970), ‘Observations on Lewisian Chronology’, *Scottish Journal of Geology,* 6(4), pp. 379-399. doi: 10.1144/sjg06040379.

Park, R., Cresswell, D. (1973) ‘The dykes of the Laxfordian belts’ in Park, R. *The early Precambrian of Scotland and related rocks of Greenland.* Keele: Department of Geology, University of Keele. pp. 119–128.

Park, R.G., Crane, A., Niamatullah, M. (1987) ‘Early Proterozoic structure and kinematic evolution of the southern mainland Lewisian’, *Geological Society, London, Special Publications’,* 27(1), pp. 139-151. doi: 10.1144/gsl.sp.1987.027.01.12.

Park, R.G., Tarney, J. (1987) ‘The Lewisian complex: a typical Precambrian high-grade terrain?’, *Geological Society, London, Special Publications*, 27(1), pp. 13-25. doi: 10.1144/GSL.SP.1987.027.01.03.

Park, R.G., Cliff, R.A., Fettes, D.J., Stewart, A.D. (1994) 'Precambrian rocks in northwest Scotland west of the Moine Thrust: the Lewisian Complex and the Torridonian' in *A Revised Correlation of Precambrian Rocks in the British Isles, Special Report of the Geological Society*. London: Geological Society of London, pp. 6–22.

Park, R. (2005) 'The Lewisian terrane model: a review', *Scottish Journal of Geology,* 41(2), pp. 105–118. doi: 10.1144/sjg41020105.

Passchier, C.W., Trouw, R.A. (2005) *Microtectonics*. 2nd edn. New York: Springer Science & Business Media.

Pattison, D.R., Chacko, T., Farquhar, J., McFarlane, C.R., 2003. Temperatures of granulite-facies metamorphism: constraints from experimental phase equilibria and thermobarometry corrected for retrograde exchange. J. Petrol. 44, 867–900.

Peach, B.N., Horne, J., Gunn, W., Clough, C.T., Teall, J.J.H., Hinxman, L.W. (1907) *The geological structure of the North-West Highlands of Scotland*. Glasgow: HM Stationery Office.

Pearce, M., Wheeler, J. (2014) 'Microstructural and metamorphic constraints on the thermal evolution of the southern region of the Lewisian Gneiss Complex, NW Scotland' *Journal of Petrology,* 55(10), pp. 2043–2066. doi: 10.1093/petrology/egu049.

Pless, J. (2012) *Characterising fractured basement using the Lewisian Gneiss Complex, NW Scotland: Implications for fracture systems in the Clair Field basement.* Ph.D. Durham University.

Roberts, N.M. Walker, R.J. (2016) 'U-Pb geochronology of calcite-mineralized faults: Absolute timing of rift-related fault events on the northeast Atlantic margin', *Geology* 44(7), pp. 531–534. doi: 10.1130/g37868.1.

Rowe, K., Rutter, E. (1990) 'Palaeostress estimation using calcite twinning: experimental calibration and application to nature', *Journal of Structural Geology,* 12(1), pp. 1–17. doi: 10.1016/0191-8141(90)90044-y.

Rutter, E., Holdsworth, R., Knipe, R. (2001) 'The nature and tectonic significance of fault-zone weakening: an introduction' *Geological Society, London, Special Publications,* 186(1), pp. 1–11. doi: 10.1144/gsl.sp.2001.186.01.01.

Rybacki, E., Evans, B., Janssen, C., Wirth, R., Dresen, G. (2013) 'Influence of stress, temperature, and strain on calcite twins constrained by deformation experiments', *Tectonophysics*, 601, pp. 20–36. doi: 10.1016/j.tecto.2013.04.021.

Schmid, S., Boland, J., Paterson, M. (1977) 'Superplastic flow in finegrained limestone', *Tectonophysics*, 43(3-4), pp. 257–291. doi: 10.1016/0040-1951(77)90120-2.

Schmid, S. (1982) 'Microfabric studies as indicators of deformation mechanisms and flow laws operative in mountain building' in Hsü, K.J. (ed) *Mountain Building Processes*. London: Academic Press.

Selby, D., Creaser, R.A. (2003) 'Re–Os geochronology of organic rich sediments: an evaluation of organic matter analysis methods', *Chemical Geology*, 200(3-4) pp. 225-240. doi: 10.1016/s0009-2541(03)00199-2.

Senshu, H., Maruyama, S., Rino, S., Santosh, M. (2009) 'Role of tonalite-trodhjemite-granite (TTG) crust subduction on the mechanism of supercontinent breakup', *Gondwana Research*, 15(3-4), pp. 433–442. doi: 10.1016/j.gr.2008.12.008.

Shelley, D. (1967) 'Myrmekite and myrmekite-like intergrowths', *Mineral Magazine*, 36(280), pp. 491–503. doi: 10.1180/minmag.1967.036.280.03.

Sheraton, J.W., Tarney, J., Wheatley, T.J., Wright, A.E. (1973) 'The Structural History of the Assynt District' in Park, R. *The Early Precambrian of Scotland and Related Rocks of Greenland*. Keele: Department of Geology, University of Keele, pp. 31–44.

Sherlock, S.C., Jones, K.A., Park, R.G. (2008) 'Grenville-age pseudotachylite in the Lewisian: laserprobe 40Ar/39Ar ages from the Gairloch region of Scotland (UK)', *Journal of the Geological Society* 165(1), pp. 73–83. doi: 10.1144/0016-76492006-134.

Shihe, L., Park, R.G. (1993) 'Reversals of movement sense in Lewisian brittle–ductile shear zones at Gairloch, NW Scotland, in the context of Laxfordian kinematic history', *Scottish Journal of Geology*, 29(1), pp. 9–19. doi: 10.1144/sjg29010009.

Sibson, R. (1977) 'Fault rocks and fault mechanisms', *Journal of the Geological Society*, 133(3), 191–213. doi: 10.1144/gsjgs.133.3.0191.

Sibson, R.H. (1983) 'Continental fault structure and the shallow earthquake source', *Journal of the Geological Society*, 140(5), 741–767. doi: 10.1144/gsjgs.140.5.0741.

Sibson, R.H., Toy, V.G. (2006) 'The habitat of fault-generated pseudotachylyte: Presence vs. absence of friction-melt' in Abercrombie, R., McGarr., Di Toro, G., Kanamori, H. *Geophysical Monograph Series 170*. New York: American Geophysical Union, pp. 153-166. doi: 10.1029/170GM16

Sills, J.D. (1983) 'Mineralogical changes occurring during the retrogression of Archaean gneisses from the Lewisian Complex of NW Scotland', *Lithos*, 16(2), pp. 113–124. doi: 10.1016/0024-4937(83)90009-9.

Sills, J., Rollinson, H. (1987) 'Metamorphic evolution of the mainland Lewisian complex', *Geological Society, London, Speical Publications*, 27(1), pp. 81–92. doi: 10.1144/gsl.sp.1987.027.01.08.

Smith, S.A.F., Strachan, R.A. and Holdsworth, R.E. (2007) 'Microstructural evolution within a partitioned midcrustal transpression zone, northeast Greenland Caledonides', *Tectonics*, 26(4). doi: 10.1029/2006tc001952.

Spencer, C.J., Cawood, P.A., Hawkesworth, C.J., Prave, A.R., Roberts, N.M., Horstwood, M.S., Whitehouse, M.J. (2015) 'Generation and preservation of continental crust in the Grenville Orogeny', *Geoscience Frontiers*, 6(3), pp. 357–372. doi: 10.1016/j.gsf.2014.12.001.

Stark, J.C., Wang, X.C., Denyszyn, S.W., Li, Z.X., Rasmussen, B., Zi, J.W., Sheppard, S. and Liu, Y. (2017) 'Newly identified 1.89 Ga mafic dyke swarm in the Archean Yilgarn Craton, Western Australia suggests a connection with India', *Precambrian Research* [Preprint]. doi: 10.1016/j.precamres.2017.12.036.

Steffen, K., Selverstone, J., Brearley, A. (2001) 'Episodic weakening and strengthening during synmetamorphic deformation in a deep-crustal shear zone in the Alps', *Geological Society, London, Special Publications',* 186(1), pp. 141–156. doi: 10.1144/gsl.sp.2001.186.01.09.

Stewart, M., Holdsworth, R.E., Strachan, R.A. (2000) 'Deformation processes and weakening mechanisms within the frictional–viscous transition zone of major crustal-scale faults: insights from the Great Glen Fault Zone, Scotland', *Journal of Structural Geology,* 22(5), pp. 543–560. doi: 10.1016/S0191-8141(99)00164-9.

Stone, P., Kimbell, G.S. and Richards, P.C. (2009) 'Rotation of the Falklands microplate reassessed after recognition of discrete Jurassic and Cretaceous dyke swarms', *Petroleum Geoscience,* 15(3), pp.279-287. doi: 10.1144/1354-079309-847.

Sutton, J., Watson, J. (1950) 'The pre-Torridonian metamorphic history of the Loch Torridon and Scourie areas in the North-West Highlands, and its bearing on the chronological classification of the Lewisian', *Quarterly Journal of the Geological Society,* 106(1-4), pp. 241-307. doi: 10.1144/gsl.jgs.1950.106.01-04.16.

Sutton, J., Watson, J. (1962) 'Further Observations on the Margin of the Laxfordian Complex of the Lewisian near Loch Laxford, Sutherland', *transactions of the Royal Society of Edinburgh,* 65(05), pp. 89–106. doi: 10.1017/s0080456800012412.

Swanson, M.T. (1989) 'Sidewall ripouts in strike-slip faults', *Journal of Structural Geology,* 11(8), pp. 933–948. doi: 10.1016/0191-8141(89)90045-x.

Tandon, R.S., Gupta, V. and Sen, K. (2015) 'Seismic properties of naturally deformed quartzites of the Alaknanda valley, Garhwal Himalaya, India', *Journal of Earth System Science*, 124(6), pp.1159-1175. doi: 10.1007/s12040-015-0605-6.

Tarney, J. (1963) 'Assynt Dykes and their Metamorphism', *Nature*, 199(4894), pp. 672–674. doi: 10.1038/199672a0.

Tarney, J. (1973) 'The Scourie dyke suite and the nature of the Inverian event in Assynt' in Park, R. *The Early Precambrian of Scotland and Related Rocks of Greenland*. Keele: Department of Geology, University of Keele, pp. 105–118.

Tarney, J., Weaver, B.L. (1987) 'Geochemistry of the Scourian complex: petrogenesis and tectonic models', *Geological Society, London, Special Publications,* 27(1), pp. 45-56. doi: 10.1144/GSL.SP.1987.027.01.05.

Teall, J.J.H. (1885) 'The metamorphosis of dolerite into hornblende-schist', *Quarterly Journal of the Geological Society,* 41(1-4), pp. 133–145. doi: 10.1144/gsl.jgs.1885.041.01-04.19.

Tikoff, B., Blenkinsop, T., Kruckenberg, S.C., Morgan, S., Newman, J., Wojtal, S.F. (2013) 'A perspective on the emergence of modern structural geology: Celebrating the feedbacks between historical-based and process-based approaches' in Bickford, M.E. *The Web of Geological Sciences: advances, impacts, and interactions*. Colorado: The Geological Society of America, Inc, pp. 65–119.

Tullis, T.E. (1980) 'The use of mechanical twinning in minerals as a measure of shear stress magnitudes', *Journal of Geophysical Research: Solid Earth,* 85(B11), pp. 6263–6268. doi: 10.1029/jb085ib11p06263.

Turnbull, M.J., Whitehouse, M.J., Moorbath, S. (1996) ‘New isotopic age determinations for the Torridonian, NW Scotland’, *Journal of the Geological Society*, 153(6), pp. 955–964. doi: 10.1144/gsjgs.153.6.0955.

Turner, F.J. (1953) ‘Nature and dynamic interpretation of deformation lamellae in calcite of three marbles’, *American Journal of Science,* 251(4), pp. 276–298. doi: 10.2475/ajs.251.4.276.

Vauchez, A., Tommasi, A., Mainprice, D. (2012) ‘Faults (shear zones) in the Earth’s mantle’ *Tectonophysics*, 558, pp. 1–27. doi: 10.1016/j.tecto.2012.06.006.

Vernon, R., Holdsworth, R.E., Selby, D., Dempsey, E., Finlay, A.J., Fallick, A.E. (2014) ‘Structural characteristics and Re–Os dating of quartz-pyrite veins in the Lewisian Gneiss Complex, NW Scotland: Evidence of an Early Paleoproterozoic hydrothermal regime during terrane amalgamation’, *Precambrian Research*, 246, pp. 256–267. doi: 10.1016/j.precamres.2014.03.007.

Vernon, R.H. (2004) *A practical guide to rock microstructure.* Cambridge: Cambridge university press.

Viljoen, M., Viljoen, R. (1969a) ‘The geology and geochemistry of the lower ultramafic unit of the Onverwacht Group and a proposed new class of igneous rocks’, *Geological Society of South Africa Special Publication,* 2, pp. 55–86.

Viljoen, R., Viljoen, M. (1969b) ‘The relationship between mafic and ultramafic magma derived from the upper mantle and the ore deposits of the Barberton region’, *Geological Society of South Africa Special Publication,* 2, pp. 221–244.

Weisenberger, T. (2009) *Zeolites in fissures of crystalline basement rocks.* Ph.D. University of Freiburg, Germany.

Wheeler, J., Park, R.G., Rollinson, H.R., Beach, A. (2010) ‘The Lewisian Complex: insights into deep crustal evolution’, *Geological Society, London, Special Publications*, 335(1), pp. 51-79. doi: 10.1144/sp335.4.

Zirkler, A., Johnson, T., White, R., Zack, T. (2012) ‘Polymetamorphism in the mainland Lewisian complex, NW Scotland–phase equilibria and geochronological constraints from the Cnoc an t’Sidhean suite’, *Journal of Metamorphic Geology,* 30(8), pp. 865–885. doi: 10.1111/j.1525-1314.2012.01003.x.

Appendices

1. Field Photographs

Fig 1.1. *Field photographs of the centre of the exposed smaller dyke at Loch Assynt down by the shore, all plan view a) NW-SW trending shear cross cutting the dyke with an obvious sharp lower base, compass clinometer for scale b) NNE-SSW trending dilational jogs of quartz mineralisation, opening direction indicated by the arrows, with hematite staining to the left of this, finger for scale c) Epidote vein within the dyke, originating from the central shear, showing fibrous crystals perpendicular to the vein margins, finger for scale. Note; field of view rotated ~90^{o} from previous photographs.*

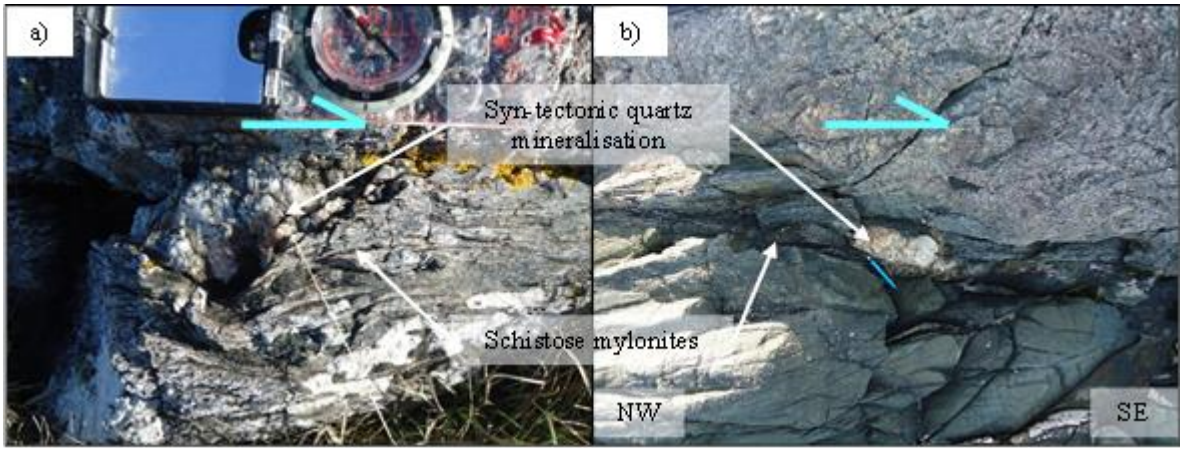

Fig 1.2. *Field photographs of quartz mineralisation and schistose fabric along the dyke margins at Achmelvich, all plan view a) syn-tectonic quartz mineralisation along with the schistose fabric at Achmelvich North, compass clinometer for scale b) syn-tectonic quartz mineralisation and schistose fabric along the southern dyke margin of Achmelvich South, pencil for scale.*

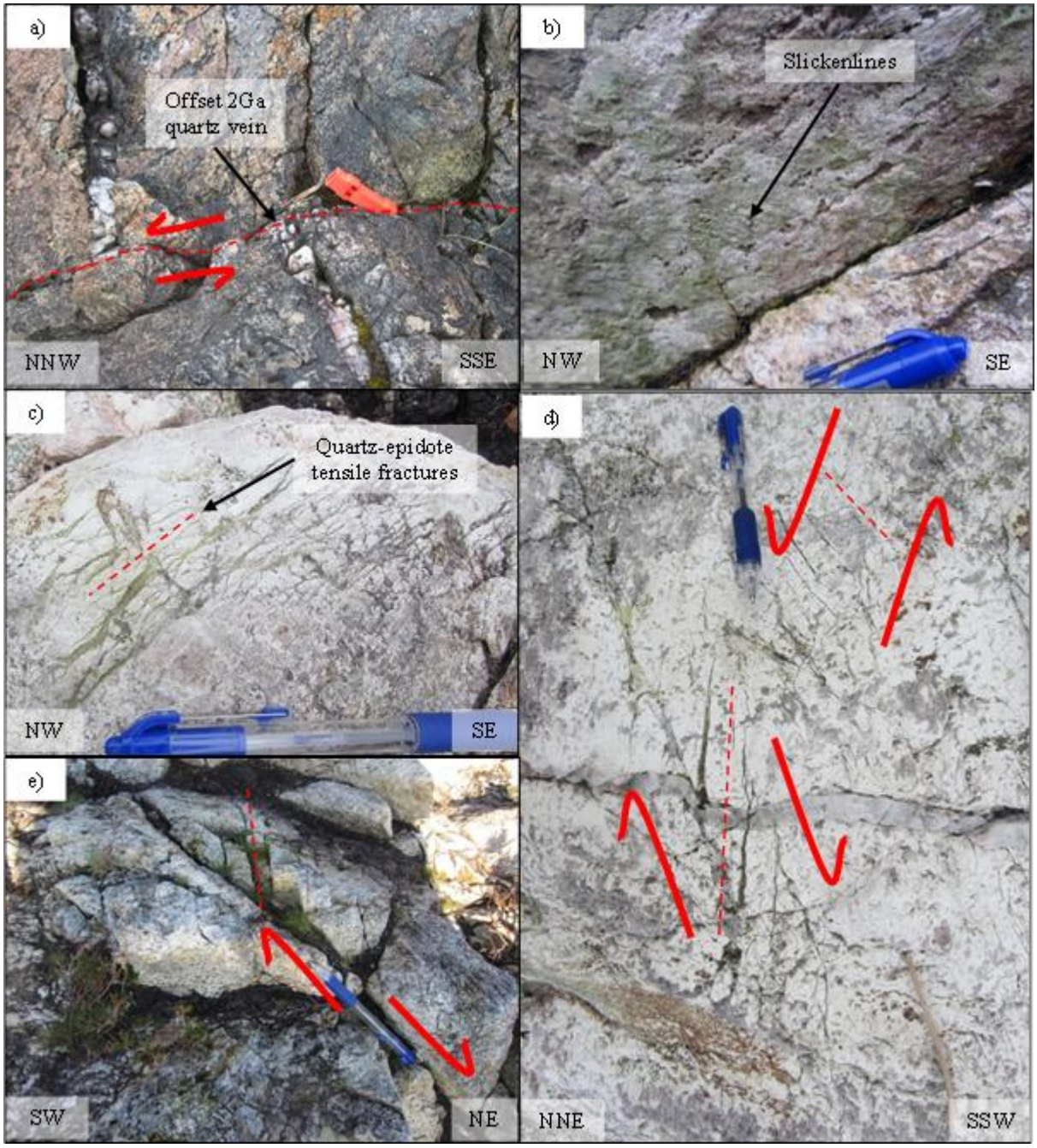

Fig 1.3. *'Late Laxfordian' fracture systems on 'Copper Island', all plan view; photos taken by R.E Holdsworth and E. Dempsey a) Sinistral offset of quartz vein by NW-SE trending brittle fractures b) Slickenlines associated with the NW-SE sinistral fractures c) En-echelon quartz-epidote WNW-ESE tensile fractures d) Antithetic sinistral and dextral shears and associated quartz-epidote filled tensile fractures e) Dextral shears and associated tensile fractures.*

Fig 1.4. *– Mineralisation along the Loch Assynt fault exposed at the tidal inlet at Clashnessie a) Chlorite mineralisation associated with a quartz-epidote vein at the edge of the fault breccia, cross sectional view, compass clinometer for scale b) Chlorite mineralisation on a sub-horizontal surface, plan view, compass clinometer for scale*

2. Thin section sample locations

Table 2.1. *Locations of samples that were subsequently sectioned for microstructural analysis; sample number, location, grid reference and a brief description are given.*

Sample No.	Location	Grid reference	Description
1	Achmelvich South, northern contact	NC 05535 24865	Predominantly gneiss, contact with dyke + pseudotachylyte (+lineations)
2	Achmelvich South, southern contact	NC 05538 24859	Biotite muscovite schist
3	Achmelvich South, southern contact	NC 05538 24859	Hornblende schist
7	Achmelvich North, central dyke	NC 05645 25066	Scourie dyke, central shear
8	Achmelvich North, southern contact	NC 05641 25055	Biotite muscovite schist
11	Assynt, southern contact (NW end)	NC 21049 25189	Ultramylonite + epidote + pseudotachylyte
15	Lochinver, southern contact	NC 08740 21927	Gneiss + dyke contact, chilled margin, undeformed
16	Lochinver, centre of dyke	NC 08740 21935	Scourie dyke, undeformed
20	Achmelvich South, northern contact	NC 05537 24864	Gneiss, pseudotachylyte + zeolite veins
21	Assynt, northern contact (SE end)	NC 21485 25025	Gneiss + dyke contact, heavy deformation + pseudotachylyte
R.E Holdsworth's samples:			
ACH1	Achmelvich South, northern contact		Gneiss + dyke contact, pseudotachylytes + zeolite/calcite mineralisation
ACH 2	Achmelvich South, northern contact		Gneiss + pseudotachylytes + zeolite/calcite mineralisation
AM	Achmelvich South, northern contact		Gneiss + dyke contact, pseudotachylytes + zeolite/calcite mineralisation
AS1	Assynt, 'Copper Island'		Gneiss + epidote mineralisation
AS2A	Assynt, 'Copper Island'		Gneiss + epidote mineralisation
AS4	Assynt, southern contact (NW end)		Ultramylonites + pseudotachylyte

3. Thin Section Photographs

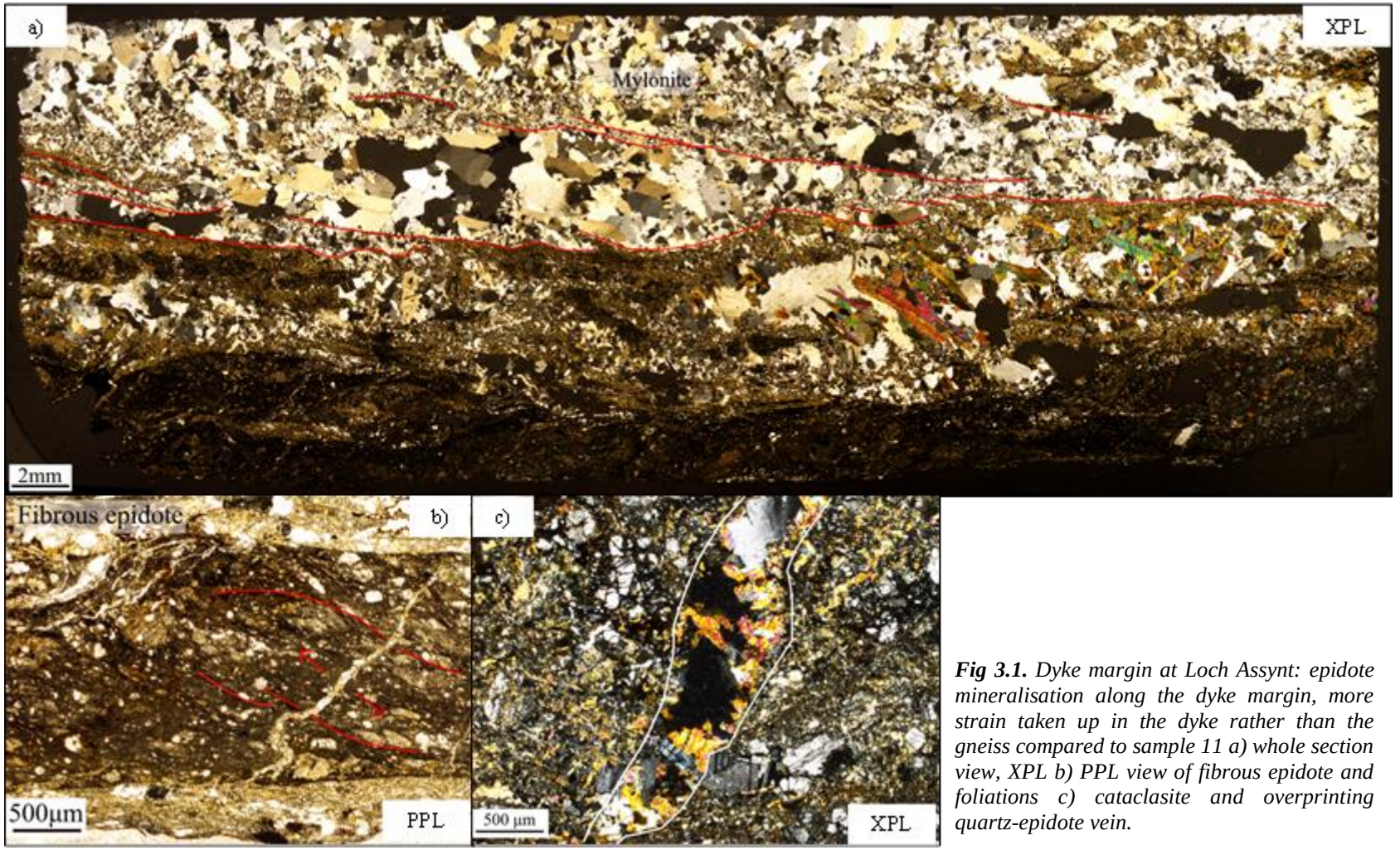

Fig 3.1. *Dyke margin at Loch Assynt: epidote mineralisation along the dyke margin, more strain taken up in the dyke rather than the gneiss compared to sample 11 a) whole section view, XPL b) PPL view of fibrous epidote and foliations c) cataclasite and overprinting quartz-epidote vein.*

Fig 3.2. *XPL whole section view of Loch Assynt sample showing overprinting relationships between ductile ultramylonites and folds, brittle structures; shears, breccias, cataclasites, and quartz epidote veins from the dyke margin. Thin section taken in a dipping plane (to the NW), lineation parallel.*

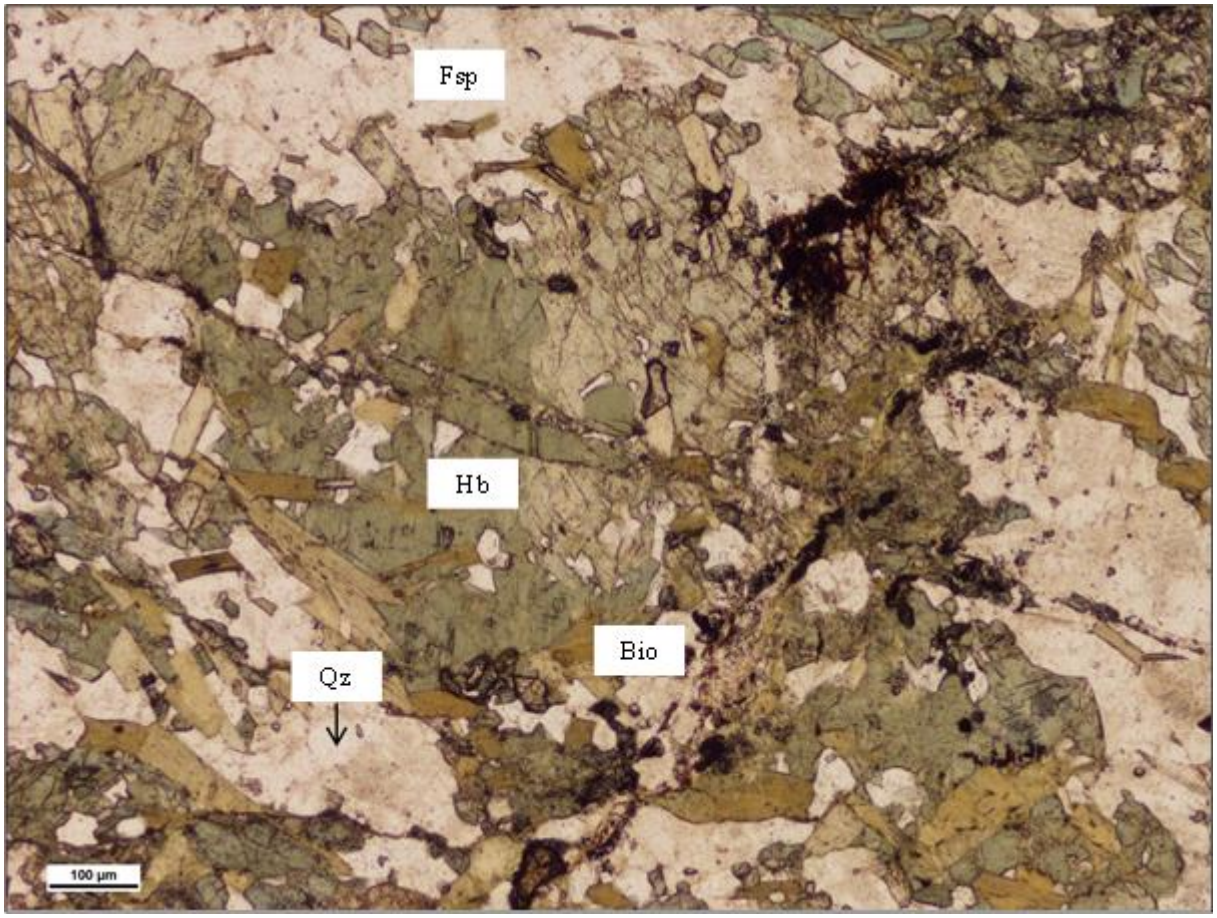

Fig 3.3. *PPL view of intercrystalline alteration of hornblende to biotite within the gneiss in samples from Achmelvich South (northern margin).*

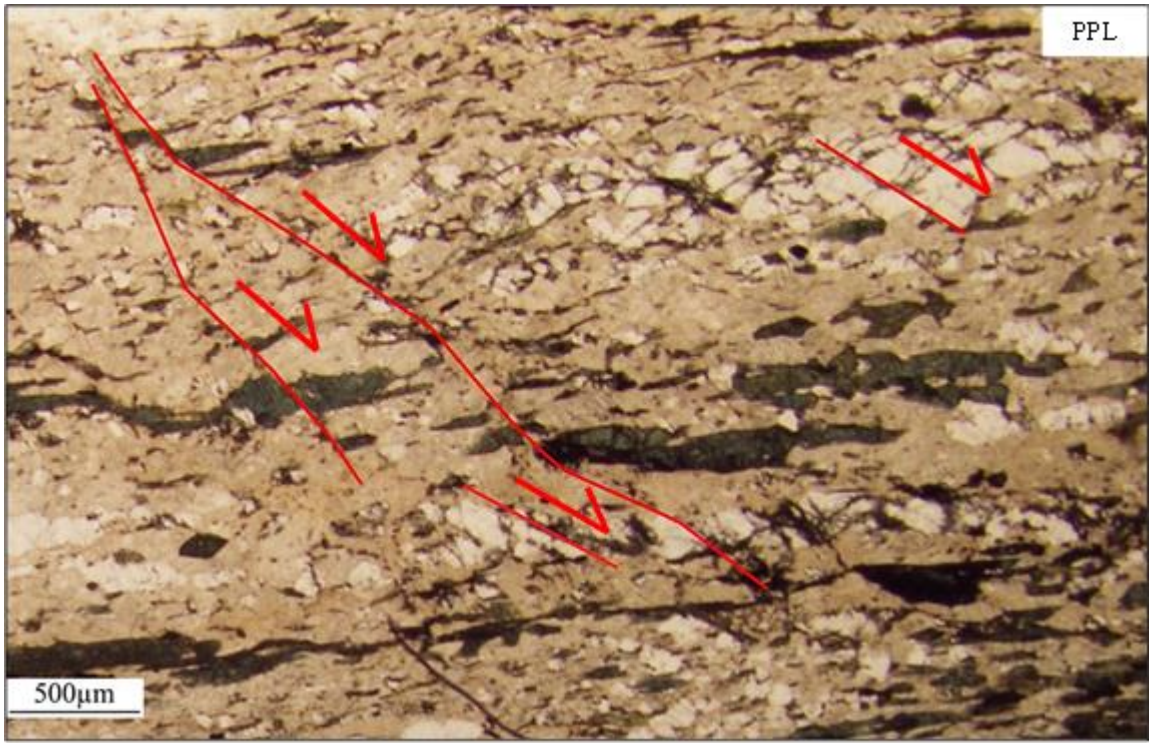

Fig 3.4. *Biotite muscovite schist cross cut by brittle dextral shears offsetting hornblendes and quartz with some clast rotation, selected shears outlined.*

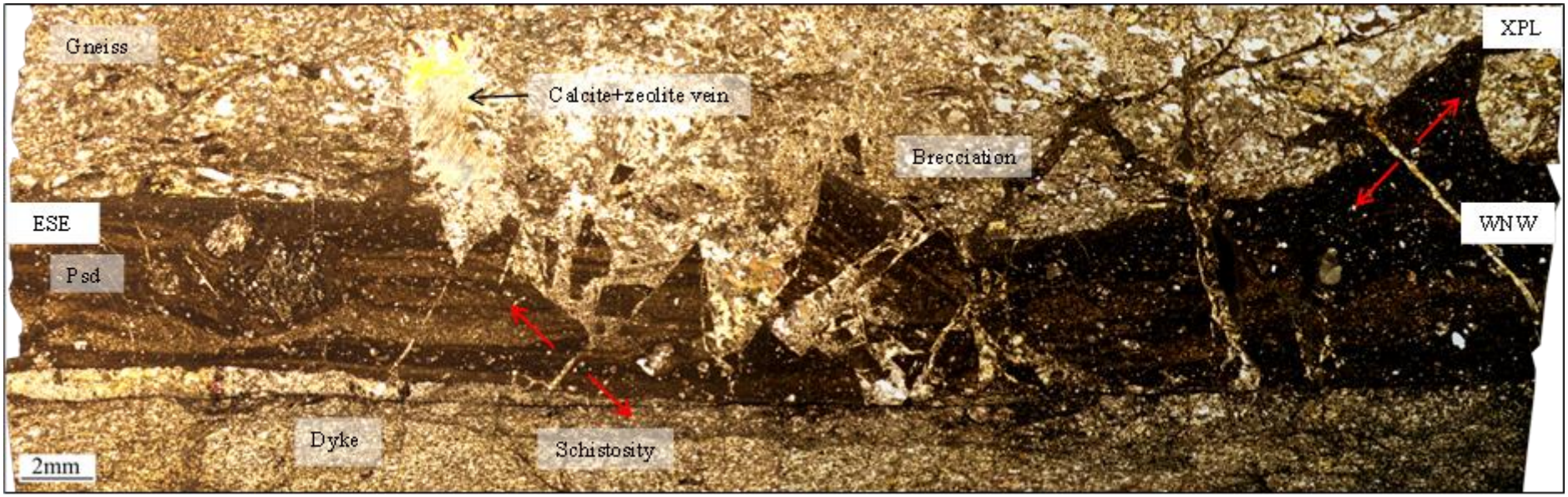

Fig 3.5. *Achmelvich South (northern margin): XPL view of flow banding within pseudotachylytes that have nucleated in the gneiss, with cataclasis associated with pseudotachylyte in the dyke. Later brecciation of the pseudotachylyte and gneiss shown by calcite + zeolite mineralisation injected along the dyke margin.*

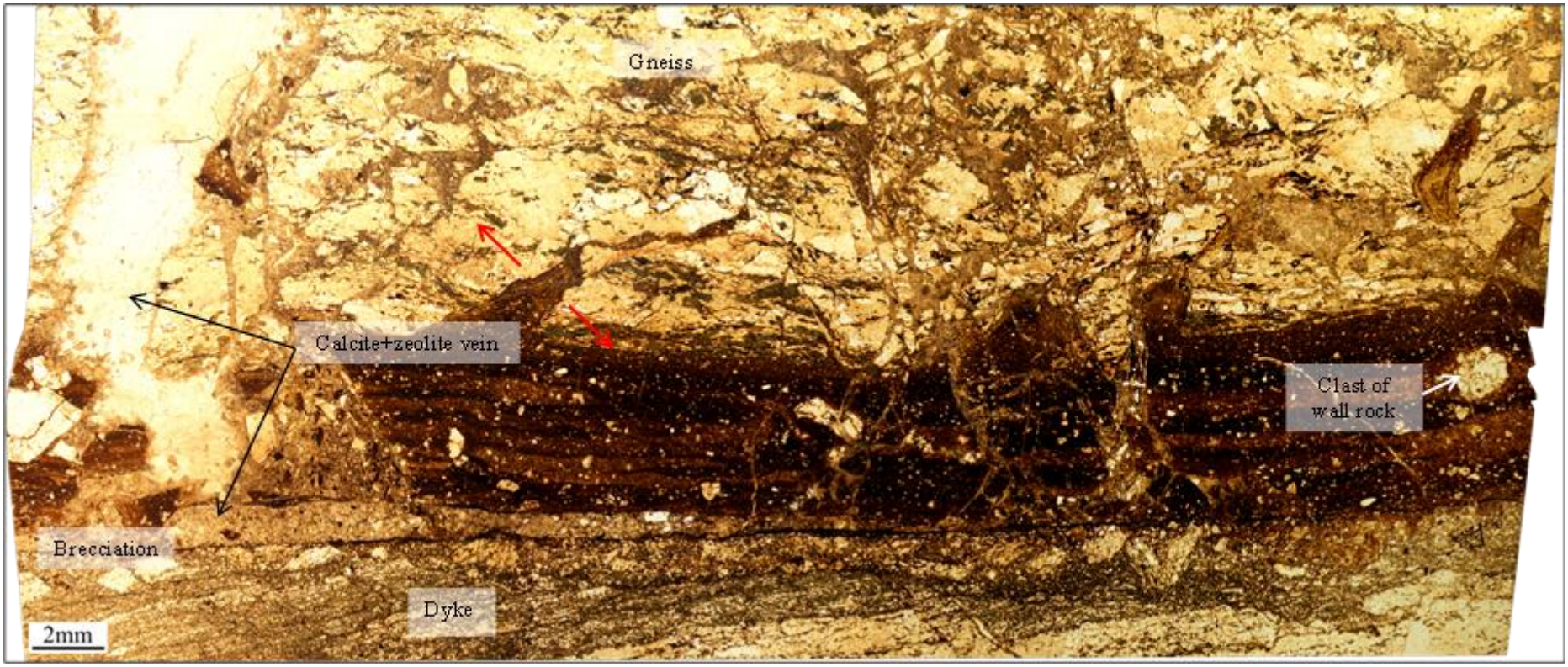

Fig 3.6. *Achmelvich South (northern margin), PPL view of flow banding within pseudotachylytes that have nucleated in the gneiss, with some earlier cataclasis in the gneiss, and cataclasis and sidewall ripout associated with pseudotachylyte in the dyke. Later brecciation of the pseudotachylyte and gneiss shown by calcite + zeolite mineralisation injected along the dyke margin.*

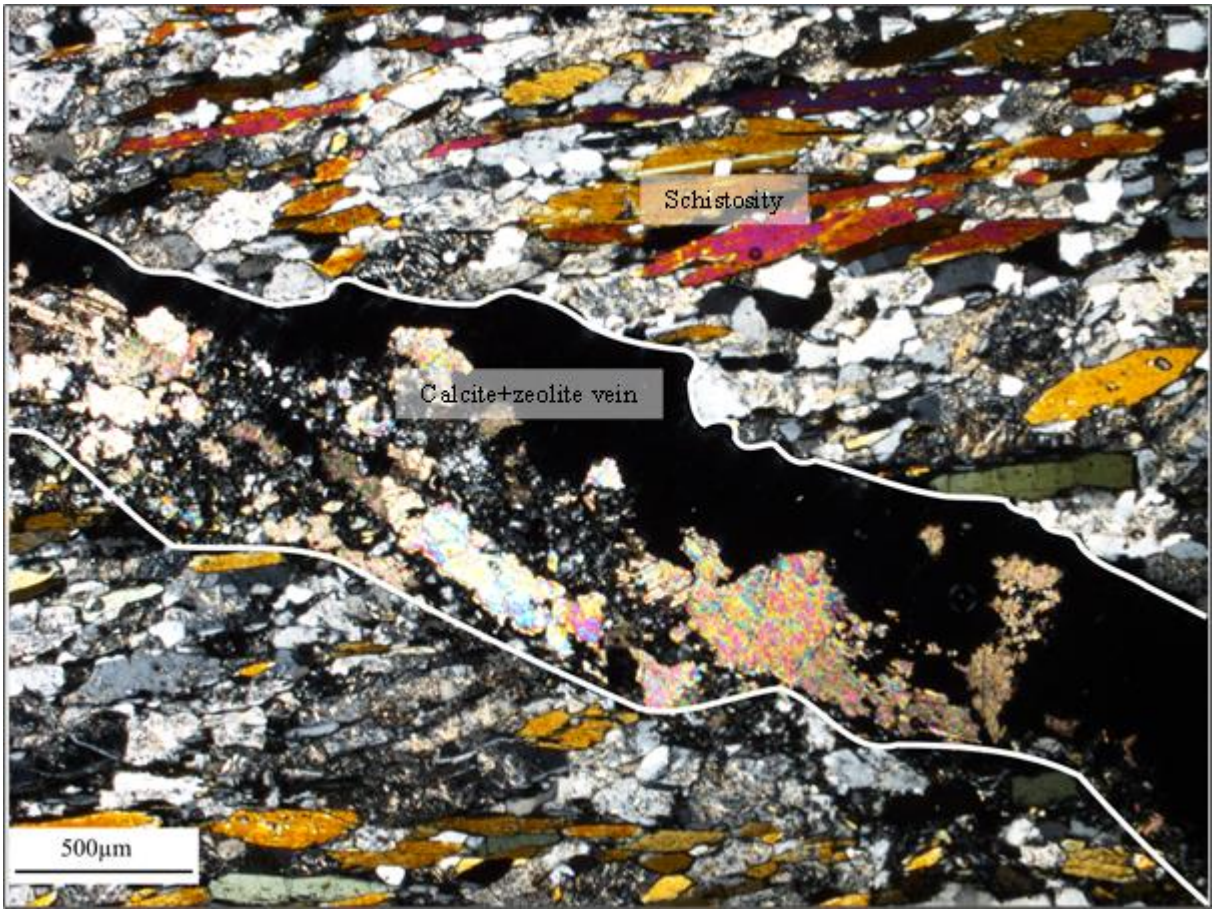

Fig 3.7. *Calcite + zeolite vein within an open fracture at Achmelvich North; overprints dextral schistose viscous mylonites*

4. Calcite twinning

Table 4.1. *Data collected from calcite veins within thin sections from Achmelvich South (northern margin), including the distance from the base of the vein and twin density. T and σ were calculated using calculations from Rybacki et al (2013) (see calculations below table).*

Sample	**Distance from vein base (mm)**	**Twin density(/mm^2)**	**T (MPa)**	**σ (MPa)**
ACH1	55	187	190	267
ACH1	12	99	138	194
ACH 1	1	296	184	335
ACH1	4	233	164	298
ACH1	65	165	138	250
ACH1	11	132	123	224
ACH1	16	76	93	170
AM	20	376	260	378

Note: Values for AM were from the only crystal to have a >1mm^2 area. As they appear as a massive outlier on the graph and are the only data from this thin section, they have been discounted.

$$\log(T) = 1.03 \pm 0.02 + (0.50 \pm 0.05) \cdot \log(N_L) \quad (1)$$

$$\log(\sigma) = 1.29 \pm 0.02 + (0.50 \pm 0.05) \cdot \log(N_L) \quad (2)$$

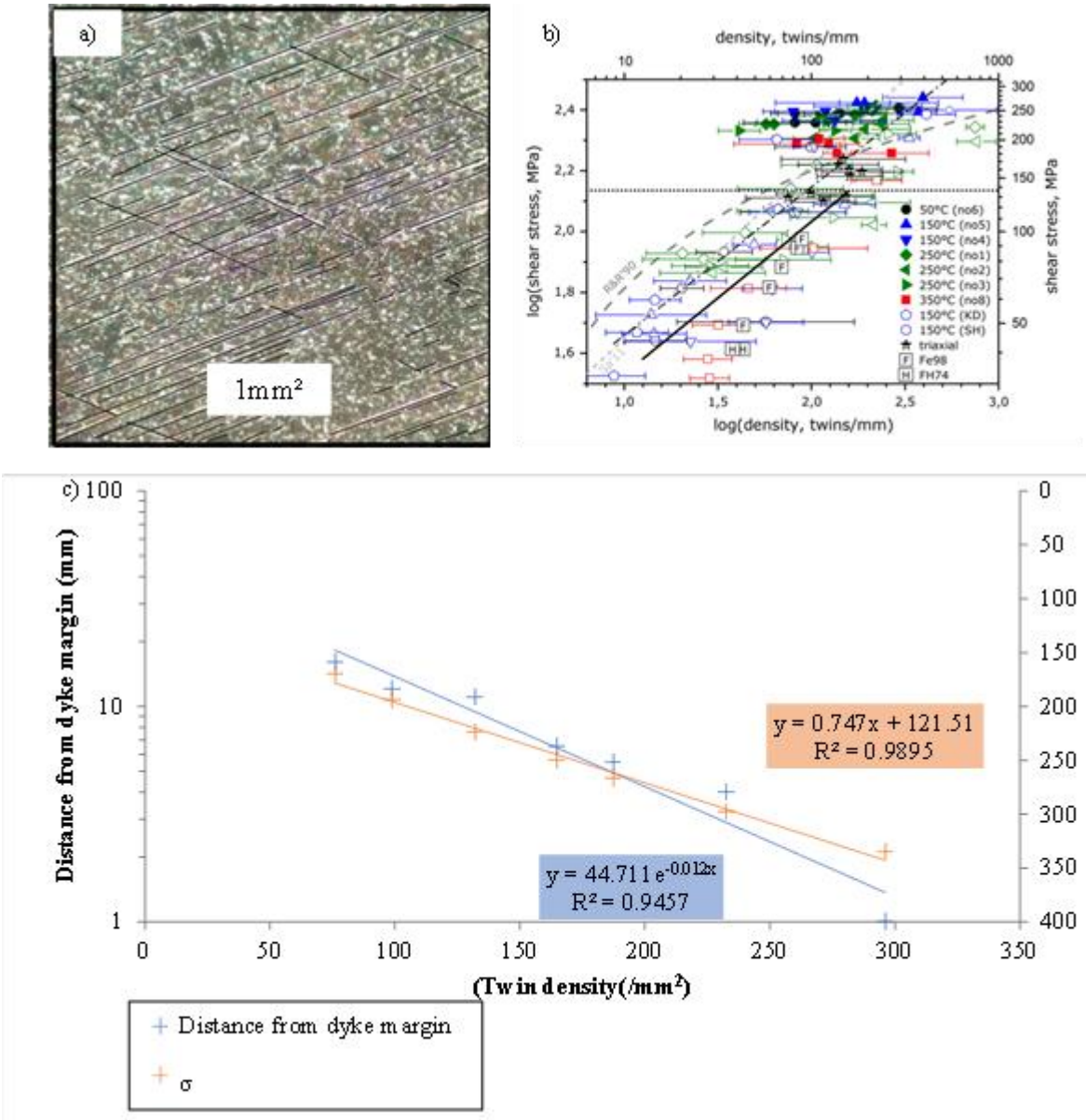

Fig 4.1. *Analysis based on calcite vein within sample ACH1 a) example of how twinning density was calculated b) Twin density vs applied shear stress in double-logarithmic scale, dotted-dashed line is a regression fit of all data, solid line shows fit of data below 140 MPa (Rybacki et al 2013) c) Twin density vs distance from dyke margin (logarithmic scale) and differential stress. Blue; distance from the dyke margin, orange; differential stresses.*

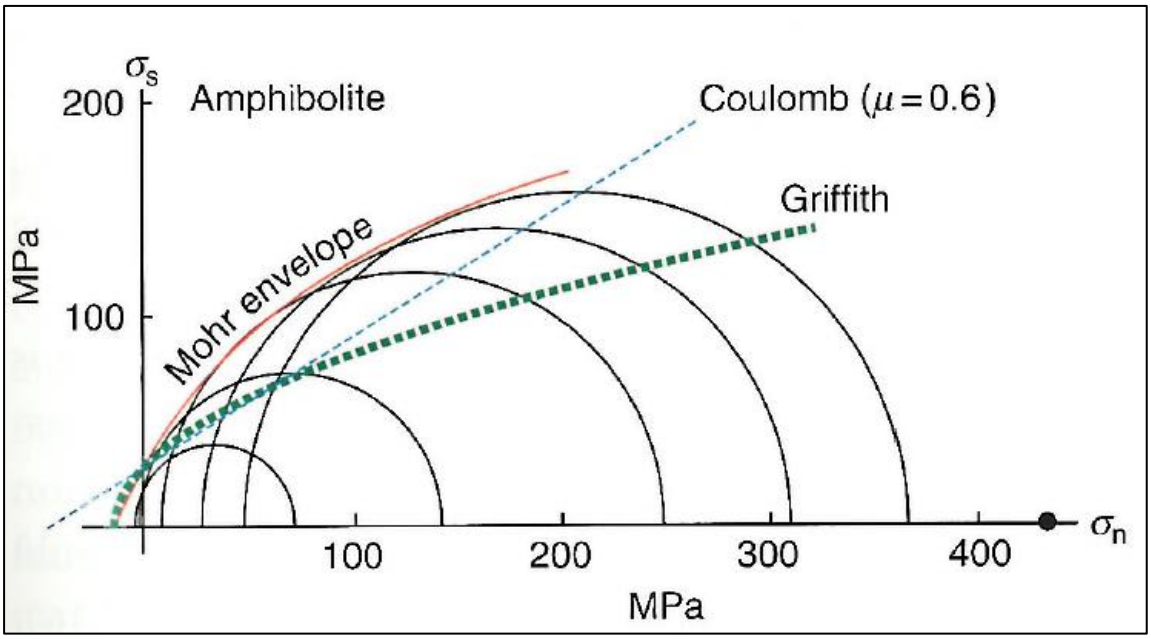

Fig. 4.2. *Griffith and Coulomb failure criteria superimposed on Mohr envelopes for amphibolite determined from triaxial tests. Neither of the criteria fit the Mohr envelope data very well. The Coulomb criterion approaches the envelope at the right side of the diagram at higher confining pressures (adapted from Fossen, 2010).*

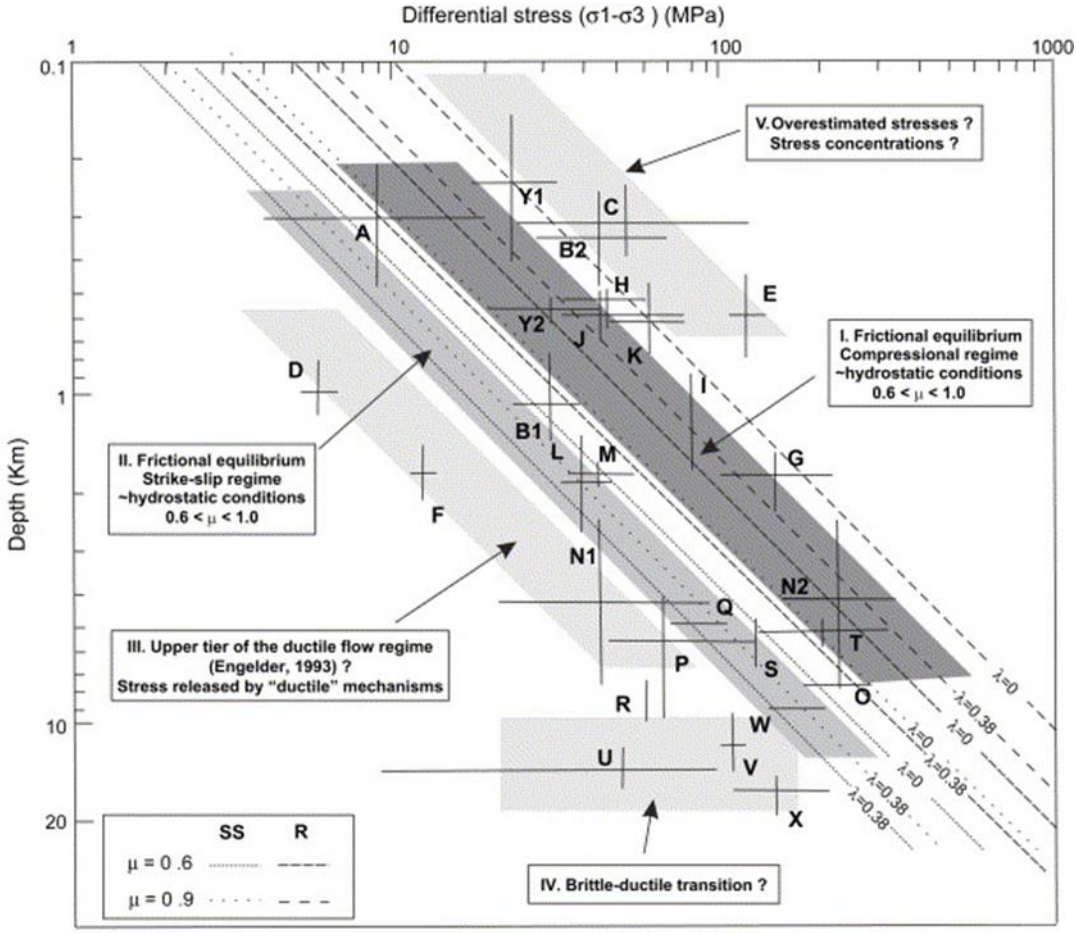

Fig 4.3 *Log-log graph of differential stress values derived from paleopiezometry vs depth relationship. Dashed lines illustrate stress-depth relationships predicted using Coulomb frictional failure theory for coefficients of friction (μ) of 0.6 and 0.9, pore pressures of 0 (λ = 0) and hydrostatic (λ = 0.38) and various tectonic regimes (SS, strike slip; R, reverse) (adapted from Lacombe, 2007)*